DISTRIBUTED-EFFECT MODAL DOMAIN OPTICAL FIBER SENSORS FOR FLEXIBLE STRUCTURE CONTROL

by

Karl Martin Reichard

Dissertation submitted to the Faculty of the
Virginia Polytechnic Institute and State University
in partial fulfillment of the requirements for the degree of
Doctor of Philosophy
in
Electrical Engineering

APPROVED:

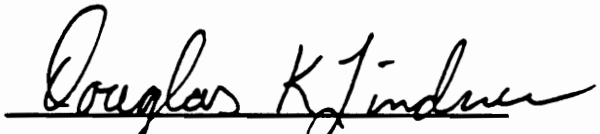

Douglas K. Lindner, Chairman

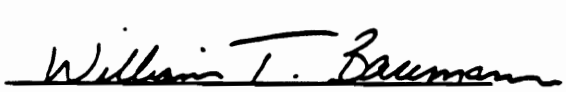

William T. Baumann

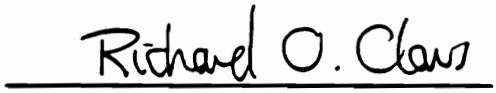

Richard O. Claus

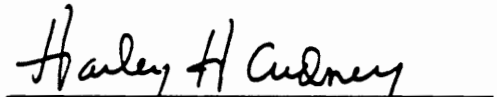

Harley H. Cudney

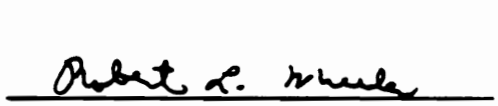

Robert L. Wheeler

June, 1991
Blacksburg, Virginia

DISTRIBUTED-EFFECT MODAL DOMAIN OPTICAL FIBER SENSORS FOR FLEXIBLE STRUCTURE CONTROL

by

Karl Martin Reichard
Douglas K. Lindner, Chairman
Electrical Engineering

(ABSTRACT)

Recently, a new class of sensors has emerged which have scalar outputs derived from distributed measurements over a significant gauge length; these sensors are known as distributed-effect sensors. The most familiar example of a distributed-effect sensor is the piezoelectric laminate PVDF film; other examples include holographic sensors and modal domain optical fiber sensors. Optical fiber sensors are particularly attractive for smart structure and materials applications because they have low mass, are flexible, and can be easily embedded in a variety of materials.

Distributed-effect sensors can be fabricated with spatially varying sensitivity to the distributed measurand and act as spatial filters. The spatial variation in the sensor sensitivity, known as the sensor's weighting function, determines the measurement provided by the spatial filter. Spatial filters can be configured to measure a variety of structural parameters, such as modal amplitudes and traveling waves, that can not be measured directly using point sensors. The mathematical model of the sensor is described and incorporated into a state-space model of a flexible structure. Several criteria are described in this dissertation for selecting the weighting functions of distributed-effect sensors for structural control laws.

The weighting function realized in the fabrication of a distributed-effect sensor may differ from the desired weighting function, causing the output of the manufactured sensor to differ from the desired measurement. In order to design reliable structural control laws, the nature and effects of errors in the

implemented weighting functions of distributed-effect sensors must be understood. This dissertation describes several causes of errors in distributed-effect sensor weighting functions. Errors in the weighting functions of distributed-effect sensors are integrated into the mathematical models of the sensors, and the effects of these errors on the sensor outputs are examined.

Acknowledgements

I would like to thank the members of my committee - Dr. Douglas K. Lindner, Dr. William T. Baumann, Dr. Richard O. Claus, Dr. Harley H. Cudney, and Dr. Robert L. Wheeler. Their insight and constructive criticism were invaluable during the course of my work. It has been a pleasure and an honor to work with each of them.

I would like express my special appreciation to Dr. Lindner, who has been both an advisor and a friend for the last several years. Dr. Lindner's dedication and insight were valuable assets during the course of this work, and it was through discussions with him that the ideas for this research evolved. I would also like to thank Dr. Claus, who has been a good friend since my days as an undergraduate, and who sparked my interest in sensor research.

I also would like to thank my family and friends for their support and constant encouragement. I am especially grateful to my parents for teaching me the value of a good education.

Finally, the one person that I can not thank enough is my wife, Karen. Not only has she made many sacrifices so that I could pursue my education, but without her love, this accomplishment would mean nothing.

This dissertation is dedicated to my wife, Karen, and to the memory of my great-uncle Theodore Taylor.

Table of Contents

List of Figures

List of Tables

1. Introduction

The use of active feedback control to suppress unwanted structural vibrations has been the subject of a great deal of research over the past decade. Much of the current research has focused on the development of structures and materials in which the required sensors, actuators, and signal processing capabilities are integrated, or even embedded, into the structure or material - so-called smart structures and materials. These smart structures and materials are designed to have enhanced performance, durability, and reliability.

Many of the proposed applications of smart structures and materials involve the control of continuous surfaces subject to deformations generated by external disturbance forces. These problems include the suppression of unwanted structural vibrations and static shape control in both flexible and rigid structures, and the control of acoustic radiation from vibrating structures. Examples of physical structures that have been mentioned in conjunction with these areas of research include large space structures such as the proposed space station and deployable antennas, airplane wings, rotating helicopter and turbine blades, submarine hulls, buildings, and bridges.

The proposed use of light-weight materials with high strength-to-weight ratios in the construction of structures such as the space station, large deployable antennas, and light-weight robotic arms will cause these structures to have little inherent structural damping. This lack of structural damping will present serious problems when these structures are employed as platforms for sensitive instrumentation and experiments. Consequently, the active suppression of unwanted structural vibrations is expected to be a primary concern in the design of these structures. In addition, active vibration suppression also has applications in earthquake protection for buildings and bridges, and the control of oscillations in aircraft components.

Increasingly stringent requirements on beam shape and pointing accuracy for space-based antennas has lead to the use of active control for both vibration

suppression and static shape control. In structures such as hoop-column antennas, active feedback is used to control the shape of the reflector and hence the nature of the beam formed by the antenna. Active feedback control is also being used in real-time adaptive optics to control the shape of segmented mirrors such as the one employed in the Keck Observatory.

The active control of acoustic radiation from structures is similar to the suppression vibrations in flexible structures, but with some slight differences in the objectives of the control laws. In the acoustic radiation problem, however, the objective isn't necessarily to damp out all vibrations, but only those vibrations that contribute to the radiated acoustic power measured in the far-field. These results have applications in the reduction of aircraft cabin noise and exterior engine noise.

Structural control laws often require a large number of sensors to provide an accurate estimate of the shape of the structure; thus sensor placement is an important problem [1-6]. Given the requirement of measuring the shape or displacement of a continuous surface, attempts have been made to choose sensor locations that optimize some performance measure. Physical restrictions on sensor placement, however, often impose limitations on the set of realizable outputs or measurements, particularly when those measurements are made by point sensors located on the structure.

Another problem related to sensor placement is observation spillover. The presence of unmodelled system dynamics in the sensor measurements can destabilize the system when those outputs are used calculate control inputs [7]. In order to reduce the effects of observation spillover, a large number of sensors is typically used to sample the behavior of the structure over its spatial domain, then modal filters are used to remove the unmodelled system dynamics from the measurements [8].

Distributed sensors provide an attractive solution to many of the sensing problems associated with structural control because they provide spatially continuous measurements of the system. Most control system designs, however, employ signal processing and computing technology which is only capable of processing scalar signals; hence, distributed measurements, if they were available, would first have to be converted into scalar signals compatible with current signal processing and computational algorithms. The challenge in converting distributed

measurements into scalar signals is to retain in the scalar signal as much of the pertinent information contained in the distributed signal as possible.

Recently, a class of sensors has emerged for structural control applications which respond to environmental changes over a significant gauge length, but have scalar outputs [9-10]. These sensor are called distributed-effect sensors. The best known examples of distributed-effect sensors have used piezoelectric film as the sensing element [11-14]. Other sensors in this class include holographic sensors [15-16] and modal domain optical fiber sensors [17-18].

Distributed-effect sensors have the unique ability to be physically altered along their gauge length to have spatially varying sensitivity to the distributed measurand. These sensors convert spatially distributed measurements into scalar signals and act as spatial filters. The spatial filter operation performed by the sensor is defined by the spatial variation in the sensor sensitivity along its gauge length; this function is known as the sensor's weighting function. The weighting function is a design parameter for the control system and can be chosen to measure directly various system quantities which can not be measured directly using point sensors.

Spatial filters have been demonstrated by Miller and Hubbard [11], Lee and Moon [14], and Collins, *et al.* [19], using piezoelectric film. Miller and Hubbard described the effects the boundary conditions associated with a distributed-effect piezoelectric sensor on the observability of the modes of a flexible beam. Lee and Moon demonstrated a spatial filter with a weighting function proportional to the shape of the first vibrational mode of a cantilevered beam; the output of the sensor was proportional to the first modal amplitude. Collins, *et al.*, [19] have demonstrated the design of spatial filters to measure traveling waves in structures. Using optimally chosen weightings, they have demonstrated spatial filters with frequency response characteristics that can not be achieved with causal temporal filters.

The use of spatial filters in structural control has received increasing attention over the last several years. Burke and Hubbard [12] applied Lyapunov stability theory to the design of a distributed actuator with spatially varying authority - the dual of a distributed-effect sensor - for controlling vibrations in a cantilevered beam. Chaing and Lee [13] demonstrated the use of weighted piezoelectric film to excite and control only the first mode of a cantilevered beam.

Spatial filters designed to measure traveling waves have been used to suppress acoustic radiation in structures [19]. The use of modal domain optical fiber sensors with uniform weightings in a vibration suppression control law for a cantilevered beam has also recently been demonstrated [20].

In addition to acting as spatial filters, distributed-effect sensors can also be viewed as generalized point sensors, since they can be configured to measure quantities that cannot be measured directly using point sensors. Although distributed-effect sensors provide scalar outputs, they differ from traditional point sensors because they are not constrained to physically locations on the structure. Consequently, distributed-effect sensors offer a possible solution to the sensor placement problem. Distributed-effect sensors have been used to realize sensors with desired observability characteristics [11] and have been proposed for the implementation of functional observers for state feedback control laws [10], and for use in control laws for the suppression of acoustic radiation [21]. The sensor's weighting function can also be chosen to eliminate observation spillover - the weighting function is chosen so that the unmodelled system dynamics are unobservable from the sensor output [10].

One issue that has received little attention is the effect that errors in implemented weighting functions will have on the performance of spatial filters in structural control laws. The weighting function that is realized in the fabrication of a distributed-effect sensor may differ from the desired weighting function. The differences between the weighting function of the ideal spatial filter and the weighting function realized in the fabrication of the sensor may significantly affect the performance of structural control algorithms which employ the spatial filter. Lee and Moon [14] reported a phenomena that they referred to as leak-through when they implemented a spatial filter designed to measure the amplitude of the first mode of a cantilevered beam - a frequency-domain analysis of the output of the spatial filter showed a noticeable component due to the beam's second vibrational mode. The sensor was fabricated by removing the metallic coating from one side of a sheet of piezoelectric film bonded to the sensor, leaving a conducting layer in the shape of the desired weighting function. Examination of the sensor, however, showed that the edges of the conducting layer were rough, not smooth as they should have been for the ideal weighting function. The difference between the implemented and the desired weighting functions caused

the presence of the additional higher-order modes in the sensor output.

This dissertation describes the use of distributed-effect sensors for the control of vibrations in flexible structures. The mathematical model for a class of distributed-effect sensors is introduced, the integration of the sensor model into state-space models of flexible structures is described, and several criteria for the selection of distributed-effect sensor weighting functions are presented. This dissertation also considers the effects of differences between the realized and ideal weighting functions on the performance of the distributed effect sensor. Several possible causes of differences between the ideal and realized weighting function for a distributed-effect sensor are discussed. Ways of characterizing the differences between ideal and realized weighting functions are described, and incorporated into the mathematical model of the sensor. Using this model, the effects of errors in the weighting functions on the sensor output are examined.

The discussion of the effects of errors in the implemented weighting functions of distributed-effect sensors in this dissertation is motivated by an interest in the use of modal domain optical fiber sensors as spatial filters. Modal domain optical fiber sensors has been employed in feedback control laws designed to suppress vibrations in a flexible beam [20,22-24], and have been proposed for use as distributed-effect sensors [10,21].

Modal domain optical fiber sensors provide a measurement proportional to the integral of the strain along the sensor gauge length. For the purpose of system analysis and control law design, the modal domain optical fiber sensor is mathematically equivalent to the piezoelectric film sensors used in the implementation of distributed-effect sensors for one-dimensional structures such as flexible beams.

The desire to develop modal domain optical fiber sensors with spatially varying sensitivity for use as weighted distributed-effect sensors is motivated by the advantages of optical fiber sensors for smart structure and materials applications [25]. The development of optical fiber sensors began over ten years ago. Different sensor configurations have been developed to measure temperature, pressure, strain, chemical concentrations, structural vibrations, and acoustic waves, and other quantities. The advantages of optical fiber sensors for smart structure applications include:

1. Immunity to electromagnetic interference.
2. Avoidance of ground loops.
3. High sensitivity.
4. Resistance to corrosion.
5. Low mass.
6. The ability to function as both a sensor and a communication channel.

Several mechanisms for implementing modal domain optical fiber sensors with spatially weighted strain sensitivity were identified by Reichard and Lindner [18], and the implementation of a modal domain optical fiber sensor with spatially varying sensitivity to strain was recently demonstrated at Virginia Tech [26]. In this dissertation, the mechanisms for weighting the sensitivity of a modal domain optical fiber sensor are reviewed, and a method for implementing arbitrary weighting functions using modal domain optical fiber sensors is proposed. This discussion serves to identify several possible sources of errors in the weighting functions that are realized in the fabrication of distributed-effect sensors.

Chapter 2 provides a brief description of modal domain optical fiber sensors. This discussion is not intended to be a complete description of this sensor technology, but should provide the level of understanding required to discuss the operation of the sensor in the context of distributed-effect sensors for structural control applications. The primary objective of this chapter is to introduce the mathematical model of the sensor model and describe the development of an expression for the sensor sensitivity. The principle sensor components and the basic mechanisms of sensor operation are described. Next, the mathematical model of the effects of applied strain on the sensor output is introduced. The sensor model is used to derive expressions for the sensor's sensitivity and dynamic range.

Chapter 3 describes the mathematical model of a simple flexible structure - a cantilevered beam. The Euler-Bernoulli beam equation is used to model the displacement of the structure from equilibrium. A state space model of the structure is derived from a modal decomposition of the structural displacement. This model is used in examples throughout this dissertation to illustrate the selection of weighting functions for distributed-effect sensors, and the effects of errors in the achieved weighting function on system performance.

In Chapter 4, the use of distributed-effect sensing for structural control is described. Key terms and concepts are defined, and the general mathematical model for a class of distributed-effect sensors is introduced. The sensor model is integrated into the state space model of the cantilevered beam, and it is shown that for certain sets of basis functions, there is a one-to-one correspondence between the distributed-effect sensor's weighting function and the output matrix for the sensor in the state space model of the structure. Using this result, several criteria for the design of distributed-effect sensors are described. The design criteria described in this chapter include the implementation of modal filters, optimizing measures of observability, and the implementation of functional observers.

Chapter 5 considers implementation of weighted modal domain optical fiber sensors. First, the effects of sensor orientation and parameter variations on sensor sensitivity are described. Next, a method is proposed for using modal domain optical fiber sensors to implement bipolar distributed-effect sensor weighting functions.

Chapter 6 is concerned with the effects that errors in the weighting functions realized in the fabrication of distributed-effect sensors have on the performance of sensors. Several possible limitations that are likely to be encountered in the process of manufacturing distributed-effect sensor are discussed and related to the generation of errors in the achieved sensor weighting function. Next, the integration of weighting function errors into the mathematical model of the sensor output is described, and it is shown that errors in the weighting functions enter the structural model as perturbations in the output matrix associated with the distributed-effect sensor. The weighting function errors generated in the fabrication of the sensors are characterized in terms of deterministic bounds on the magnitude of the error and as a random processes. The performance of distributed-effect sensors with errors in their weighting functions is compared to the performance of the corresponding ideal distributed-effect sensors for several of the design criteria described in Chapter 5.

Chapter 7 contains a summary of the results presented in this dissertation. Several areas of further research are also discussed.

2. Modal Domain Optical Fiber Sensors

The purpose of this chapter is to provide an brief introduction into the use of modal domain optical fiber sensors to sense structural strain. The basic components and operating principles of the sensor are described, and the derivation of a mathematical model of the effects of arbitrary strain on the sensor output is outlined. The response of the sensor to applied strain is characterized in terms of the sensor sensitivity and dynamic range. A more detailed treatment of the material presented in this chapter can be found in Reichard and Lindner [18].

The use of modal domain optical fiber sensors for the measurement of strain has been studied in some detail [27]. Previous sensor models derived for use in system theoretic analysis and design, however, have only accounted for strain in the direction of the fiber's longitudinal axis. While these models are adequate for sensing applications involving beams and other structures in which the resulting strain field is predominantly one-dimensional, the use of the modal domain optical fiber sensor in sensing applications involving more general structural geometries requires a more detailed model of the effects of strain on the sensor output. Sirkis and Haslach [28] have described the effects of arbitrary strain on the output of a traditional optical fiber interferometer; the sensor model described in this chapter is based on an extension of their analysis to modal domain optical fiber sensors.

The simulation model of the sensor described in this chapter is based on a complete analysis of the mechanical, optical, and photoelastic effects of arbitrary strain on the sensor output, however, it does not provide a closed-form expression for the sensor output in response to applied strain. The derivation of two simplified sensor models is also described. The simplified models provide closed-form expressions for the sensor output and are better suited for the design and analysis of systems that employ modal domain optical fiber sensors. These models are used to derive expressions for the sensor's sensitivity and dynamic range.

Section 2.1 describes the primary components of the modal domain optical fiber sensor. Section 2.2 outlines the issues that must be addressed in

development of a mathematical model of the effects of arbitrary strain on the output of the fiber sensor, and Section 2.3 describes the derivation of the sensor models. Expressions for the sensor's sensitivity and dynamic range are derived in Section 2.4.

2.1. SENSOR DESCRIPTION

This section describes the primary components of modal domain optical fiber sensors, and the operating configurations employed when the sensor is used to measure strain. For strain sensing, the sensor can be operated in two configurations which determine the type of output produced by the sensor.

2.1.1. Sensor components

The block diagram in Figure 2.1.1 shows a modal domain optical fiber sensor attached to a structure. The modal domain optical fiber sensor is composed of five primary components:

1. Laser light source
2. Lead-in fiber section
3. Fiber sensing section
4. Lead-out fiber section
5. Detection electronics.

In the analysis presented here, the input to the sensor is the strain induced in the core and cladding of the sensing-section fiber, and the sensor's output is the electrical signal produced by the detection electronics. The intensity pattern produced at the output of the sensing-section fiber is referred to as the sensor's optical output.

The laser provides coherent light for the sensor, and is assumed to provide monochromatic light at a single frequency. The effects of the laser light source on the electromagnetic waves propagating in an optical fiber depend on the wavelength of the light and the conditions under which the light is launched into

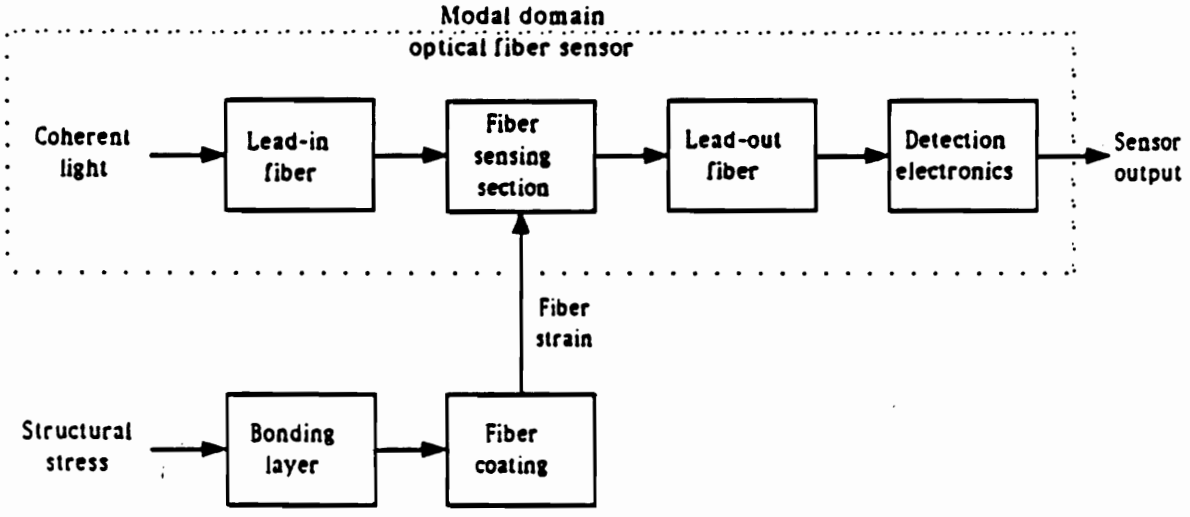

Figure 2.1.1. Modal domain optical fiber sensor attached to a structure.

the fiber, called the launch conditions. The launch conditions correspond to boundary conditions for Maxwell's equations governing the propagation of light in the fiber, and determine the distribution of optical power between the electromagnetic modes excited in the optical fiber [29]. In the modal domain optical fiber sensor, the launch conditions depend on the frequency and wavelength of the laser and the alignment between the lead-in, and sensing-section fibers.

The practical implementation of the modal domain optical fiber sensor employs three sections of optical fiber: a sensing section, and lead-in and lead-out sections [17]. The lead-in fiber serves as a conduit for the transfer of optical power to the sensor's sensing section and eliminates the need to place the coherent light source at the measurement site. The parameters of the sensor's sensing-section fiber are chosen such that light at the wavelength of the laser source excites the propagation of two electromagnetic modes in the fiber. The two electromagnetic modes propagating in the sensing-section fiber generate a standing interference pattern that changes in a predictable manner when the fiber is subject to strain along its length. This intensity pattern is monitored at the output of the sensing section and constitutes the sensor's optical output. The length of the sensing section is called the sensor's gauge length. The lead-out fiber carries the sensor's optical output to the detection electronics. The parameters of the optical fibers employed in the lead-in and lead-out sections of the sensor are chosen so that they are insensitive to the quantity being measured.

The configuration of the modal domain optical fiber sensor considered in this research was proposed by Layton and Bucaro [30], and employed circular-core fiber in the sensing section. Current sensor configurations employ elliptical-core (e-core) fiber to improve the stability of the intensity distribution monitored at the endface of the sensing-section fiber [17,31]. The use of e-core fiber, however, complicates the analysis of the electromagnetic modes propagating in the fiber because there are no closed-form solutions to Maxwell's equations for elliptical-core waveguides. In the analysis presented here, the elliptical cross-section of the sensing-section fiber's core is approximated by a circular core to simplify the analysis. This approximation is widely used and is sufficient for this analysis. Recent advances in the theory of elliptical-core waveguides [32] suggest that this analysis can be extended to sensors employing e-core fiber.

The detection electronics convert the sensor's optical output into an electrical signal. A photodetector converts the intensity pattern monitored at the endface of the sensing-section fiber into an electrical signal. Additional signal processing is often employed to convert the photodetector output into a form compatible with the particular sensor application, and may be either analog or discrete depending on the sensor configuration.

2.1.2. Sensor operating configurations

For the measurement of structural strain, the modal domain optical fiber sensor can be operated in two configurations:

1. Analog configuration
2. Fringe-counting configuration.

The two operating configurations are defined by the type of signal processing employed in the sensor's detection electronics - the analog sensor configuration uses of analog detection electronics, and the fringe counting configuration employs discrete electronics.

In both the analog configuration and the fringe-counting configuration, the output of the photodetector employed in the detection electronics is a signal of the form

$$y_d(\bar{\epsilon}) = \bar{I}_1(\bar{\epsilon}) + \bar{I}_2(\bar{\epsilon}) \sin\left(\Gamma(\bar{\epsilon}) \right), \tag{2.1.1}$$

where $\bar{\epsilon}$ denotes dependence on the strain in the sensing section fiber - the exact form of this equation is described in Section 2.2. In the analog configuration, the sensor output is proportional to the output of the photodetector. For strain such that

$$\sin\left(\Gamma(\bar{\epsilon}) \right) \simeq \Gamma(\bar{\epsilon}), \tag{2.1.2}$$

and the sensor is said to be operating in its linear range. The analog configuration is typically used when the strain in the sensor satisfies (2.1.2); hence, the analog

configuration is often referred to as the sensor's "linear range" configuration.

As the strain in the sensor increases, the signal produced by the photodetector will vary in a roughly sinusoidal nature as a function of $\Gamma(\bar{\epsilon})$. A 2π radian change in Γ is called a fringe, and when Γ changes by

$$\Delta\Gamma = 2n\pi \tag{2.1.3}$$

the sensor output is said to have gone through n fringes. For values of strain such that the sensor output becomes sinusoidal, discrete detection electronics are employed to monitor the Γ by count fringes [17,33]. Sensor configurations that employ this type of discrete detection electronics are referred to as fringe-counting configurations.

2.2. MODEL DEVELOPMENT

This section describes the development of a mathematical model of the effects of arbitrary strain in the sensing-section fiber on the output of a modal domain optical fiber sensor. An optical fiber mounted on the surface of, or embedded in, a structure inherits the characteristics of the stress and strain in the structure. By propagating coherent light through the optical fiber and monitoring an appropriate optical output information is obtained about the strain in the optical fiber, which can be used to infer information about the stress and strain in the structure.

In modeling the effects of applied stress on the output of the sensor, the following issues must be taken into account [18]:

1. The optical interrogation of the fiber.
2. The transfer of stress between the structure and the sensor.
3. The effects of strain on the propagation of light in the sensor.
4. The conversion of the sensor's optical output into an electrical signal.

Each of these issues is accounted for in the development of the sensor model described below. In addition, the effects of strain in the lead-in and lead-out fibers on the sensor output are also considered.

2.2.1. Optical interrogation of the fiber

Under certain conditions that depend on the wavelength of the laser light source, the geometry and dimensions of the fiber core, and the indices of refraction of the fiber core and cladding, the optical fiber acts as an electromagnetic waveguide [34]. When the fiber parameters and the laser wavelength are such that the fiber can be considered weakly guiding [35], the solutions to Maxwell's equations for the light propagating in the fiber can be described as a linear combination of electromagnetic modes known as Linearly Polarized, or LP modes.

The wavelength of the laser source and the parameters of the optical fiber used in the sensor's sensing section are chosen so that two modes, the LP_{01} and LP_{11}, propagate in the fiber. These modes have different propagation constants, $\beta_{\ell m}$, interfere with each other, and generate an intensity pattern along the length of the fiber of the form

$$I_f(r,\theta,z\ ;\ a,\lambda,n_{co},n_{cl},\beta_{\ell m}) = I_1(r,\theta\ ;\ a,\lambda,n_i,\beta_{\ell m}) + I_2(r,\theta\ ;\ a,\lambda,n_i,\beta_{\ell m})\cos(\ \Gamma(z;a,\lambda,n_i,\beta_{\ell m}))\ , \qquad (2.2.1)$$

where Γ denotes the relative phase shift between the modes over the sensor gauge length and (r,θ,z) denotes the cylindrical coordinates of a point in the fiber core. Equation (2.2.1) is written in a form which emphasizes the dependence of I_f on the sensor parameters - the fiber core radius, a, the laser wavelength, λ, the indices of refraction of the fiber core and cladding, n_i - and the solutions to the propagation constants $\beta_{\ell m}$, which depend on the solutions to the waveguide characteristic equation [34].

2.2.2. Strain transfer

Figure 2.1.1 shows the modal domain optical fiber sensor attached to a structure. Strain is induced in the sensor through the mechanical attachment of the sensing-section fiber to the structure. The stress transferred from the structure to the sensor depends on the way in which the sensor is attached to the structure and the mechanical properties of any adhesives or fiber coatings [36-37].

In this analysis, the strain induced in the sensing-section fiber is considered the sensor input; the effects of fiber coatings, adhesives, and the manner in which the sensor is attached to the test article can be modeled separately.

In this analysis it is assumed that, from a mechanical point of view, the optical fiber behaves like a linear homogeneous isotropic material. The strain at a point in the fiber is described by a tensor, which can be represented by the a vector of the form:

$$\bar{\epsilon} = \begin{bmatrix} \epsilon_1 \\ \epsilon_2 \\ \epsilon_3 \\ \epsilon_4 \\ \epsilon_5 \\ \epsilon_6 \end{bmatrix} = \begin{bmatrix} \epsilon_z \\ \epsilon_x \\ \epsilon_y \\ \gamma_{xy} \\ \gamma_{yz} \\ \gamma_{zx} \end{bmatrix}. \tag{2.2.2}$$

In the tensor $\bar{\epsilon}$, the elements ϵ_z, ϵ_x, and ϵ_y denote normal strains in the directions of the $z, x,$ and y axes in Cartesian coordinates, and the elements γ_{xy}, γ_{yz}, and γ_{zx} denote shear strains.

The effects of strain on light propagating in an optical material depend primarily on the normal strain in directions perpendicular to or in the direction of the propagation of light in the material; hence, the strain in the sensor's sensing-section fiber is typically represented in a coordinate system defined with respect to the fiber's longitudinal axis. The direction of propagation of light through the fiber is referred to as the fiber's longitudinal axis, or simply the axial direction, and the directions perpendicular to the fiber's longitudinal axis are referred to as transverse. Local, fiber-based Cartesian and cylindrical coordinate systems are defined such that their respective positive z-directions are aligned with the fiber's longitudinal axis at each point along the sensor gauge length.

2.2.3. Strain-optic interaction

The intensity pattern generated by the interference of the electromagnetic modes propagating in the sensing section of the modal domain optical fiber sensor depends on the wavelength of the laser source, the radius of the fiber core, the indices of refraction of the fiber core and cladding. Strain-induced changes in the interference pattern and the sensor gauge length combine to alter the intensity monitored at the endface of the sensor's sensing section.

When an optical fiber is subjected to mechanical stress, the strain induced in the fiber is related to changes in the dimensions of the fiber core and cladding, and the sensor gauge length. In this analysis the fiber core is assumed to remain approximately circular with radius equal to the average strained core radius. The sensor gauge length changes by an amount given by

$$\Delta L(\bar{\epsilon}) = \int_S \epsilon_z(s)\, ds \tag{2.3.3}$$

where S denotes the fiber path on the structure and ϵ_z denotes the normal strain in the direction of the fiber's longitudinal axis at the point $s \in S$. The indices of refraction of the fiber core and cladding change as a result of the photoelastic effect [38]. The wavelength of the laser source is unaffected by strain in the fiber.

Strain-induced changes in the sensor parameters affect the solutions to the waveguide characteristic equation, and hence affect the propagation constants of the LP modes in the fiber. Including the dependence of the sensor parameters and the propagation constants of the LP modes on the strain in the sensor, the expression for the intensity pattern monitored at the endface of the sensing section becomes

$$\begin{aligned} I_f(r,\theta,z_f(\bar{\epsilon})\ ;\ a(\bar{\epsilon}),\lambda,n_i(\bar{\epsilon}),\beta_{\ell m}(\bar{\epsilon})) = I_1(r,\theta\ ;\ a(\bar{\epsilon}),\lambda,n_i(\bar{\epsilon}),\beta_{\ell m}(\bar{\epsilon})) + \\ I_2(r,\theta\ ;\ a(\bar{\epsilon}),\lambda,n_i(\bar{\epsilon}),\beta_{\ell m}(\bar{\epsilon}))\cos(\ \Gamma(z_f(\bar{\epsilon});a(\bar{\epsilon}),\lambda,n_i(\bar{\epsilon}),\beta_{\ell m}(\bar{\epsilon}))\ )\ , \end{aligned} \tag{2.2.4}$$

where $z = z_f(\bar{\epsilon})$ denotes the strained position of the fiber endface.

2.2.4. The effects of lead-in and lead-out strain

The parameters of the lead-in and lead-out fibers are chosen such that for light at the wavelength of the laser source, the lead-in and lead-out fibers support only one LP mode. Strain in the lead-in fiber affects the amplitude and phase of the light entering the sensing section, and has the same effect on both of the LP modes propagating in the sensing section. The interference pattern monitored at the endface of the sensing-section fiber depends on the relative phase difference between the two LP modes; therefore, phase changes induced by lead-in fiber strain have no effect on the sensor output. Strain-induced changes in the

magnitude of the light launched into the sensing section are the result of strain-induced losses in the lead-in fiber and their effect on the sensor output is typically assumed to be small compared to the effect of strain in the sensing section. The effect, on the sensor output, of strain in the lead-out fiber is similar to the effect of strain in the lead-in fiber, and is typically ignored.

2.2.5. Electro-optical conversion

For operation in the sensor's analog configuration, the sensor output is proportional to the output of the photodetector. Assuming that the dynamics of the photodetector can be neglected, the sensor output is given by Equation (2.1.1) where $\bar{I}_1$ and $\bar{I}_2$ denote the spatial integrals of I_1 and I_2 over the area monitored by the photodetector. For operation in the sensor's fringe-counting configuration, the output of the sensor's discrete detection electronics corresponds to an estimate of the relative phase difference difference between the two LP modes and is given by

$$y_d(\bar{\epsilon}) = K_d\, \Gamma(\, z_f(\bar{\epsilon})\, ;\, \bar{\epsilon}\,) \quad . \tag{2.2.5}$$

The effects of nonideal detection electronics can be modelled and added to the sensor model.

2.3. SENSOR MODELS

This section describes three sensor models based on the expression given in Equation (2.2.4) for the intensity pattern generated by the interference of the LP_{01} and LP_{11} modes propagating in the sensor's sensing section. The simulation model includes all of the effects of strain on the sensor output indicated in Equation (2.2.4). The nonlinear and linear design models are approximations of the simulation model that are more useful for system theoretic analysis and design.

2.3.1. Simulation model

The sensor output predicted by the simulation model is given by I_f in Equation (2.2.4). The output predicted by the simulation model depends on the effects of strain-induced changes in the fiber core radius, the indices of refraction of the fiber core and cladding, the sensor gauge length, and the solutions to the waveguide characteristic equation.

The sensor operating point, or Q-point, is typically chosen so that the expression for the intensity monitored at the endface of the sensing section fiber becomes

$$I_f(\bar{\epsilon}) = I_1(\bar{\epsilon}) + I_2(\bar{\epsilon}) \sin (\Gamma(\bar{\epsilon}) - \Gamma_0) , \tag{2.3.1}$$

where Γ_0 denotes the nominal value of $\Gamma(\bar{\epsilon})$. The strain-induced relative phase shift between the two LP modes propagating in the sensor's sensing section, over the sensor gauge length, is given by

$$\Gamma(\bar{\epsilon}) = \int_S \Delta\beta(\bar{\epsilon}(s)) (1 + \epsilon_1(s)) \, ds , \tag{2.3.2}$$

[28], where $\Delta\beta$ denotes the difference between the propagation constants of the two LP modes. In Equation (2.3.2), S denotes the path of the fiber in or on the test article, $\bar{\epsilon}(s)$ denotes the strain tensor at the point s, and ϵ_1 denotes the component of the strain in the direction of fiber's longitudinal axis. In order to simplify notation, the explicit dependence of $\bar{\epsilon}$ on s is dropped with the understanding that $\bar{\epsilon}$ denotes the representation of the strain tensor in the local coordinate system of the fiber sensor.

2.3.2. Design model

In the expression for the intensity pattern monitored at the endface of the sensing-section fiber, I_1, I_2, and Γ all depend on the solutions to the waveguide characteristic equation for each value of $\bar{\epsilon}$ [18]. Because of this dependence on the solutions to the waveguide characteristic equation, the simulation model does not provide closed-form description of the effects of strain on the sensor output. In order to be useful for system analysis and design, however, the sensor model should provide a closed-form expression for the sensor output applications.

Therefore, in order to develop a sensor model that does not depend on the exact solutions to the waveguide characteristic equation for each value of $\bar{\epsilon}$, the terms $I_1(\bar{\epsilon})$, $I_2(\bar{\epsilon})$, and $\Gamma(\bar{\epsilon})$ in Equation (2.3.1) must be replaced with suitable approximations.

The strain-induced modal phase shift is approximated by linearizing $\Gamma(\bar{\epsilon})$ about some nominal strain distribution represented by $\bar{\epsilon}^0$. Expanding the integrand in Equation (2.3.2) in a Taylor series about $\bar{\epsilon} = \bar{\epsilon}^0$ yields

$$\Delta\beta(\bar{\epsilon})(1+\epsilon_1) = \Delta\beta(\bar{\epsilon}^0)(1+\epsilon_1) \; + \; \sum_{j=1}^{6} \frac{\partial \Delta\beta(\bar{\epsilon}^0)}{\partial \epsilon_j} (1+\epsilon_1^0)(\epsilon_j - \epsilon_j^0) \; + (\text{h.o.t.}), \quad (2.3.3)$$

where ϵ_j^0 denotes the j-th element of the strain tensor $\bar{\epsilon}^0$, and "h.o.t." denotes higher order terms involving products of elements of the strain tensors of the form $\epsilon_j^n \epsilon_k^m$ with $n+m > 1$. Ignoring the effects of the higher order terms in Equation (2.3.3), $\Gamma(\bar{\epsilon})$ is approximately equal to

$$\tilde{\Gamma}(\bar{\epsilon}) \triangleq \int_S \left\{ \Delta\beta(\bar{\epsilon}^0)(1+\epsilon_1) \; + \sum_{j=1}^{6} \frac{\partial \Delta\beta(\bar{\epsilon}^0)}{\partial \epsilon_j} (1+\epsilon_1^0)(\epsilon_j - \epsilon_j^0) \right\} ds \; . \quad (2.3.4)$$

This approximation of $\Gamma(\bar{\epsilon})$ does not depend on the solutions of the waveguide characteristic equation for each value of $\bar{\epsilon}$. It depends on the nominal difference between the propagation constants, $\Delta\beta(\bar{\epsilon}^0)$, and the first partial derivatives of $\Delta\beta(\bar{\epsilon}^0)$ with respect to the elements of the strain tensor [38].

The terms $I_1(\bar{\epsilon})$ and $I_2(\bar{\epsilon})$ in the simulation model also depend on the solutions to the waveguide characteristic equation. Simulations of the effects of strain on the sensor output predicted by the simulation model indicate that the strain-induced changes in I_1 and I_2 are several orders of magnitude smaller than the corresponding changes in Γ, and can be approximated by their respective nominal values. This leads to the following approximation of the sensor output predicted by the simulation model:

$$\tilde{I}_f(\bar{\epsilon}) \triangleq I_1(\bar{\epsilon}^0) \; + \; I_2(\bar{\epsilon}^0) \sin\left(\tilde{\Gamma}(\bar{\epsilon}) - \tilde{\Gamma}_0 \right), \quad (2.3.5)$$

where $\tilde{\Gamma}_0 = \Gamma_0$. Equation (2.3.5) is referred to as the design model of the modal domain optical fiber sensor.

2.3.3. Linear design model

Although the design model does not depend on the exact solutions of the waveguide characteristic equation for each value of the strain tensor $\bar{\epsilon}$, it does contain a sinusoidal nonlinearity which may be undesirable in many applications. For small values of strain, such as those typically associated with operation in the sensor's linear range,

$$\sin\left(\tilde{\Gamma}(\bar{\epsilon}) - \tilde{\Gamma}_0\right) \approx \left(\tilde{\Gamma}(\bar{\epsilon}) - \tilde{\Gamma}_0\right). \tag{2.3.6}$$

Therefore, the sensor output can be approximated by

$$\tilde{I}_{f_l}(\bar{\epsilon}) = I_1(\bar{\epsilon}^0) + I_2(\bar{\epsilon}^0)\left(\tilde{\Gamma}(\bar{\epsilon}) - \Gamma(\bar{\epsilon}^0)\right). \tag{2.3.7}$$

Equation (2.3.7) is referred to as the linear sensor model.

2.4. SENSOR RESPONSE CHARACTERIZATION

This section, described the characterization of the response of the modal domain optical fiber sensor to strain in terms of the sensor's sensitivity and dynamic range. Because the sensor output is a function of a tensor quantity, traditional notions of sensitivity and dynamic range lead to characterizations of the sensor response in terms of tensor quantities. For special classes of applied strain, however, it is possible to derive scalar expressions for the sensor sensitivity and dynamic range.

2.4.1. Parametric strain

The strain tensor $\bar{\epsilon}$ is said to represent parametric strain if each element of the strain tensor can be expressed as function of some single scalar variable; that is, there exists scalar functions f_j and a scalar parameter ϵ such that

$$\epsilon_j = f_j(\epsilon), \tag{2.4.1}$$

for $j = 1, 2, \ldots, 6$, and the complete strain tensor has the form given in Equation (2.2.2).

If an optical fiber is subject to an applied force that generates a uniaxial normal stress σ at an angle θ with respect to the fiber's longitudinal axis, then the strain induced in the fiber is given by

$$\bar{\epsilon} = \begin{bmatrix} \epsilon\,(\,\cos^2\theta - \nu\,\sin^2\theta\,) \\ \epsilon\,(\,\sin^2\theta - \nu\,\cos^2\theta\,) \\ -\nu\epsilon \\ -\epsilon\,(1-\nu)\,\sin 2\theta\,/\,2 \\ 0 \\ 0 \end{bmatrix}, \tag{2.4.2}$$

where ϵ depends on the mechanical properties of the fiber and the magnitude of the applied force [39]. This type of strain is called planar parametric strain, since it results from an applied normal stress acting in a plane containing the fiber's longitudinal axis.

Of particular interest are two special types of planar parametric strain. Axial parametric strain is produced by normal stress in the direction of the fiber's longitudinal axis, and has the representation in terms of the fiber's local coordinate system given by Equation (2.4.2) with $\theta = 0$. Transverse parametric strain is produced by normal stress perpendicular to the fiber's longitudinal axis, and is described by tensors of the form given in Equation (2.4.2) with $\theta = \pi/2$. Both of these types of parametric strain are illustrated in Figure 2.4.1.

2.4.2. Sensor sensitivity

Sensor sensitivity is traditionally defined as the slope of the sensor response, or some linear approximation of the sensor response, at the sensor Q-point. The input to the modal domain optical fiber sensor, however, is a tensor quantity - the strain in the sensing-section fiber. Therefore, applying the traditional definition of sensitivity to the modal domain optical fiber sensor, the sensor sensitivity is a tensor quantity with elements

Axial strain

(a)

Transverse strain

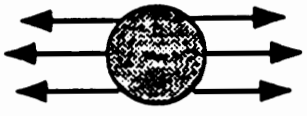

(b)

Figure 2.4.1. Applied stress configurations resulting in planar parametric strain.

$$\Delta\tilde{\beta} = \Delta\beta_0 \frac{\partial\epsilon_1^0}{\partial\epsilon} + (1+\epsilon_1^0)\sum_{j=1}^{6} \frac{\partial\Delta\beta_0}{\partial\epsilon_j}\frac{\partial\epsilon_j^0}{\partial\epsilon}\,, \tag{2.4.7}$$

and $\Delta\beta_0$ denotes the nominal difference between the propagation constants of the two LP modes. Substituting Equation (2.4.6) into the approximate expression for the sensor sensitivity yields

$$S_Q = I_2(\bar{\epsilon}^0) \int_S \Delta\tilde{\beta}\ ds. \tag{2.4.8}$$

Equation (2.4.8) shows that the sensor sensitivity depends on the Q-point values of I_2 and $\Delta\tilde{\beta}$, and the sensor orientation - determined by the path S. The effects of variations in the sensor parameters and sensor orientation on sensor sensitivity are discussed in Chapter 5.

2.4.3. Dynamic range

The sensor's dynamic range is defined as the range of strain over which the deviation of the sensor output from the output predicted by the linear design model is less than some maximum allowable value; hence, the terms dynamic range and linear range are used interchangeably. Let

$$e_l(\bar{\epsilon}) \triangleq \frac{\tilde{I}_{f_l}(\bar{\epsilon}) - I_f(\bar{\epsilon})}{I_f(\bar{\epsilon}) - I_f(\bar{\epsilon}^0)}\,, \tag{2.4.9}$$

be defined as the linear model error, where I_f represents the actual sensor output, and $\tilde{I}_{f_l}$ denotes the sensor output predicted by the linear design model. The sensor's linear range is defined with respect to some maximum allowable error, e_{max}, as the set of all $\bar{\epsilon}$, such that

$$\left| e_l(\bar{\epsilon}) \right| \leq e_{max}\,. \tag{2.4.10}$$

The dynamic range of the sensor as defined by Equation (2.4.10) corresponds to a region in a six-dimensional space defined by the allowable elements of the strain tensor; therefore, interpreting the relationship between the sensor's dynamic range and sensor operation is difficult. As in the

$$\bar{S}_{Q_j} = \left.\frac{\partial I_f(\bar{\epsilon})}{\partial \epsilon_j}\right|_{\bar{\epsilon}=\bar{\epsilon}^0} , \tag{2.4.3}$$

where $\bar{\epsilon}^0$ denotes the Q-point strain. Each element of the tensor $\bar{S}_Q$ denotes the sensitivity of the sensor output with respect to the corresponding element of strain tensor.

Unfortunately, the sensitivity tensor $\bar{S}_Q$ does not provide the same intuitive understanding of the sensor behavior normally associated with the sensor sensitivity. When the strain in the sensor is parametric, however, each element of the strain tensor is a function of the same scalar parameter, and the sensitivity can be defined as a weighted sum of the elements of the tensor $\bar{S}_Q$:

$$\begin{aligned} S_Q &\triangleq \sum_{j=1}^{6} \left.\frac{\partial I_f}{\partial \epsilon_j}\frac{\partial \epsilon_j}{\partial \epsilon}\right|_{\bar{\epsilon}=\bar{\epsilon}^0} \\ &= \left.\frac{dI_f(\bar{\epsilon})}{d\epsilon}\right|_{\bar{\epsilon}=\bar{\epsilon}^0} . \end{aligned} \tag{2.4.4}$$

The scalar quantity S_Q in Equation (2.4.4) depends on the type of parametric strain in the sensor through the partial derivatives of the elements of the strain tensor with respect to the scalar parameter, ϵ.

In order to derive a closed-form expression for S_Q in Equation (2.4.4), I_f can be approximated by $\tilde{I}_f$, the sensor output predicted by the design mode; so that,

$$\begin{aligned} S_Q &\approx \frac{d}{d\epsilon}\left.\tilde{I}_f(\bar{\epsilon})\right|_{\bar{\epsilon}=\bar{\epsilon}^0} \\ &= I_2(\bar{\epsilon}^0)\ \left.\frac{d}{d\epsilon}\tilde{\Gamma}(\bar{\epsilon})\right|_{\bar{\epsilon}=\bar{\epsilon}^0} . \end{aligned} \tag{2.4.5}$$

From the definition of $\tilde{\Gamma}$,

$$\left.\frac{d\tilde{\Gamma}(\bar{\epsilon})}{d\epsilon}\right|_{\bar{\epsilon}=\bar{\epsilon}^0} = \int_S \Delta\tilde{\beta}\ ds , \tag{2.4.6}$$

where

characterization of the sensor sensitivity, however, the sensor's linear range can be defined in terms of the sensor's response to parametric strain. The dynamic range can then be described in terms of bounds on some scalar strain parameter.

In order to develop a closed-form expression for e_l, the sensor output I_f in Equation (2.4.10) can be approximated by the output predicted by $\tilde{I}_f$, which yields

$$e_l(\bar{\epsilon}) \approx \frac{\tilde{I}_{f_l}(\bar{\epsilon}) - \tilde{I}_f(\bar{\epsilon})}{\tilde{I}_f(\bar{\epsilon}) - \tilde{I}_f(\bar{\epsilon}^0)} = \frac{\tilde{\Gamma}(\bar{\epsilon})}{\sin\left(\tilde{\Gamma}(\bar{\epsilon})\right)} - 1 \; . \tag{2.4.11}$$

For a straight section of optical fiber subject to uniform parametric strain, the linear model error can be expressed as the following function of the strain parameter, ϵ:

$$e_l(\epsilon) = \frac{\Delta\tilde{\beta}\epsilon L}{\sin\left(\Delta\tilde{\beta}\epsilon L\right)} - 1 \; . \tag{2.4.12}$$

Figure 2.4.2 shows the percent linear model error ($100 \times e_l$) as a function of the strain-induced relative phase shift between the LP modes in the fiber ($\tilde{\Gamma}(\epsilon) = \Delta\tilde{\beta}\epsilon L$).

The relationship between e_l and $\tilde{\Gamma}$ in Figure 2.4.2 is independent of the sensor parameters and the type of parametric strain in the sensor. For a particular value of the e_{max} Figure 2.4.2 shows the maximum allowable value for $\tilde{\Gamma}$, from which the corresponding allowable range of strain can be calculated. For a straight section of optical fiber subject to planar parametric strain, the sensor's linear range corresponds to the set

$$\mathcal{L} = \left\{ \epsilon : |\epsilon| \leq \epsilon_{max} = \tilde{\Gamma}_{max} \,/\, \Delta\tilde{\beta}L \right\} . \tag{2.4.13}$$

Table 2.4.1 shows the maximum values of ϵ for axial and transverse parametric strain, for several different values of e_{max}.

2.5. SUMMARY

This chapter described the derivation of mathematical models of the effects of arbitrary strain on the output of a modal domain optical fiber sensor. The response of the sensor to parametric strain was characterized in terms of the

Table 2.4.1. Sensor linear range for axial and transverse parametric strain for different maximum acceptable values of the percent linear model error.

error	Linear range (μ-strain)	
	Axial	Transverse
5 %	±33.4	±44.4
10 %	±42.3	±56.3
15 %	±48.7	±64.7
20 %	±53.8	±71.4

sensor's sensitivity and dynamic range.

The sensor's sensitivity and dynamic range both depend on the sensor gauge length and the quantity $\Delta\tilde{\beta}$. The term $\Delta\tilde{\beta}$ is a function of the difference in the propagation constants of the two LP modes propagating in the sensor's sensing section, and the difference in their respective partial derivatives with respect to the elements of the strain tensor in the fiber.

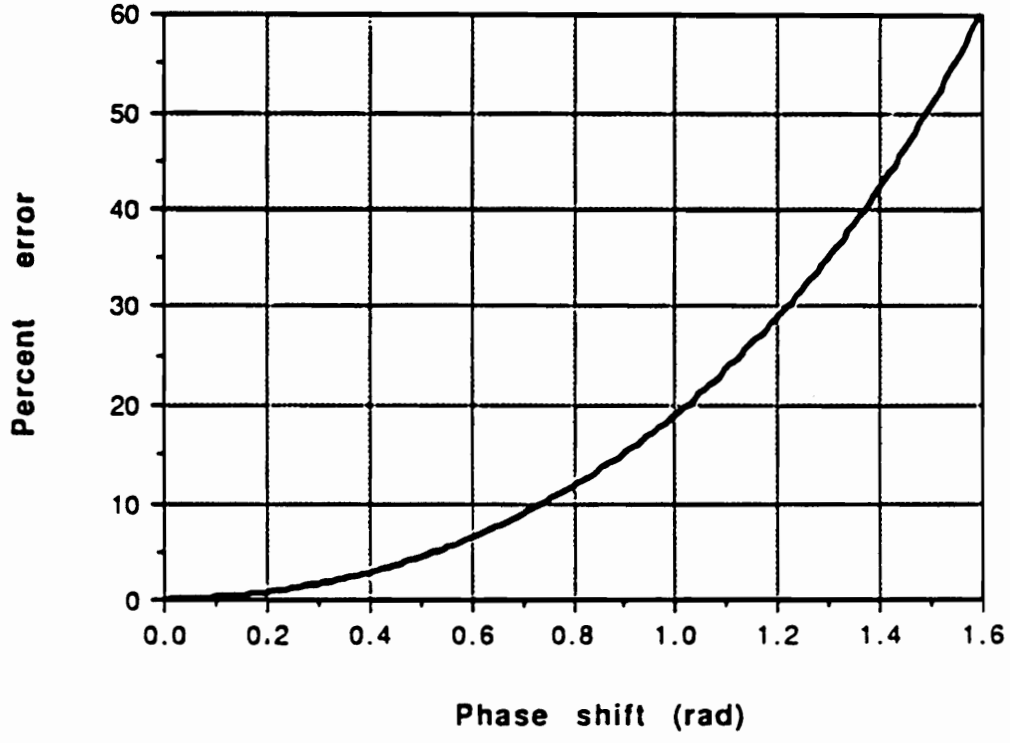

Figure 2.4.2. Percent linear model error versus strain-induced modal phase difference.

3. Flexible structure example

This chapter describes a mathematical model for a simple flexible structure - a cantilevered beam. This model is used in several examples throughout this dissertation. The numerical values used in this model correspond to the parameter values for a flexible beam experiment constructed at Virginia Tech [24].

Section 3.1 describes the mathematical model of the cantilevered beam. Section 3.2 describes the integration of the modal domain optical fiber sensor model into the model of the flexible structure.

3.1. FLEXIBLE BEAM MODEL

Figure 3.1.1 shows a cantilevered beam subject to an arbitrary distributed force, $f(z,t)$. For small deflections, the displacement of a thin flexible beam from equilibrium is described by the Bernoulli-Euler beam equation:

$$\frac{\partial^2}{\partial z^2}\left[\mathrm{E\ I}(z)\frac{\partial^2 w(z,t)}{\partial z^2}\right] + \frac{\rho(z)}{A(z)}\frac{\partial^2 w(z,t)}{\partial t^2} = f(z,t)\ , \tag{3.1.1}$$

subject to the boundary conditions:

$$\begin{aligned} &w(0,t) = 0, && \frac{\partial w(0,t)}{\partial z} = 0 && \text{(clamped end)} \\ &\frac{\partial^2 w(l,t)}{\partial^2 z} = 0, && \frac{\partial^3 w(l,t)}{\partial^3 z} = 0 && \text{(free end)}\ , \end{aligned} \tag{3.1.2}$$

for $0 \le z \le l$ and $t \ge 0$, where $w(z,t)$ denotes the displacement of the beam, and $f(z,t)$ denotes external forces acting on the beam. The parameter values used in the numerical examples presented in this dissertation were derived from a flexible beam experiment constructed at Virginia Tech and are listed in Table 3.1.1 [24].

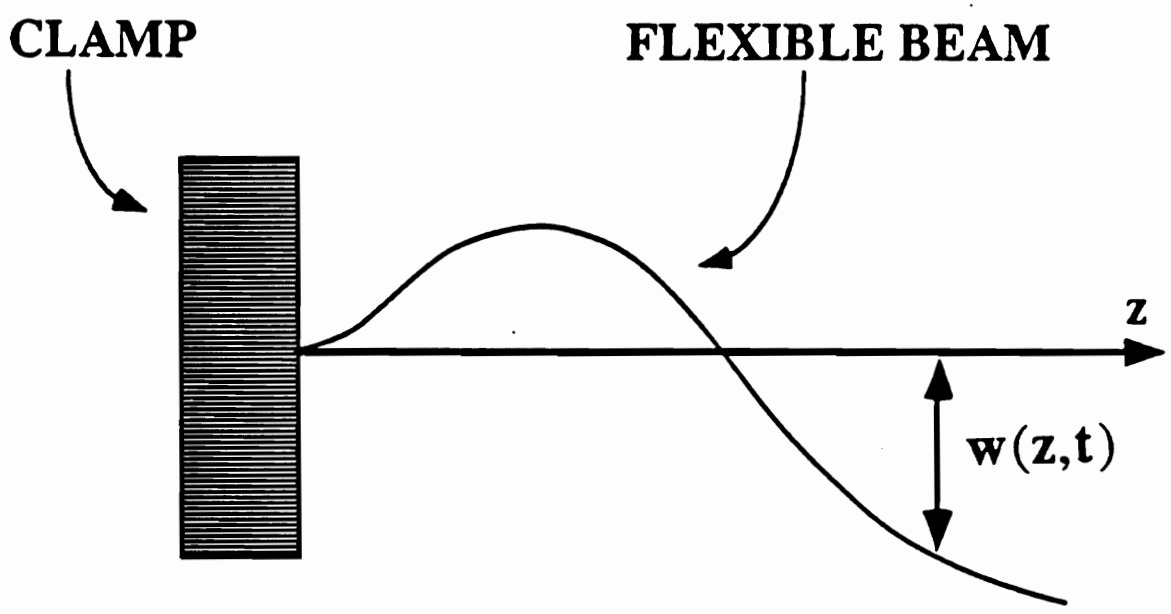

Figure 3.1.1 Flexible cantilevered beam.

Table 3.1.1 Cantilevered beam parameter values [24].

Beam material	Steel
Young's modulus, E_b	200 GPa
Density, ρ	7860 Kg/m^3
Length, l	0.614 m
Height, h_b	0.05 m
Thickness, t_b	0.74 mm
Piezo height, h_p	0.0317 m
Fiber end points:	
f^-	0.0 m
f^+	0.566 m
Piezo end points:	
p^-	0.012 m
p^+	0.05 m

The set of points, $\Omega = \{z \mid 0 \le z \le l\}$, over which the structural model in (3.1.1) is defined is referred to as the structural domain. The displacement $w(z,t)$ describes the shape of the structure as a function of time. For structures such as the cantilevered beam, there exists a set of functions $\{\phi_j(z)\}$ which form an orthonormal basis for the set of all square-integrable functions defined on Ω [40]; hence, at any time t, there exists a set of weights $\{\eta_j(t)\}$ such that

$$w(z,t) = \sum_{j=1}^{\infty} \eta_j(t)\phi_j(z). \tag{3.1.3}$$

The basis functions $\{\phi_j(z)\}$ are commonly referred to as mode shapes, and the time varying functions $\{\eta_j(t)\}$ are called modal amplitudes or weights. For the cantilevered beam, the mode shapes are given by

$$\phi_j(z) = \frac{1}{\sqrt{l}}\{\ \cos(\beta_j z) - \cosh(\beta_j z) - e_j[\ \sin(\beta_j z) - \sinh(\beta_j z)\ ]\ \}\ , \tag{3.1.4}$$

where

$$e_j = \frac{\cos(\beta_j l) + \cosh(\beta_j l)}{\sin(\beta_j l) + \sinh(\beta_j l)}\ , \tag{3.1.5}$$

and β_j is the j-th solution to the characteristic equation for the structure:

$$1 + \cos(\beta_j l)\cosh(\beta_j l) = 0\ . \tag{3.1.6}$$

Figure 3.1.2 shows a plot of the first five mode shapes for the cantilevered beam, $\phi_j(z), j = 1,\ldots,5$.

For structures such as cantilevered and simply supported beams, the second derivatives of the mode shapes, $\{\phi_j''(z)\}$, are also orthogonal, and are normalized by scaling each mode shape by $1/\beta_j^2$. Figure 3.1.3 shows the second derivatives of the first five mode shapes.

For computational purposes the infinite series (3.1.6) is typically truncated to a finite number of modes, N, so that

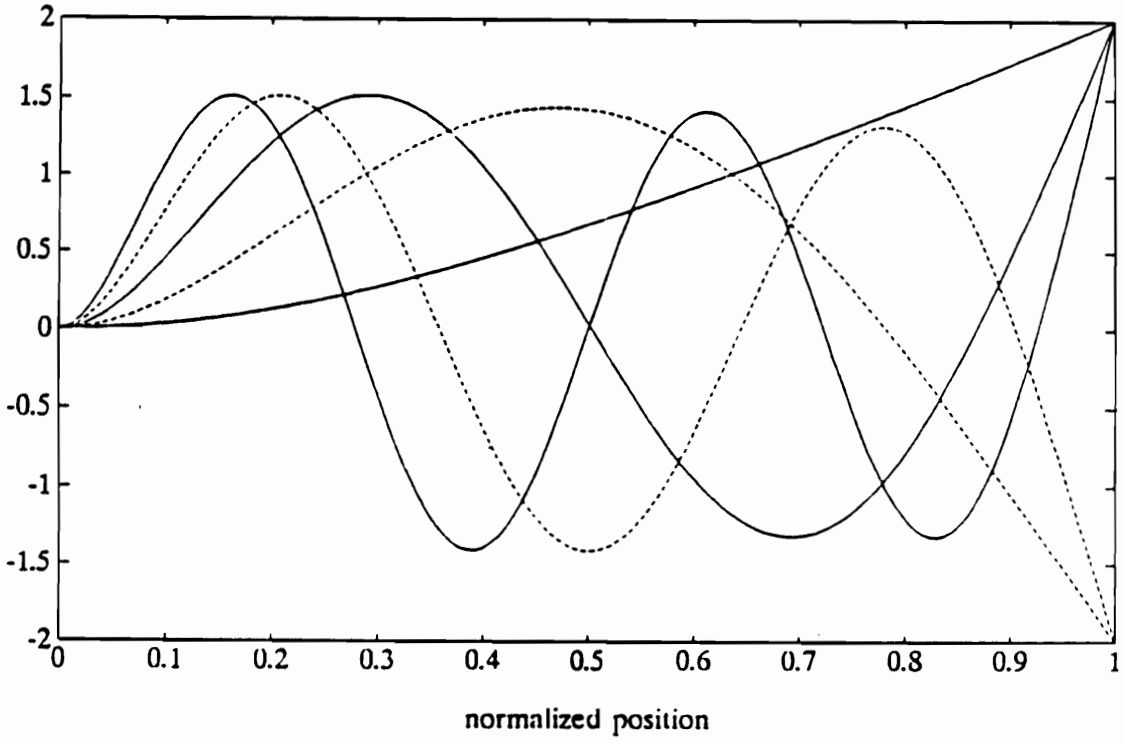

Figure 3.1.2 Mode shapes for a cantilevered beam.

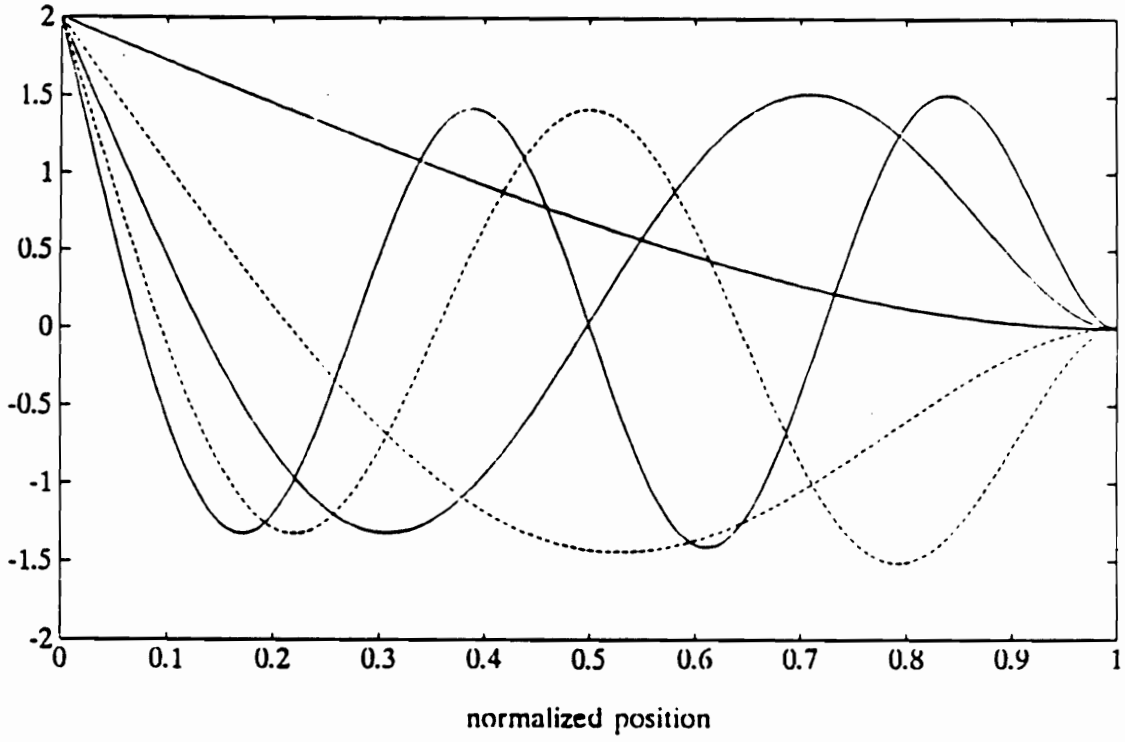

Figure 3.1.3 Second derivatives of the mode shapes for a cantilevered beam.

$$w(z,t)=\sum_{j=1}^{N}\eta_j(t)\phi_j(z). \tag{3.1.7}$$

For many flexible structure models the number of modes, N, required to provide an acceptable approximation of the shape $w(z,t)$ may be very large. The finite-dimensional approximation of $w(z,t)$ in Equation (3.1.7) leads to a reduced order model of the structure of the form

$$\ddot{\eta}(t)+2\zeta\Lambda^{1/2}\dot{\eta}(t)+\Lambda\eta(t)=Qu(t), \tag{3.1.8}$$

where vector $\eta(t)$ is defined as

$$\eta(t)=[\ \eta_1(t)\ \eta_2(t)\cdots\eta_N(t)]^{\mathrm{T}}\ , \tag{3.1.9}$$

and the matrices Λ and ζ are given by

$$\Lambda=\begin{bmatrix}\omega_1^2 & 0 & 0\\ 0 & \ddots & 0\\ 0 & 0 & \omega_N^2\end{bmatrix}, \tag{3.1.10}$$

and

$$\zeta=\begin{bmatrix}\zeta_1 & 0 & 0\\ 0 & \ddots & 0\\ 0 & 0 & \zeta_N\end{bmatrix}, \tag{3.1.11}$$

with ω_j and ζ_j denoting the modal frequency and damping ratio of the j-th structural mode. Although the proportional damping is not present in the Bernoulli-Euler beam equation, a small amount of damping is usually assumed for each mode to more accurately reflect the behavior of real structures. The modal frequencies are related to the solutions of the structure's characteristic equation, Equation (3.1.6), by

$$\omega_j^2=\frac{\mathrm{EI}}{\rho}\beta_j^4\ . \tag{3.1.12}$$

The matrix in Q Equation (3.1.9) is known as the input influence matrix, and $u(t)$ denotes external forces (control or disturbance) acting on the structure. For the cantilevered beam considered here the input to the system is supplied by two piezoelectric patches mounted at the base of the beam and configured to supply a bending moment [24].

Defining the state vector

$$x(t) = [\eta^{\mathrm{T}}(t) \;\; \dot{\eta}^{\mathrm{T}}(t)]^{\mathrm{T}} , \tag{3.1.13}$$

yields the state space model

$$\dot{x}(t) = \mathrm{A}x(t) + \mathrm{B}u(t) , \tag{3.1.14}$$

where the matrix A can be partitioned in $N \times N$ blocks as

$$\mathrm{A} = \begin{bmatrix} 0 & \mathrm{I} \\ -\Lambda & -2\zeta\Lambda^{1/2} \end{bmatrix}, \tag{3.1.15}$$

and the matrix B matrix has the form

$$\mathrm{B} = \begin{bmatrix} 0 \;\mid\; \mathrm{Q}^{\mathrm{T}} \end{bmatrix}^{\mathrm{T}} = [0 \,,\, 0 \,,\ldots,\, 0 \,,\, b_1 \,,\, b_2 \,,\ldots,\, b_N]^{\mathrm{T}} . \tag{3.1.16}$$

System measurements or outputs are typically modelled as linear combinations of the system states. Measurements that only depend on the system's position states are called position type outputs. If $y(t)$ denotes a position type measurement, then there exists an output matrix C such that

$$y(t) = \mathrm{C}\eta(t) , \tag{3.1.17}$$

or, for the choice of the state vector x in (3.1.13),

$$y(t) = [\ C\ \ 0\ ]x(t)\ . \tag{3.1.18}$$

Another common choice for the state vector x is

$$x = [\eta_1,\ \dot{\eta}_1,\ \eta_2,\ \dot{\eta}_2,\ \ldots \eta_N,\ \dot{\eta}_N]^T\ . \tag{3.1.19}$$

For this choice of the state vector, the matrix A in Equation (3.1.14) is block diagonal with diagonal blocks

$$A_i = \begin{bmatrix} 0 & 1 \\ -\omega_i^2 & -2\zeta_i\omega_i \end{bmatrix}, \tag{3.1.20}$$

the input matrix has the form

$$B = [0,\ b_1,\ 0,\ b_2,\ \ldots,\ 0,\ b_N]^T\ , \tag{3.1.21}$$

and the output matrices for position type measurements have the form

$$C = [c_1,\ 0,\ c_2,\ 0,\ \ldots,\ c_N,\ 0]\ . \tag{3.1.22}$$

The two choices for the state vector in Equations (3.1.13) and (3.1.19), and the corresponding A, B, and C matrices, are related by a similarity transform.

3.2. THE MODAL DOMAIN OPTICAL FIBER SENSOR MODEL

Chapter 2 described the development of a mathematical model of the modal domain optical fiber sensor for use in system theoretic design and analysis. The sensor model is incorporated into flexible structure models of the form given in Equations (3.1.8) and (3.1.14) by decomposing the strain in the sensor in terms of the second derivatives of the structural mode shapes.

Using the linear design model of the sensor described in Chapter 2 and assuming that the nominal strain distribution in the sensor is equal to zero, the sensor output is proportional to

$$I(t) = I_1 + I_2 \int_S \left\{ \Delta\beta_0 \epsilon_1(s,t) + \sum_{j=1}^{6} \frac{\partial \Delta\beta_0}{\partial \epsilon_j} \epsilon_j(s,t) \right\} ds , \tag{3.2.1}$$

where ϵ_j denotes the j-th element of the tensor which describes the representation of the strain transferred to the sensor in the fiber's local coordinate system, $\Delta\beta_0$ denotes the difference between the propagation constants of the two electromagnetic modes propagating in the optical fiber, and S denotes the fiber path along the structure. If the sensor is mounted on the surface of the beam in a straight line along the length of the beam parallel to the beam's longitudinal, then

$$I(t) = I_1 + I_2 \int_\Omega \Delta\tilde{\beta}\epsilon(z,t) \, dz , \tag{3.2.2}$$

where $\epsilon(z,t)$ denotes the strain at the surface of the beam, and $\Delta\tilde{\beta}$ denotes the sensor sensitivity to axial strain. If the sensor output is filtered by an ideal high-pass filter to remove the DC component, I_1, the effective sensor output becomes

$$y_f(t) = K_f \int_\Omega \Delta\tilde{\beta}\epsilon(z,t) \, dz , \tag{3.2.3}$$

where Ω denotes the structural domain, and K_f denotes the sensor gain.

For small deflections, the strain at the surface of the beam is proportional to the second derivative of the deflection, so that

$$\epsilon(z,t) = -\frac{h}{2} \frac{\partial^2 w(z,t)}{\partial z^2} , \tag{3.2.4}$$

where h denotes the thickness of the beam. Writing the deflection in terms of the modal decomposition described in Section 3.1, the strain is approximated by

$$\epsilon(z,t) = -\frac{h}{2} \sum_{j=1}^{N} \phi_j''(z) \, \eta_j(t). \tag{3.2.5}$$

Substituting this approximation into Equation (3.2.3), the sensor output becomes

$$y_f(t) = -\frac{h}{2} K_f \int_\Omega \Delta\tilde{\beta} \sum_{j=1}^{N} \phi_j''(z) \, \eta_j(t) \, dz . \tag{3.2.6}$$

Interchanging the orders of integration and summation,

$$y_f(t) = -\frac{h}{2} K_f \sum_{j=1}^{N} \left(\int_{\Omega} \Delta\tilde{\beta}\, \phi_j''(z)\ dz \right) \eta_j(t) . \tag{3.2.7}$$

Therefore,

$$y_f(t) = C_f \eta(t) , \tag{3.2.8}$$

where the matrix C_f has elements c_j given by

$$c_j = -\frac{h}{2} K_f \int_{\Omega} \Delta\tilde{\beta}\, \phi_j''(z)\, dz . \tag{3.2.9}$$

Equations (3.2.7) and (3.2.9), show that the output of the modal domain optical fiber sensor is a position type measurement and depends on a linear combination of the structure's modal position states.

3.3. SUMMARY

This chapter described the mathematical model of a simple flexible structure - a cantilevered beam. A state-space description of the structure was derived from the Bernoulli-Euler beam equation. The general forms of the system, input and output matrices which comprise the state-variable description of the system in modal coordinates were described for two choices of the state vector. Finally, the mathematical model of the modal domain optical fiber sensor was incorporated into the state-variable model of the structure.

4. Distributed-effect sensing

The modal domain optical fiber sensor described in Chapter 2 belongs to the class of sensors known as distributed-effect sensors. Distributed-effect sensors respond to distributed quantities over a significant gauge length but have scalar outputs. The best known example of a distributed-effect sensor is piezoelectric film. By altering the sensors' sensitivity along their gauge lengths, distributed-effect sensors can be configured to provide a much wider variety of structural measurements than comparable point sensors.

Section 4.1 compares the concepts of distributed sensing, distributed-effect sensing, and point sensing, and described the forms of the mathematical models associated with each type of sensor. Section 4.2 describes different sensing technologies that have been applied or proposed to implement distributed-effect sensors. Section 4.3 described the integration of the mathematical models of the distributed-effect sensors into the state space models for flexible structures. Section 4.4 describes several criteria for the design of distributed-effect sensors.

4.1. SENSOR MODEL

Although distributed-effect sensors respond to environmental changes over a significant gauge length, their outputs are scalar signals; hence, they do not conform to the traditional notion of distributed sensors. When the sensitivity of these sensors varies along their gauge lengths the sensors spatially filter the distributed quantities to which they respond. This section describes the general mathematical model for a class of distributed-effect sensors, and compares distributed-effect sensors to distributed sensors and point sensors.

4.1.1 Distributed vs Point sensing

Definition 4.1.1: A signal m is a distributed signal if it depends on a spatial

variable, z, which belongs to a domain Ω with dimension greater than or equal to one. □

Many of the signals, $m(z,t)$, of interest in the control of flexible structures are distributed signals. Examples of distributed signals associated with flexible structures include structural displacement and velocity, strain, and the rate of change of strain.

Let $m(z,t)$ denote a distributed signal associated with a flexible structure, and let Ω denote the spatial domain over which the sensor responds (i.e. $m(z,t)$ is only defined for $z \in \Omega$).

Definition 4.1.2: A sensor is a distributed sensor if the sensor output, $s(z,t)$, is a distributed signal proportional to a distributed signal, $m(z,t)$, associated with the structure. □

Distributed sensors are attractive for structural control because they contain information about the behavior of a system over some continuous domain Ω. The spatially distributed nature of the sensor outputs, however, make them difficult to incorporate into existing control, identification, or monitoring systems. With the exception of some recent advances in optical signal processing, most signal processing algorithms and hardware only accept scalar signals; therefore, even when they are available, distributed measurements must first be converted into scalar signals before they can be used.

Definition 4.1.3: A sensor is a distributed-effect sensor if the sensor output, $y(t)$, is a scalar function of time derived from a distributed signal, $m(z,t)$. □

One method of combining the spatially distributed information in a distributed signal to produce a scalar output is to weight (multiplying point-by-point) the signal by a spatially varying gain then integrate the signal over the domain of the spatial variable. Distributed-effect sensors of this type are modelled as

$$y(t) = \int_{\Omega} g(z)m(z,t)\, dz \tag{4.1.1}$$

where $m(z,t)$ is a distributed quantity, $g(z)$ is a distributed gain which depends on the sensor placement and fabrication, and K is a scalar proportionality constant.

In some sensors, the gain $g(z)$ can be selected independently of the sensor and represents an additional design parameter in the design of control laws for the structure. In such cases, the distributed-effect sensor in (4.1.1) can be interpreted as filtering the distributed signal $m(z,t)$ according to the distributed gain $g(z)$ to produce the output $y(t)$.

Definition 4.1.4: If the function $g(z)$ in (4.1.1) can be chosen independently of the sensor, then $g(z)$ is called a weighting function. □

Definition 4.1.5: Any device which produces a scalar output signal $y(t)$ based on a distributed input signal $m(z,t)$ according to (4.1.1) where $g(z)$ is a weighting function is called a spatial filter. □

Figure 4.1.1 shows a distributed-effect sensor in a control loop for a flexible structure. Once a distributed measurement is converted into a scalar signal by a distributed filter there is no difference between that scalar signal and the output of a distributed-effect sensor. The only difference between the output of a distributed-effect sensor and the spatially filtered output of a distributed sensor is whether the spatial filter is considered part of the sensor or part of the control system.

Although the output of the distributed-effect sensor is a scalar quantity, there are important differences between distributed-effect sensors and point sensors, which also provide scalar system outputs.

Definition 4.1.6: A sensor is a point sensor if the sensor output, $p(t)$, only depends on the behavior of the structure at a single point $z_0 \in \Omega$. □

Choosing the weighting function

$$g(z) = \delta(z - z_0) \tag{4.1.2}$$

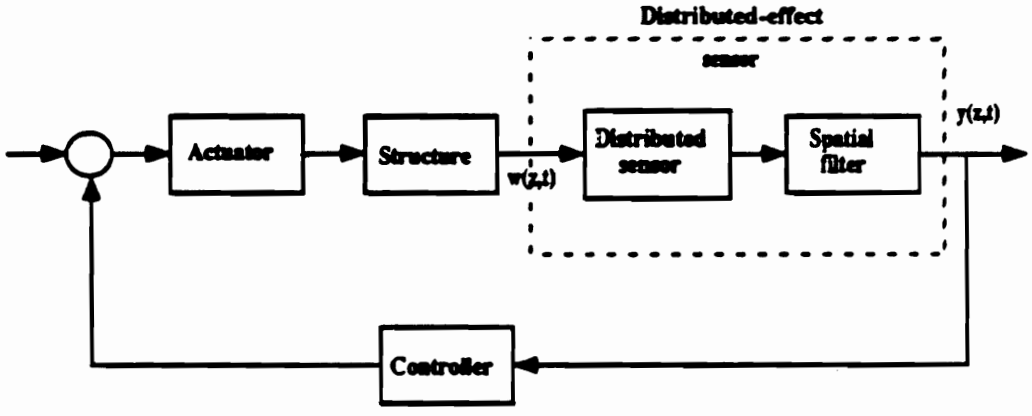

Figure 4.1.1 Distributed-effect sensor in a control system for a flexible structure.

in (4.1.1) yields the point measurement

$$p(t) = \int_{\Omega} \delta(z - z_0) m(z,t)\, dz = m(z_0, t)\ . \tag{4.1.3}$$

Hence, distributed-effect sensors can be used to extract point measurements from distributed signals.

One interpretation of distributed-effect sensors is as distributed sensors followed by spatial filters. The spatial filter serves to provide a desired scalar structural measurement, $y(t)$, determined by the selection of the weighting function $g(z)$. For example, the weighting function may be chosen to measure specific structural modes that are to be controlled [13-14]. From this point of view, the distributed-effect sensor is equivalent to a generalized point sensor.

From another point of view, the weighting function in the distributed-effect sensor is a distributed control gain [10,12]. From this point of view the output of the transfer function used in the controller design is the distributed signal $m(z,t)$ and the spatial filter serves as part of the feedback control system.

From both points of view, the weighting function, $g(z)$, can be considered a design parameter for the control system. The important issue in the design of distributed-effect sensors is the choice of the sensor weighting function $g(z)$ in Equation (4.1.1) to provide measurements of desired quantities.

4.2. DISTRIBUTED-EFFECT SENSOR TECHNOLOGY

This section describes three sensor technologies that have been used or proposed for use as distributed-effect sensors. These sensor technologies include piezoelectric sensors, modal domain optical fiber sensors, and holographic sensors.

4.2.1. Piezoelectric sensors

Piezoelectric materials have been used in the control of flexible structures as both distributed sensors and actuators [11,13,14,41]. Piezoelectric sensors can be configured to produce a scalar signal proportional to the spatial integral of the distributed strain or the rate of change of the strain over the surface of the sensor.

Both piezoelectric ceramic crystals and piezoelectric polymer films have

been used as distributed sensors, however, most weighted distributed-effect sensor implementations have used piezoelectric polymer film. The most common commercially available piezoelectric polymer film is Polyvinylidene Fluoride (PVDF), a polymer material that is polarized (and made piezoelectric) by poling in an electric field during processing. The film usually has a layer of conducting metal deposited on either side to facilitate the application or measurement of a voltage or electric field.

The piezoelectric film acts like a capacitor. Longitudinal strain in the material causes an electrical charge to develop at a point on the surface of the material. If the voltage induced by the accumulated surface charge is measured directly (using a high impedance measurement circuit), then the output of the sensor is proportional to the spatial integral of the distributed structural strain over the surface area of the sensor. If, however, the sensor if shunted with a resistor, the surface charge produces a current in the resistor that is proportional to the rate of change of the spatial integral of the strain in the structure.

There are primarily two ways of implementing distributed filter weights with piezoelectric film sensors: a) by spatially varying the piezoelectric constant of the material; or, b) by physically limiting the sensor's sensing area. The second method appears to be more popular. The sensor's sensing area is limited by either cutting the film or removing the metallic conducting layer in a pattern that corresponds to the desired spatial filter function. For structures subject to one dimensional vibrations such as flexible beams, this translates into using sensors that are shaped like the desired spatial weighting function.

Consider the flexible beam example described in Chapter 3, and suppose $k(z,x)$ describes the shape of a layer of piezoelectric film bonded to the surface of the beam (i.e. $k(z,x) = 1$ if the sensor responds to strain at the point (z,x), and is equal to zero elsewhere). The output of the piezoelectric sensor is proportional to

$$y_p(t) = K \int_0^l \int_0^b k(z,x)\, \epsilon(z,t)\, \mathrm{d}x\, \mathrm{d}z, \tag{4.2.1}$$

where b denotes the width of the beam. Since the strain in the flexible beam only depends on the longitudinal coordinate z, Equation (4.2.1) simplifies to

$$y_p(t) = K_p \int_0^l g(z)\, \epsilon(z,t)\, \mathrm{d}z, \tag{4.2.2}$$

where

$$g(z) = \int_0^b k(z,x)\, \mathrm{d}x. \tag{4.2.3}$$

Therefore, the "width" of the sensor (in the unstrained direction) at a point z determines the value of the spatial filter weighting function at the point z. Sign changes are implemented by reversing the direction of the poling field, or by simply reversing the polarity of the leads attached to the sensor.

4.2.2. Holographic sensor

Holographic sensors are noncontacting optical sensors that provide a spatially distributed measurement of the displacement of a structure [9,15,42]. Interference between two beams of coherent light with slightly different frequencies - a reference beam which travels over a fixed optical path length, and an object beam which is reflected from the structure - form a holographic image of the structure inside a photo-refractive crystal. When the holographic image is "read" from the photo-refractive crystal, the sensor output is an optical image with spatially varying intensity proportional to the spatial variation in the structural displacement [15].

The output of the holographic sensor is a truly distributed signal which can be processed optically by passing the optical signal through masks or transparencies with spatially varying optical transmittance proportional to the desired weighting function [15]. A photodetector converts the filtered distributed optical signal into a scalar electrical signal.

If $w(z,t)$ denotes the displacement of the cantilevered beam described in Chapter 3, then the output of the holographic sensor would be a distributed optical signal,

$$s(z,t) \propto w(z,t)\ . \tag{4.2.4}$$

If the sensor output is passed through a transparency with spatially varying transmittance $g(z)$ and converted to an electrical signal by a photodetector, then

photodetector output is given by

$$y_h(t) = K_h \int_0^l g(z)\, s(z,t)\, \mathrm{d}z. \tag{4.2.5}$$

where the spatial integration is performed by the photodetector.

At this time, holographic sensors for structural vibration control applications are still in the developmental stage [16]. The potential advantages of holographic sensor technology, however, lie in the possibility of implementing complex control and signal processing algorithms optically [15].

4.2.3 Modal domain optical fiber sensor

The modal domain optical fiber sensor described in Chapter 2 is another example of a distributed-effect sensor [10,24]. When the sensor is mounted on the surface of a structure, the sensor responds primarily to the component of the structural strain in the direction tangent to the fiber's path [28]. For the flexible beam example considered in Chapter 3, the sensor output is given by

$$y_f(t) = K_f \int_0^l \Delta\tilde{\beta}\epsilon(z,t)\, \mathrm{d}z, \tag{4.2.6}$$

where $\Delta\tilde{\beta}$ denotes the sensor sensitivity, $\epsilon(z,t)$ denotes the strain in the beam, and K_f is a proportionality constant. The sensor sensitivity depends on the fiber parameters [18], the orientation of the sensor's sensing section fiber relative to the structure, and the material properties of coatings and adhesives applied to the fiber [28,38]. The realization of modal domain optical fiber sensors with spatially varying sensitivity, $\Delta\tilde{\beta}$, is focus of Chapter 5.

4.3. SENSOR MODEL INTEGRATION

This section describes the integration of the distributed-effect sensor model into structural models of the type described in Chapter 3. The model of the weighting function is developed from two points of view. The first approach assumes that the desired weighting function, $g(z)$ is known; the second approach assumes that the a desired system output matrix, C, is known and a

corresponding weighting function is determined to realize the desired system output.

Assume that the distributed signal $m(z,t)$ is described by a set of orthogonal basis functions $\{\xi_j(z)\}$ defined over the spatial domain of the structure, Ω. Then $m(z,t)$ can be written as

$$m(z,t) = \sum_{j=1}^{N} \xi_j(z)\eta_j(t) \tag{4.3.1}$$

Substituting this expression into the spatial filter model (4.1.1) yields

$$\begin{aligned} y(t) &= \sum_{j=1}^{N} \left\{ \int_{\Omega} g(z)\ \xi_j(z)\ \mathrm{d}z \right\} \eta_j(t) \\ &= \sum_{j=1}^{N} c_j\ \eta_j(t)\ , \end{aligned} \tag{4.3.2}$$

where

$$c_j = \int_{\Omega} g(z)\ \xi_j(z)\ \mathrm{d}z\ . \tag{4.3.3}$$

Thus, if $g(z)$ is known, Equation (4.3.2) and the finite dimensional model of the structural dynamics described in Chapter 3 define the input output model of the system used in control system design.

Now suppose that the output matrix C corresponding to a desired scalar system output is known. The question is: Does there exist a weighting function, $g(z)$, such that a distributed-effect sensor which measures the distributed signal $m(z,t)$ will provide the desired output? Again assume that the distributed signal $m(z,t)$ is described by a set of orthogonal basis functions defined over the spatial domain Ω. Also assume there exists another set of basis functions $\{\gamma_j(z)\}$ defined over Ω, such that

$$g(z) = \sum_{k=1}^{N} g_k\ \gamma_k(z) \tag{4.3.4}$$

Substituting (4.3.4) into Equation (4.3.3) yields

$$c_j = \sum_{k=1}^{N} g_k \int_{\Omega} \gamma_k(z)\ \xi_j(z)\ \mathrm{d}z. \tag{4.3.5}$$

Defining the $N \times N$ matrix Q with elements

$$q_{kj} = \int_{\Omega} \gamma_k(z)\, \xi_j(z)\, \mathrm{d}z, \tag{4.3.6}$$

Equation (4.3.5) can be written in matrix form as

$$\mathrm{C} = \mathrm{GQ}\ , \tag{4.3.7}$$

where

$$\mathrm{G} = [g_1\ g_2 \cdots g_N]\ . \tag{4.3.8}$$

If the matrix Q is invertible, then G is uniquely defined by (4.3.7), and $g(z)$ can be computed from equation (4.3.4).

Remark: If the basis functions $\{\xi_j(z)\}$ are chosen such that they are orthonormal and $\gamma_j(z) = \xi_j(z)$ for all j, then Q is the identity matrix and

$$\mathrm{C} = \mathrm{G}. \tag{4.3.9}$$

For the cantilevered beam, the structures mode shapes, $\{\phi_j(z)\}$, form an orthonormal basis.

Remark: For the cantilevered beam, the second derivatives of the mode shapes form an orthogonal basis for the structure's spatial domain, Ω. If $\xi_j(z) = \gamma_j(z) = \phi_j''(z)$ in Equation (4.3.6), the matrix Q in (4.3.7) is a diagonal matrix with diagonal elements

$$q_{ii} = \beta_i^4 \tag{4.3.10}$$

where β_i is the solution of the waveguide characteristic equation corresponding to the i-th structural mode.

4.4. SENSOR DESIGN CRITERIA

One interpretation of distributed-effect sensors is as spatial filters that process distributed signals - the sensor's weighting function determines how the spatially distributed information in the distributed measurement is combined in the sensor output. Another interpretation of distributed-effect sensors is as generalized point sensors where the weighting function determines the quantity being measured. From this perspective, traditional point sensors are equivalent to distributed-effect sensors with unit impulse functions for spatial filter gains.

An important problem in structural control is sensor placement [43]. Although various approaches have been used to optimize sensor selection, the problem often reduces to a nonlinear programming problem because of constraints imposed by realizable point sensor locations. Distributed-effect sensors remove these constraints because the sensor output is determined by the sensor's weighting function not by the sensor's geographical location.

One common criterion for sensor selection is uses measures of observability associated with the sensor output. The weighting functions for distributed-effect sensors can be chosen to realize sensor outputs with specified measures of observability. Considering distributed-effect sensors as spatial filters, the sensor's weighting function can be chosen to implementation of modal filters [8]. Another criterion for weighting function selection is the implementation of control and signal processing algorithms [10], and the realization of desired system frequency response characteristics [19].

4.4.1. Arbitrary system output realization

The problem of determining the weighting function $g(z)$ which realizes the desired system output matrix C occurs frequently in the sensor placement problem: the matrix C is determined through some optimality criteria and the problem is to find a sensor location which corresponds to this output matrix. Until the advent of spatial filters, the sensor was restricted to be a point sensor or a finite sum of point sensors, which is equivalent to requiring that the weighting function be of the form

$$g(z) = \sum_{i=1}^{M} g_i \delta(z - z_i) \ . \tag{4.4.1}$$

If $\xi_j(z) = \phi_j(z)$, the mode shapes, then the output matrix for a single point sensor must satisfy

$$c_j = \phi_j(z_0), \tag{4.4.2}$$

for $j = 1, 2, \ldots, N$, where $z = z_0$ denotes the point sensor location. In general, an arbitrary output matrix, C, can not be realized using point sensors, but can be realized using distributed-effect sensors. Clearly, therefore, spatial filters allow additional flexibility for solving the sensor placement problem.

Example 4.4.1

Consider the flexible beam example presented in Chapter 3, and suppose that a desired measurement is given by

$$y(t) = [\ 1\ 0\ 0\ 0\ ]\ \eta(t)$$

where $\eta(t)$ denotes a vector of the structures modal position states. From Equations (4.3.7) and (4.3.10), the corresponding weighting function for a distributed-effect strain measurement is given by

$$g(z) = \frac{1}{\beta_1^4}\, \phi_1''(z) \ ,$$

and is plotted in Figure 4.4.1. Clearly, it would be difficult to approximate $g(z)$ by any finite number of delta functions; hence, the desired sensor output can not be realized using point sensors. Trying to realize the desired measurement using a strain gauge located at the root of the beam yields an output matrix proportional to

$$\hat{C} = [1.0 \quad 5.1 \quad 11.3 \quad 16.5] \ . \qquad \square$$

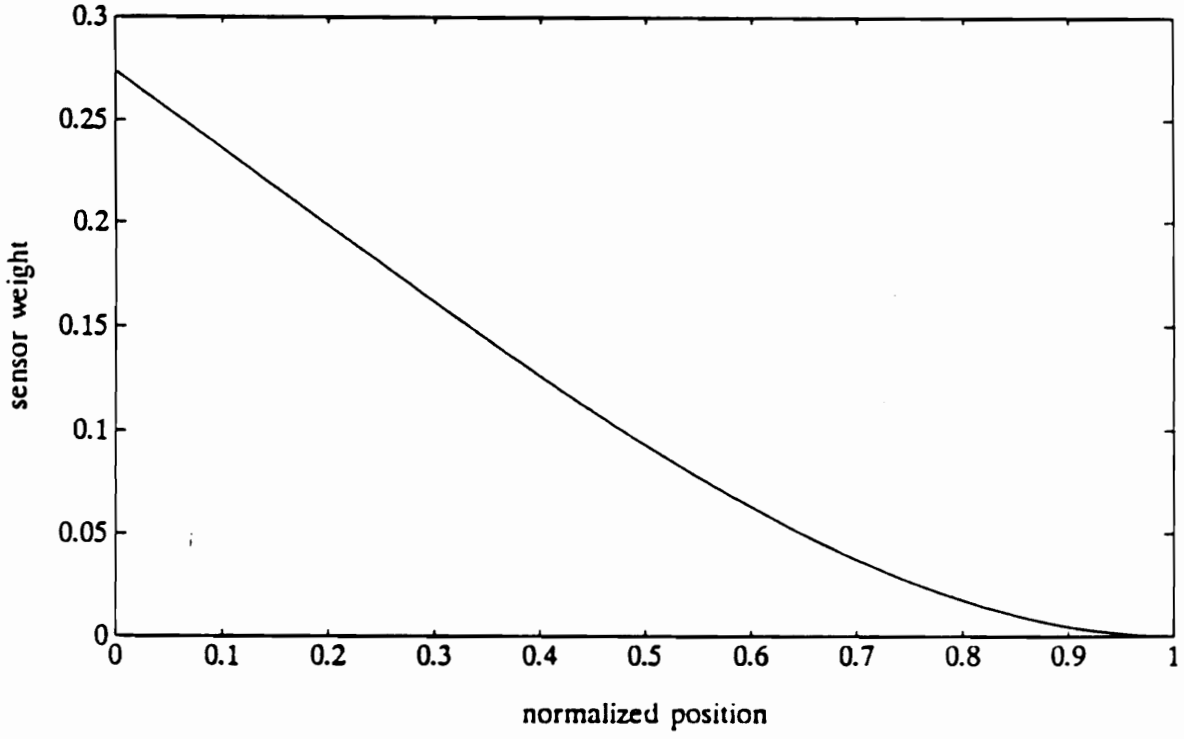

Figure 4.4.1 Weight function $g(z)$ for Example 4.4.1.

4.4.2. Observability

The weighting function $g(z)$ determines the observability of the structure from the output of a distributed-effect sensor. The weighting function can be chosen to make particular modes observable or unobservable [11,13,14], or to assign specified measures of observability for the system.

Miller and Hubbard [11] described the effects of the weighting function on the observability of a flexible beam from the output of a distributed-effect piezoelectric sensor, for a number of different boundary conditions. The following example illustrates this point.

Example 4.4.2

Suppose the distributed signal $m(z,t)$ in Equation (4.1.1) represents the strain in a flexible beam. For $g(z) \equiv 1$, then the output of the distributed-effect sensor is proportional to

$$\begin{aligned} y(t) &= \int_0^l \epsilon(z,t)\mathrm{d}z \\ &= \int_0^l \sum_{j=1}^{N} \phi_j''(z)\eta_j(t)\ \mathrm{d}z \\ &= \sum_{j=1}^{N} \left(\phi_j'(l) - \phi_j'(0) \right) \eta_j(t). \end{aligned}$$

For certain clamped or sliding boundary conditions, however, the slope at the ends of the beam is always equal to zero; hence the system would be unobservable from the sensor output. For a simply supported beam,

$$\phi_j(z) \propto \sin\left(\frac{j\pi z}{l}\right),$$

so that

$$\left(\phi_j'(l) - \phi_j'(0) \right) \propto (1 - \cos(j\pi)).$$

Therefore, the odd numbered modes (i.e. j odd) are observable, but the even

numbered modes are unobservable. □

A common criteria for sensor selection is to assign a measure of observability to the sensor output, then choose the sensor location that optimizes the specified measure. The measure of observability is an indication of the ability of the sensor to observe the system dynamics [44]. The weighting functions for distributed-effect sensors can be chosen to optimize a specified measure of observability for the system. Using an appropriate measure of observability, the sensor output can be selected to optimize the performance of structural control systems or maximize disturbance rejection [21].

The observability Grammian (with respect to a system output) defines an ellipsoid in the state space that represents the set of all system states that can be observed by extracting unit energy from the system (with respect to the L^2 norm) [45]. There are several measures of observability defined by the orientation of the observability Grammian with respect to the system eigenvectors. The distributed filter gain determines the orientation of the observability Grammian with respect to the system eigenvectors; therefore, we can choose the distributed filter weighting function to maximize or minimize some measure of observability for certain system modes.

One measure of observability is defined by the distance in the direction of each of the system eigenvectors from the origin to the ellipsoid in the state space defined by the observability Grammian.

Definition 4.4.1: The observability Grammian at time t_0, is defined by

$$W_o^2(t_0) = \int_0^{t_0} e^{A^T\tau} C^T C e^{A\tau} d\tau \ , \tag{4.4.3}$$

where $e^{A^T\tau}$ denotes the state transition matrix for the system and C defines the system output. □

Remark: The observability Grammian is a symmetric, positive semi-definite matrix with the singular value decomposition:

$$W_o^2 = V_o \Sigma_o^2 V_o^T \tag{4.4.4}$$

where

$$\Sigma_o^2 = \text{diag}\{\sigma_{o_1}^2, \sigma_{o_2}^2, \ldots, \sigma_{o_N}^2\}\ , \text{ and} \qquad V_o = [v_{o_1}\ v_{o_2} \ldots v_{o_N}]\ . \tag{4.4.5}$$

The quantity σ_{o_i} is defined as the i-th principle component magnitude of the observability Grammian, and the vector v_{o_i} is defined as the i-th principle component vector of the observability Grammian.

For $u(t) = 0$, the output of the system is given by

$$y(t) = Ce^{At}x(0)\ , \tag{4.4.6}$$

where e^{At} defines the system's state transition matrix. The set of observable initial states under the constraint of extracting unit norm energy in time t_0 is given by

$$S_o(t_0) = \left\{x(0)\ \Big|\ \int_0^{t_0} |y(\tau)|^2\, d\tau \le 1\right\}\ . \tag{4.4.7}$$

The boundary of the set $S_o(t_0)$ is defined as the set

$$\hat{S}_o = \left\{x(0)\ \big|\ x(0) = V_o \Sigma_o^{-1} \rho,\ \|\rho\| = 1\right\}\ , \tag{4.4.8}$$

which is an ellipsoid in the state space with semi-axes equal to $\sigma_{o_i}^{-1} v_{o_i}$.

Remark: The ellipsoid corresponding to $\hat{S}_o$ defines a surface in the state space on which all states are equally observable. The direction in which states lie closest to the origin is the most observable, and the direction in which states lie farthest from the origin is the least observable direction. The distance from the origin to this ellipsoid in the direction of a system eigenvector provides a measure of the observability of that eigenvector or mode.

The state transition matrix has the following decomposition:

$$e^{At} = \sum_{i=1}^{N} p_i \, e^{\lambda_i t} q_i^T \,, \tag{4.4.9}$$

where λ_i denotes the i-th system eigenvalue and p_i and q_i^T denote the corresponding right and left eigenvectors respectively, of the system's A matrix. Therefore, from Equation (4.4.6),

$$\begin{aligned} \| y(T) \|_2^2 &= \int_0^T | \, y(t) \, |^2 \, dt \\ &= \int_0^T x^T(0) \, e^{A^T t} C^T \, C e^{At} x(0) \, dt \\ &= \int_0^T \left\{ \sum_{k=1}^{N} x^T(0) \, q_k \, e^{\bar{\lambda}_k t} p_k^T \, C^T \right\} \left\{ \sum_{i=1}^{N} C \, p_i \, e^{\lambda_i t} q_i^T x(0) \right\} dt \,. \end{aligned} \tag{4.4.10}$$

If $x(0)$ lies in the direction of the j-th eigenvector, then there exists scalar α_j, such that $x(0) = p_j \alpha_j$, and

$$\| y(T) \|_2^2 = \int_0^T \left\{ \sum_{k=1}^{N} \alpha_j \, p_j^T \, q_k \, e^{\bar{\lambda}_k t} p_k^T \, C^T \right\} \left\{ \sum_{i=1}^{N} C \, p_i \, e^{\lambda_i t} q_i^T \, p_j \, \alpha_j \right\} dt \,. \tag{4.4.11}$$

The left and right eigenvectors are orthogonal; therefore,

$$q_j^T p_k = \; p_j^T q_k = \delta_{jk} \,, \tag{4.4.12}$$

and Equation (4.4.11) becomes

$$\begin{aligned} \| y(T) \|_2^2 &= \int_0^T \left\{ \alpha_j \, e^{\bar{\lambda}_j t} p_j^T \, C^T \right\} \left\{ C \, p_j \, e^{\lambda_j t} \alpha_j \right\} dt \\ &= \alpha_j^2 \int_0^T | \; C \, p_j \, e^{\lambda_j t} \, |^2 \, dt. \end{aligned} \tag{4.4.13}$$

When $x(0)$ lies on the ellipsoid defined by the observability Grammian, $\|y(T)\|^2 = 1$, which implies

$$\alpha_j = \left\{ \int_0^T | \, C \, p_j \, e^{\lambda_j t} \, |^2 \, dt \right\}^{-1/2} . \tag{4.4.14}$$

The quantity α_j in Equation (4.4.14) is the distance from the origin to the ellipsoid in the state space defined by the observability Grammian in the direction of the j-th system eigenvector and defines a measure of observability for the j-th structural mode.

Definition 4.4.2: If C denotes the output matrix corresponding to a scalar system output, $y(t)$, and λ_j and p_j denote the j-th system eigenvalue and eigenvector respectively, then

$$\mu_j \triangleq \left\{ \int_0^T | \, C \, p_j \, e^{\lambda_j t} \, |^2 \, dt \right\}^{1/2} . \tag{4.4.15}$$

defines a measure of observability of the j-th mode of a system from the output $y(t)$. □

Remark: The measure of observability μ_j is the inverse of α_j in Equation (4.4.14), which is equal to the distance from the origin to the boundary of the observability ellipsoid in the state space on which all states are equally observable. States on the ellipsoid that lie closest to the origin are more observable, and states that lie farthest from the origin are less observable; hence, $\mu_j > \mu_k$ ($\alpha_j < \alpha_k$) implies that the j-th mode is more observable than the k-th mode, since one has to travel farther in the state space along the corresponding eigenvector for the k-th mode to extract unit L^2 norm energy from the system. When $\mu_k = 0$, the k-th mode is unobservable from the sensor output.

Squaring both sides of Equation (4.4.15) and evaluating the integral

expression yields

$$\mu_k^2 = |\, C\ p_k \,|^2 \int_0^T |\, e^{\lambda_k t} \,|^2\, dt\ ,$$

$$= |\, C\ p_k \,|^2 \int_0^T e^{2Re\{\lambda_k\}t}\ dt\ , \tag{4.4.16}$$

$$= |\, C\ p_k \,|^2\ \frac{e^{2Re\{\lambda_k\}T} - 1}{2Re\{\lambda_k\}}\ ,$$

where $Re\{\lambda_k\}$ denotes the real part of λ_k. For stable systems, $Re\{\lambda_k\} < 0$ for all k; therefore, for $T = \infty$,

$$\mu_k^2 = |\, C\ p_k \,|^2\ \frac{-1}{2Re\{\lambda_k\}}\ . \tag{4.4.17}$$

Taking the positive square root of both sides yields

$$\mu_k = \frac{|\, C\ p_k \,|}{\sqrt{2\,|\, Re\{\lambda_k\} \,|}}\ . \tag{4.4.18}$$

For structural models of the type described in Chapter 3, the eigenvalues and corresponding eigenvectors of the system occur in complex conjugate pairs. When the state vector is defined as

$$x(t) = [\eta_1,\ \dot{\eta}_1,\ \eta_2,\ \dot{\eta}_2,\ \cdots,\ \eta_N,\ \dot{\eta}_N]^T\ , \tag{4.4.19}$$

the output matrix C for a position type measurement has the form

$$C = [c_1\ 0\ c_2\ 0\ \ \ldots\ c_N\ 0\ ]\ , \tag{4.4.20}$$

and the k-th eigenvector has the form

$$p_k = \frac{1}{\sqrt{1+\omega_k^2}}\,[0\ 0\ \cdots\ 0\ 0\ 1\ \lambda_k\ 0\ 0\ \cdots\ 0\ 0]^T, \tag{4.4.21}$$

where

$$\lambda_k = -\zeta_k\omega_k \pm \omega_k\sqrt{\zeta_k^2 - 1}\,, \tag{4.4.22}$$

denotes the corresponding eigenvalue. Therefore, for position type measurements

$$Cp_k = \frac{c_k}{\sqrt{1+\omega_k^2}}\,, \tag{4.4.23}$$

and

$$\mu_k = \frac{|\,c_k\,|}{\sqrt{2\zeta_k\omega_k(1+\omega_k^2)}}\,. \tag{4.4.24}$$

Equation (4.4.24) can be used to choose the output matrix, and hence the weighting function for a distributed-effect sensor, to achieve desired measures of observability for different structural modes. Suppose $\{\tilde{\mu}_k\}$, $k = 1,2,\ldots,N$, denotes the desired measures of observability for the first N structural modes. From (4.4.24) choosing

$$c_k = \pm\ \tilde{\mu}_k\sqrt{2\zeta_k\omega_k(1+\omega_k^2)}\,, \tag{4.4.25}$$

yields

$$\mu_k = \tilde{\mu}_k\,. \tag{4.4.26}$$

The weighting function necessary to realize the desired system output using a distributed-effect sensor that measures a distributed signal $m(z,t)$ can be determined from Equation (4.3.7).

Example 4.4.3

Consider the flexible structure model described in Chapter 3, and suppose it is desirable for each of the structure's first four modes to have the same measure of observability, $\tilde{\mu}$, and all of the remaining modes to be unobservable, i.e. $\mu_k = 0$, $k = 5,\ldots,N$. If

$$g(z) = \sum_{k=1}^{N} g_k \frac{1}{\beta_k^2} \phi_k''(z) ,$$

then for a distributed-effect sensor that measures structural strain, the nonzero elements of the corresponding output matrix are given by

$$c_k = \beta_k^2 g_k .$$

Therefore, from Equation (4.4.25), $\mu_k = \tilde{\mu}_k$ if

$$g_k = \pm \frac{\tilde{\mu}_k}{\beta_k^2} \sqrt{2\zeta_k \omega_k (1 + \omega_k^2)} ,$$

for all k.

For the modal measures of observability described above, the desired weighting function is given by

$$g(z) = \tilde{\mu} \sum_{k=1}^{4} \frac{\sqrt{2\zeta_k \omega_k (1 + \omega_k^2)}}{\beta_k^4} \phi_k''(z) .$$

Figure 4.4.2 shows a plot of $g(z)$ for $\tilde{\mu} = 1$. □

The dual criterion to choosing the distributed filter gain to specify the observability of the system is to design the distributed-effect sensor based on the controllability of the system. The controllability Grammian corresponding to a given system input defines the set of system states that are reachable with L^2 unit energy from that input. By selecting the distributed filter gain which aligns the corresponding measurement vector with the direction in the state space in which the system is least controllable for a given disturbance input the effect of that disturbance on the system measurement is minimized, and the effect of the disturbance on the closed loop performance of the system is minimized.

Conversely, aligning the measurement vector in the direction in which the system is most controllable insures that the measurement provides the maximum information on the effect of the control input on the system [6,46]. A similar technique has been proposed for the control of acoustic radiation - the distributed-

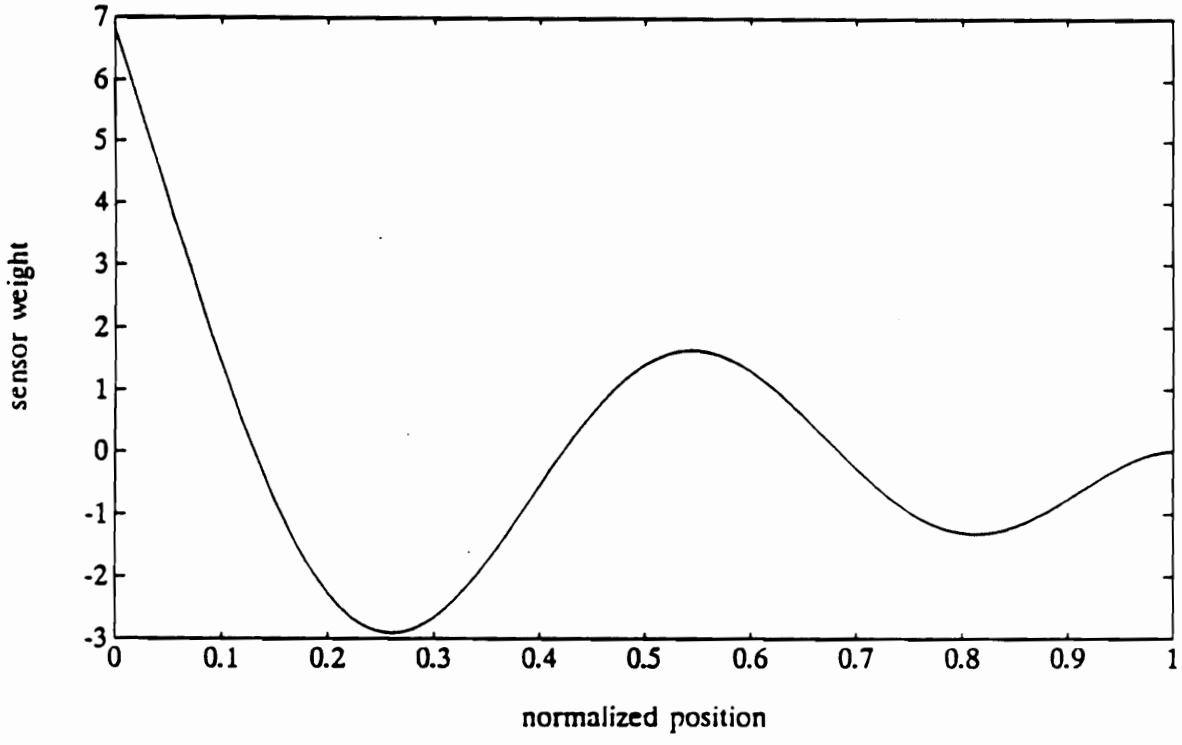

Figure 4.4.2 Weighting function $g(z)$ for Example 4.4.3.

effect sensor gain is chosen to align the measurement vector in the direction in the state space in which the system radiates the most acoustic power [21].

4.4.3. Modal filtering

Another application of distributed-effect sensing is modal filtering. Utilizing the orthogonality of the mode shapes of structures such as flexible beams, the weighting functions for distributed-effect sensors may be chosen to eliminate certain modes from the sensor output. Modal filtering is analogous to the familiar notion of band-limited filtering in conventional signal processing.

The use of modal filters is particularly useful for reducing observation spillover when the control system is designed using a reduced order model of the system since it permits removal of any unmodelled system dynamics from the measurement signal [40]. This can be very important, since unmodelled dynamics in the measurement signal can destabilize the system [7]. The implementation of modal filters using point sensors requires at least as many sensors as the number of modes included in the system model [8]. Distributed-effect sensors, however, can used to implement modal filters directly [11,13,14,41].

The usefulness of distributed sensors for modal filtering is a result of the orthogonality of the structure's mode shapes. Consider a distributed-effect strain sensor, and suppose

$$B=\{\phi_{j_m}(z) \mid 1 \leq m \leq M\} , \tag{4.4.27}$$

denotes the set of structural modes contained in the finite-dimensional model of the system. If the weighting function for the distributed-effect sensor is chosen such that

$$g(z)=\sum_{m=0}^{M} g_m \frac{1}{\beta_{j_m}^2} \phi''_{j_m}(z), \tag{4.4.28}$$

and the quantity measured by the distributed-effect sensor is structural strain, then the sensor output is given by

$$y(t) = \int_{\Omega} \sum_{m=0}^{M} g_m \frac{1}{\beta_{j_m}^2} \phi_{j_m}''(z)\, \epsilon(z,t)\, \mathrm{d}z. \tag{4.4.29}$$

Substituting the representation of the structural strain based on the (infinite-dimensional) modal decomposition of the structural displacement given in Equation (3.1.3), the expression for the sensor output becomes

$$\begin{aligned} y(t) &= \int_{\Omega} \sum_{m=1}^{M} g_m \frac{1}{\beta_{j_m}^2} \phi_{j_m}''(z) \sum_{i=1}^{\infty} \phi_i''(z)\, \eta_i(t)\, \mathrm{d}z \\ &= \sum_{m=0}^{M} g_m \sum_{i=1}^{\infty} \int_{\Omega} \frac{1}{\beta_{j_m}^2} \phi_{j_m}''(z)\, \phi_i''(z)\, \mathrm{d}z\, \eta_i(t) \\ &= \sum_{m=0}^{M} g_m \sum_{i=1}^{\infty} \beta_{j_m}^2\, \delta_{i,j_m}\, \eta_i(t) \\ &= \sum_{j_m=0}^{M} g_m \beta_{j_m}^2 \eta_{j_m}(t). \end{aligned} \tag{4.4.30}$$

Hence, because the basis functions $\{\phi_j''\}$ are mutually orthogonal, any modes contained in the distributed measurement $\epsilon(z,t)$ but not contained in the set B are removed by the filter and do not appear in the filtered output, $y(t)$.

It should be noted that these modal results are equivalent to the observability criteria presented earlier. Modes included in the set B in Equation (4.4.27) are observable from the output of the distributed-effect sensor with the weighting function $g(z)$ defined by Equation (4.4.28); structural modes that are not included in the weighting function are unobservable. In the analogy to temporal frequency-domain filters, the set B defines the modal filter's pass band.

Example 4.4.4

The desired sensor output in Example 4.4.1 represents the output of a modal filter for the first mode of the cantilevered beam; that is, the set B in (4.4.27) is given by

$$B=\{\phi_1(z)\}.$$

The corresponding distributed sensor weight, $g(x)$, shown in Figure 4.4.1, is proportional to the second derivative of the structure's first mode shape,

$$g(z) \propto \phi''(z),$$

and the sensor output is a direct measurement of the first modal amplitude, $\eta_1(t)$□

4.4.4. Control law implementation (functional observers)

Several control schemes for flexible structures require the implementation of high order compensators. The complexity of the compensator can be significantly reduced, however, by choosing the weighting function for the distributed-effect sensor to implement partial state feedback. One method for doing this is to use distributed-effect sensors to implement functional observers for the desired state feedback control law [10].

Suppose the state feedback control law

$$u(t) = -\mathrm{K}x(t) \tag{4.4.31}$$

is designed for the flexible structure described in Chapter 3, where the state vector is composed of the modal positions and velocities for each of the modeled structural modes. Unless the controller has direct access to the system states, an observer of the form

$$\dot{\hat{x}}(t) = \mathrm{A}\ \hat{x}(t) + \mathrm{B}\ u(t) + \mathrm{L}(\ y(t) - \mathrm{C}\hat{x}(t)\ )\ , \tag{4.4.32}$$

is typically used to provide an estimate, $\hat{x}$, of of the state vector, x, and the feedback law in Equation (4.4.32) is replaced by

$$u(t) = -\mathrm{K}\hat{x}(t)\ . \tag{4.4.33}$$

If the structural model includes N modes, the full-order state observer in Equation (4.4.32) has order $2N$. For models of complicated structures, the model dimension can be quite high; hence, a reduction in the order of the observer required to implement the control law is desirable.

If the dimension of the measurement $y(t)$ in Equation (4.4.32) is m, then a reduced-order observer of dimension $2N$-m can be used to provide an estimate of x. To reduce the compensator dimension still further, consider the case where $y(t) = \eta(t)$, so $m = N$. The observability index for such a system is 2; thus, a functional observer of dimension 1 can be constructed, which will provide an estimate of the feedback control signal $u(t)$ instead of the full state vector $x(t)$ [47].

Functional observers have the form

$$\begin{aligned} \dot{z}(t) &= \mathrm{F}z(t) + \mathrm{G}\eta(t) + \mathrm{H}u(t) \\ w(t) &= \mathrm{M}z(t) + \mathrm{P}\eta(t) \end{aligned} \tag{4.4.34}$$

and are designed so that

$$\lim_{t \to \infty} w(t) = \mathrm{K}x(t) \,, \tag{4.4.35}$$

with time constants determined by the eigenvalues of F. The functional observer can be implemented using two distributed-effect sensors which provide the measurements

$$y_G(t) = \mathrm{G}\eta(t), \tag{4.4.36.a}$$

and

$$y_P(t) = \mathrm{P}\eta(t). \tag{4.4.36.b}$$

The $1 \times N$ matrices G and P depend on the system parameters, the state feedback gain, and the functional observer design parameters F and M.

If the matrices G and P have elements γ_j and p_j respectively, then from Equations (4.3.7) and (4.3.10), the desired measurements can be realized using distributed-effect strain sensors with weighting functions

$$g(z) = \sum_{k=1}^{N} \frac{\gamma_k}{\beta_k^4} \phi_k''(z) \tag{4.4.37.a}$$

and

$$p(z) = \sum_{k=1}^{N} \frac{p_k}{\beta_k^4} \phi_k''(z) \ , \tag{4.4.37.b}$$

respectively. Using distributed-effect sensors with the weighting functions $g(z)$ and $p(z)$ defined in Equation (4.4.37), the equations defining the dynamics and output of the functional observer become

$$\begin{aligned} \dot{z}(t) &= \mathrm{F}z(t) + y_G(t) + \mathrm{H}u(t) \\ w(t) &= \mathrm{M}z(t) + y_P(t) \end{aligned} \tag{4.4.38}$$

where

$$y_G(t) = \int_{\Omega} g(z)\epsilon(z,t)\mathrm{d}z \tag{4.4.39}$$

and

$$y_P(t) = \int_{\Omega} p(z)\epsilon(z,t)\mathrm{d}z \ . \tag{4.4.40}$$

Example 4.4.5

Consider once again the cantilevered beam described in Chapter 3. The open-loop system is assumed to have approximately 0.15% damping in each mode. Using LQG control techniques a feedback matrix K can be determined such that for

$$u(t) = -\mathrm{K}x(t)$$

the first four modes of the structure have the closed-loop damping shown in Table 4.4.1. A full-order observer for this system would have the form

$$\dot{\hat{x}}(t) = \mathrm{A}\hat{x}(t) + \mathrm{B}u(t) + \mathrm{L}(y(t) - \mathrm{C}\hat{x}(t))$$

Table 4.4.1 Open and closed-loop poles for Example 4.4.5.

mode	% damping	
	open loop	closed loop
1	0.15	5.22
2	0.15	4.26
3	0.15	3.40
4	0.15	2.50

and would double the size of the closed-loop system. For a functional observer of the form

$$\dot{z}(t) = \mathrm{F}z(t) + y_G(t) + \mathrm{H}u(t)$$
$$w(t) = \mathrm{M}z(t) + y_P(t)$$

the order of the closed-loop system is only one greater than the order of the open-loop system. The additional closed-loop pole corresponds to an eigenvalue at $\lambda = -\mathrm{F}$. For this example, F=18, so the functional observer dynamics are twice as fast as the fastest pole of the closed-loop system. The normalized distributed-effect sensor weighting functions, $g(z)/\parallel g \parallel_\infty$ and $p(z)/\parallel p \parallel_\infty$, which realize the required measurements $y_G(t)$ and $y_P(t)$ are plotted in Figures 4.4.3 and 4.4.4. Figure 4.4.5 shows the ideal closed-loop system response with

$$u(t) = -Kx(t)$$

and the closed-loop system response when the functional observer provides the control signal

$$u(t) = -w(t)$$

for an arbitrary set of initial conditions. Figure 4.4.5 shows that the functional observer does an adequate job of estimating the necessary feedback control signal□

4.5. SUMMARY

The output of a distributed-effect sensor is equivalent to the spatially filtered output of a distributed sensor. Distributed-effect sensors can be designed to realize arbitrary scalar system outputs because there is a one-to-one correspondence between the distributed-effect sensor's weighting function and the output matrix associated with the state-space representation of the distributed-effect sensor output. The set of system measurements realizable using a finite number of point sensors is a subset of the set of scalar system measurements that

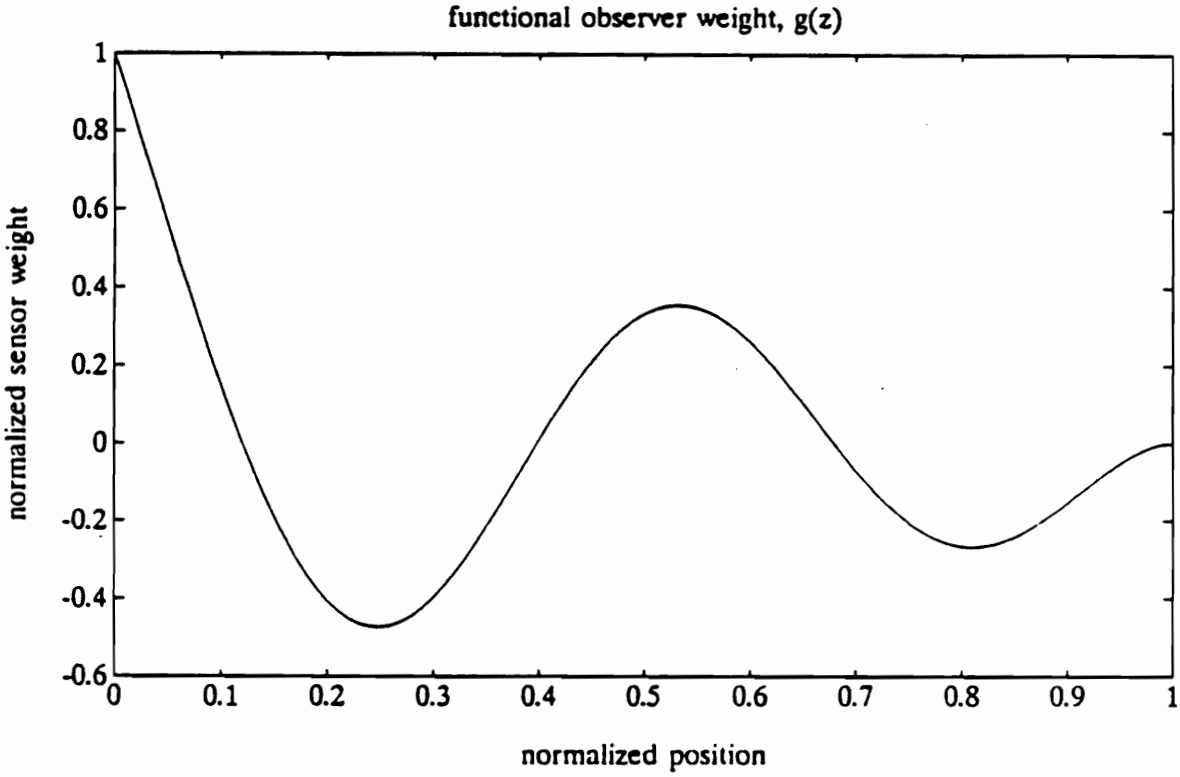

Figure 4.4.3 Normalized weighting function, $g(z)/||g(z)||_\infty$, for the functional observer described in Example 4.4.5.

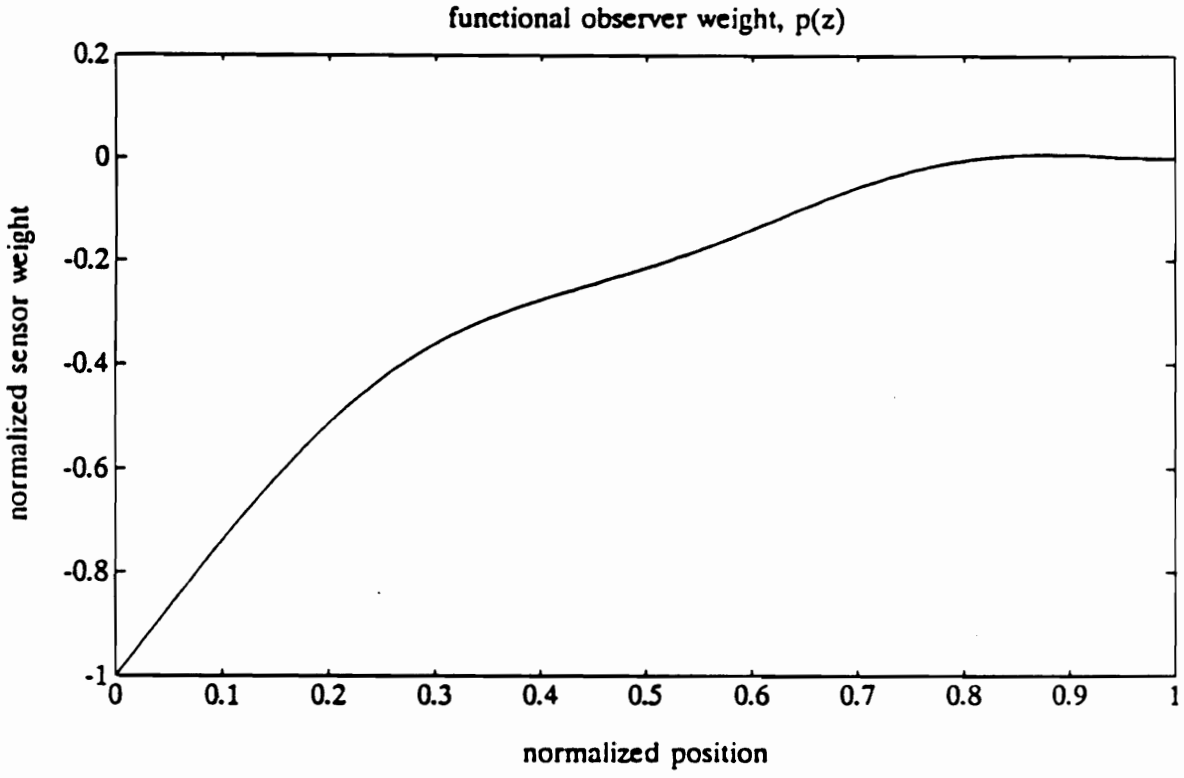

Figure 4.4.4 Normalized weighting function, $p(z)/\parallel p(z) \parallel_{\infty}$, for the functional observer described in Example 4.4.5.

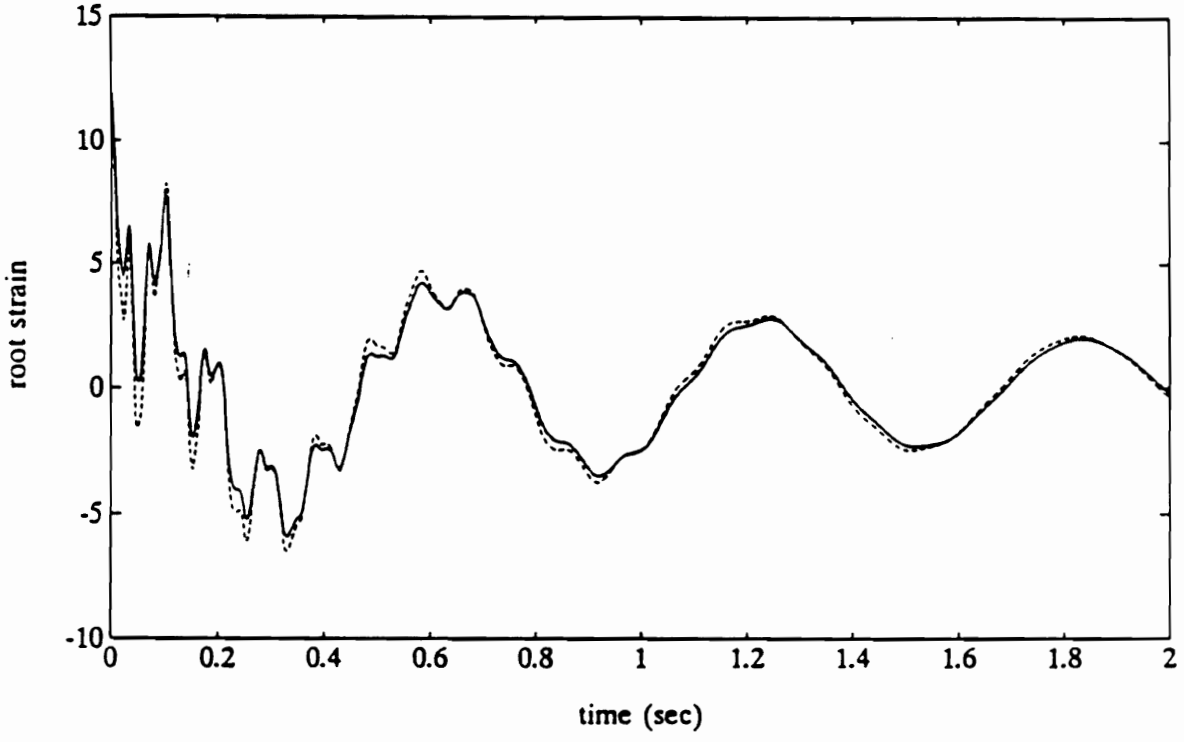

Figure 4.4.5 Ideal closed-loop system response and closed-loop response using the functional observer.

are realizable using distributed-effect sensors. Several design criteria for the selection of distributed-effect sensor weighting functions were described and several of these design techniques were applied to the selection of sensor weights for the control of a cantilevered beam.

5. Distributed-effect modal domain optical fiber sensors

The purpose of this chapter is to explore the use of modal domain optical fiber sensors as distributed-effect sensors. The sensor sensitivity depends on the sensor parameters and the orientation of the sensor with respect to the test article. By varying these design parameters, the sensor sensitivity can be altered in a prescribed manner along the sensor gauge length to implement the distributed-effect sensor designs described in Chapter 4

Section 5.1 describes the effects of parameter variations on the sensitivity of modal domain optical fiber sensors. Section 5.2 describes a proposed method for implementing distributed-effect sensor designs using modal domain optical fibers with spatially varying sensitivity to strain.

5.1. THE EFFECTS OF PARAMETER VARIATIONS ON SENSOR SENSITIVITY

In Chapter 2, expressions for the sensitivity of modal domain optical fiber sensors to applied strain were derived from the mathematical model of the sensor. This section describes the effects of variations in the sensor parameters and the sensor orientation on the sensor sensitivity.

The expression for the sensor sensitivity derived in Chapter 2 shows that the sensor sensitivity is proportional to a quantity $\Delta\tilde{\beta}$ which depends on the sensor orientation and the solutions to the waveguide characteristic equation. The solutions to the waveguide characteristic equation depend on the laser wavelength, the radius of the fiber core, and the indices of refraction of the fiber core and cladding. The solutions to the waveguide characteristic equation are more sensitive to the relative difference between the indices of refraction of the core and cladding than their actual values; hence, in this study the index of refraction of the fiber core remains constant and only variations in the index of refraction of

the cladding are considered.

5.1.1. Parameter variation constraints

The intensity pattern monitored at the endface of the sensor's sensing-section fiber is generated by the interference of electromagnetic modes propagating in the fiber. Which modes propagate in the sensing-section fiber depend on the sensor parameters, and the conditions under which light is launched into the fiber. The normalized frequency, or V-number

$$V = \frac{2\pi}{\lambda} a \, (n_{co}^2 - n_{cl}^2)^{1/2} , \tag{5.1.1}$$

relates the sensor parameters to the solutions of the waveguide characteristic equation, which determine the propagation constants of the modes propagating in the fiber sensing section. To insure that the desired electromagnetic modes propagate in the sensor's sensing section, the normalized frequency is restricted to the range

$$2.405 < V < 3.832.$$

Figure 5.1.1 shows the effect of variations in the laser wavelength, fiber core radius, and cladding index of refraction on the normalized frequency. In each plot, one parameter is varied while the others are maintained at their nominal values. If

$$\mathcal{P} = \{(a, \lambda, n_{co}, n_{cl}) \,|\, 0 < \lambda \, , \, 0 < a \, , \, 1 < n_{co} < n_{cl} \} , \tag{5.1.2}$$

denotes the set of all possible combinations of sensor parameters, the restriction on the range of V for the modal domain optical fiber sensor defines a subset

$$\mathcal{S} = \{ (a, \lambda, n_{co}, n_{cl}) \in \mathcal{P} \,|\, 2.405 < V < 3.832 \} \subset \mathcal{P} , \tag{5.1.3}$$

containing the permissible combinations of the sensor parameters. If the index of refraction of the fiber core is fixed at some nominal value the dimension of the

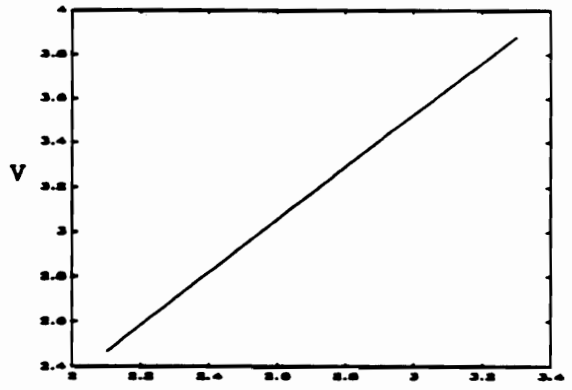

(a)

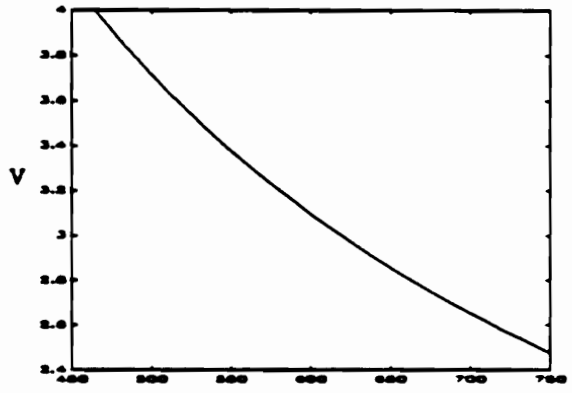

(b)

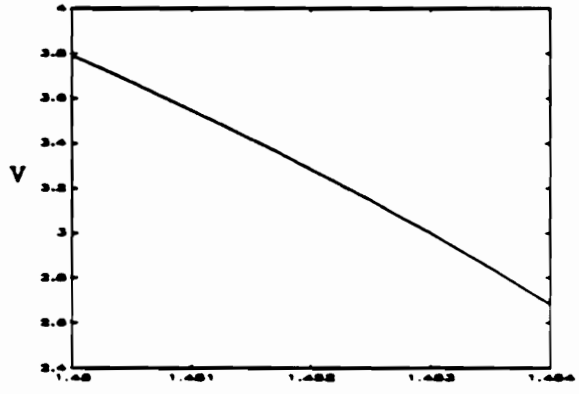

(c)

Figure 5.1.1 Effects of parameter variations on normalized frequency: (a) fiber core radius, (b) laser wavelength, (c) cladding index of refraction.

parameter space is reduced to 3.

The set $\mathcal{S}$ also defines absolute limits on the sensor's operating range. For a given set of nominal sensor parameters, the sensor's operating range is defined by the range of $\bar{\epsilon}$, for which

$$(a(\bar{\epsilon}), \lambda, n_{co}(\bar{\epsilon}), n_{cl}(\bar{\epsilon})) \in \mathcal{S}.$$

If the strained values of the sensor parameters correspond to a point outside the set $\mathcal{S}$, then the V-number of the sensor's sensing-section fiber will be outside the required range and the sensor will fail to behave in the expected manner. Consequently, the expected range of the strain to which the sensor will be exposed must be considered when choosing the sensor parameters.

5.1.2. The effects of parameter variations on sensitivity

From Chapter 2, for operation in the sensor's linear range, the sensor sensitivity to parametric strain is given by

$$S_Q^l = I_2 \int_S \Delta\tilde{\beta} \, ds \, . \tag{5.1.4}$$

For $\bar{\epsilon}^0 = 0$,

$$\Delta\tilde{\beta} = \Delta\beta_0 \frac{\partial\epsilon_1}{\partial\epsilon} + \sum_{j=1}^{6} \frac{\partial\Delta\beta_0}{\partial\epsilon_j} \frac{\partial\epsilon_j}{\partial\epsilon} \, , \tag{5.1.5}$$

where $\Delta\beta_0$ denotes the nominal difference in the propagation constants of the two electromagnetic modes propagating in the sensor's sensing section, and ϵ_j denotes the j-th component of the tensor representation of the strain induced in the fiber core. The quantity $\Delta\tilde{\beta}$ depends on the sensor orientation through the partial derivatives $\partial\epsilon_j/\partial\epsilon$, and on the sensor parameters through the solutions to the waveguide characteristic.

Experimental evidence suggests that modal domain optical fiber sensors mounted on the surface of flexible structures respond primarily to the component of the structural strain in the direction tangent to the fiber path [38]. Therefore, for one-dimensional structures such as flexible beams, the strain transferred to the

optical fiber sensor is proportional to the tensor

$$\bar{\epsilon} = \begin{bmatrix} 1 \\ -\nu_f \\ -\nu_f \\ 0 \\ 0 \\ 0 \end{bmatrix} \cos^2\theta \; \epsilon(z,t) \; , \tag{5.1.6}$$

where $\epsilon(z,t)$ denotes the strain at the surface of the beam, ν_f and ν_b denote Poisson's ratios for the fiber and beam respectively, and θ denotes the orientation of the sensor with respect to the longitudinal axis of the beam at the point z.

From (5.1.6), $\Delta\tilde{\beta}$ for an optical fiber sensor mounted on the surface of a flexible beam is given by

$$\Delta\tilde{\beta} = \left\{ \Delta\beta_0 + \frac{\partial\Delta\beta_0}{\partial\epsilon_1} - \nu_f \frac{\partial\Delta\beta_0}{\partial\epsilon_2} - \nu_f \frac{\partial\Delta\beta_0}{\partial\epsilon_3} \right\} \cos^2\theta \; . \tag{5.1.7}$$

Figure 5.1.2 shows the dependence of $\Delta\tilde{\beta}$ on the orientation of the sensor's sensing section fiber with respect to the longitudinal axis of the beam. Figure 5.1.2 shows that the sensor is most sensitive when $\theta = 0$, and least sensitive for $\theta = \pm 90^{\circ}$. For a nominal value of $\Delta\tilde{\beta}$, say $\Delta\tilde{\beta} = \Delta\tilde{\beta}_0$, varying the sensor orientation permits variations in the sensitivity such that

$$\Delta\tilde{\beta}_0 \geq \Delta\tilde{\beta}(z) \geq 0 \; . \tag{5.1.8}$$

When $\theta = 0$, the sensor is said to be subject to axial parametric strain [18].

Figure 5.1.3 shows the effects of variations in the fiber core radius, the laser wavelength, and the cladding index of refraction on $\Delta\tilde{\beta}$ for axial parametric strain. Figure 5.1.4 compares the effects of relative variations in each sensor parameter - in terms of a percentage of their respective nominal values - on $\Delta\tilde{\beta}$, and Figure 5.1.5 shows plots of $\Delta\tilde{\beta}$ versus V for variations in the fiber core radius, laser wavelength, and cladding index of refraction.

Figures 5.1.3-5 show that, for the parameter variations considered, $\Delta\tilde{\beta}$ is most sensitive to variations in the index of refraction of the fiber cladding, and least sensitive to variations in the fiber core radius. Figure 5.1.5 shows that for

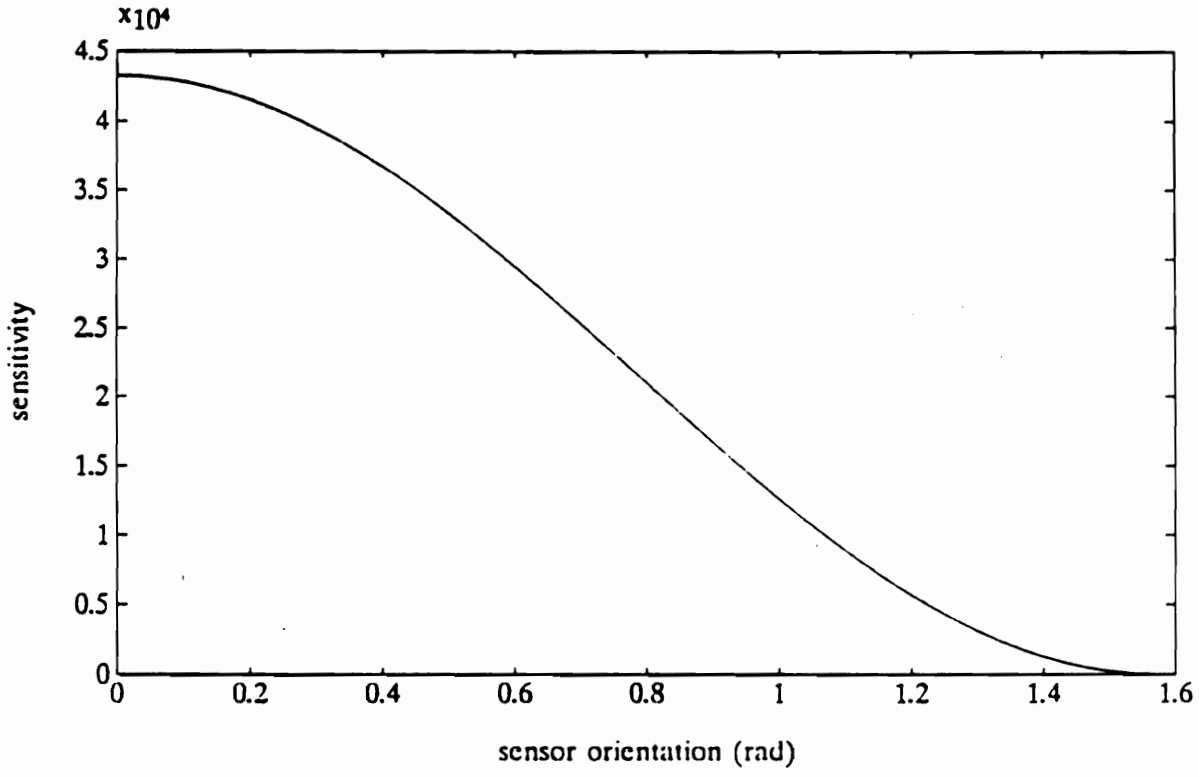

Figure 5.1.2 Effect of sensor orientation on sensitivity.

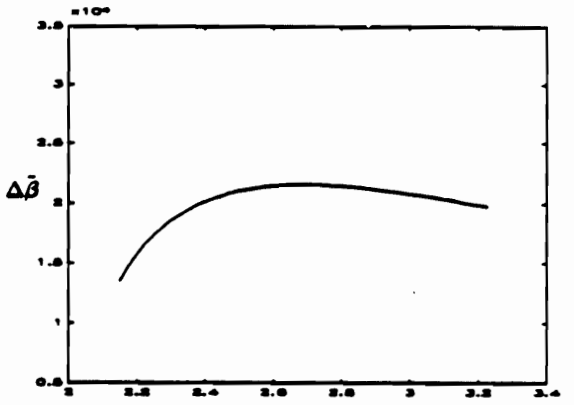

(a)

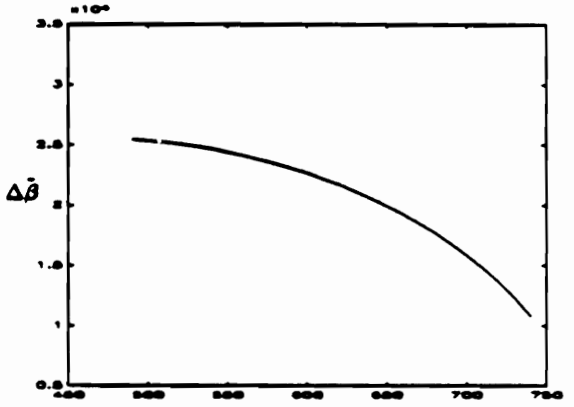

(b)

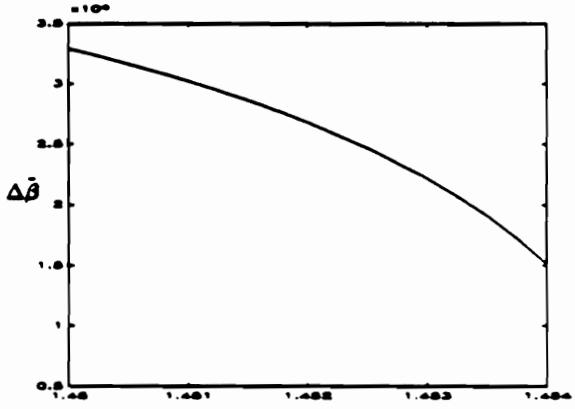

(c)

Figure 5.1.3 Effects of parameter variations on $\Delta\tilde{\beta}$ for axial strain: (a) fiber core radius, (b) laser wavelength, (c) cladding index of refraction.

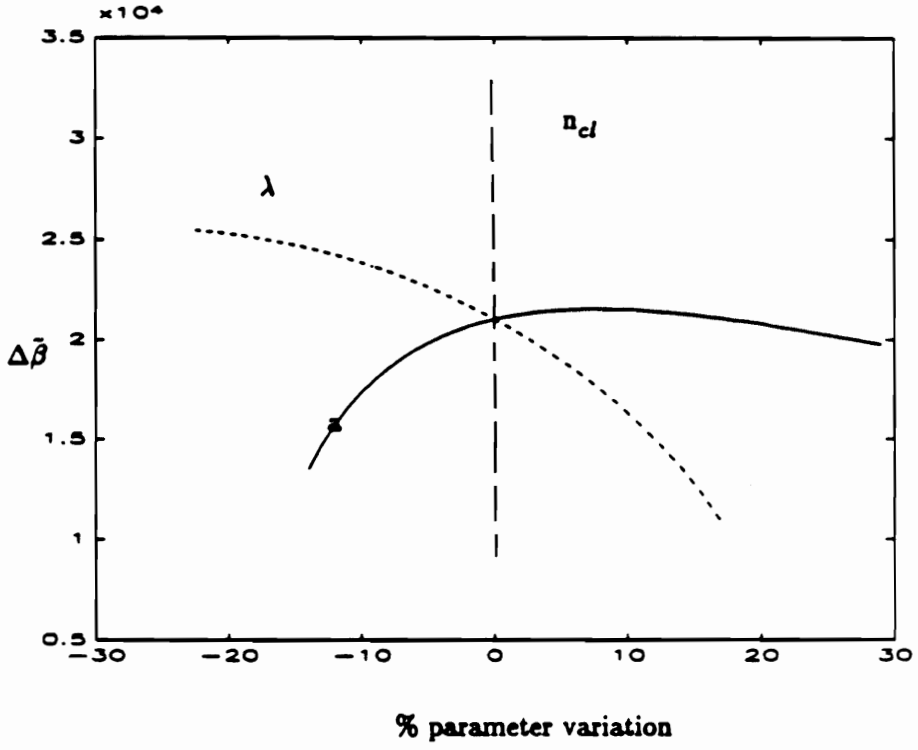

Figure 5.1.4 Effects of relative parameter variations (in % of their nominal values) on $\Delta\tilde{\beta}$ for axial parametric strain.

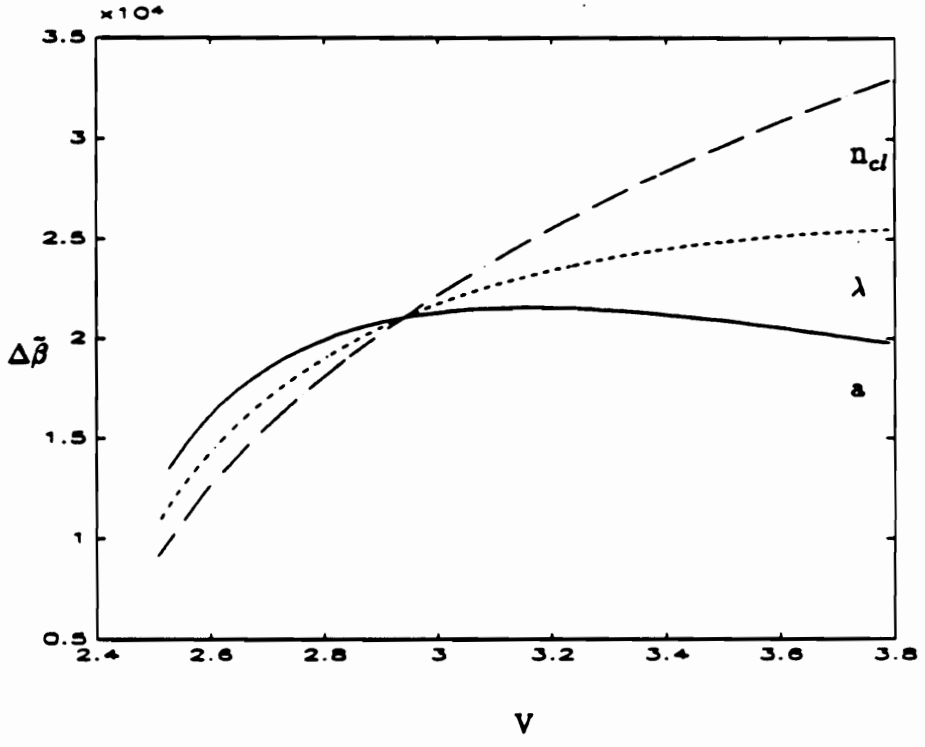

Figure 5.1.5 $\Delta\tilde{\beta}$ for axial parametric strain versus normalized frequency (V) for variations in the sensor parameters.

variations in the laser wavelength and cladding index of refraction, the sensitivity is maximized by operating at the largest allowable normalized frequency. For variations in the fiber core radius, however, the maximum value of $\Delta\tilde{\beta}$ does not correspond to the maximum of V.

Table 5.1.1 shows the nominal value of $\Delta\tilde{\beta}$ for axial parametric strain, and the minimum and maximum values of $\Delta\tilde{\beta}$ that can be achieved by varying the laser wavelength, cladding index of refraction, and fiber core radius as shown in Figure 5.1.2. The maximum value of $\Delta\tilde{\beta}$ listed in Table 5.1.1 corresponds to an 86% increase over the nominal value, while the minimum value corresponds to a 46% decrease. This demonstrates the range of sensor sensitivity that might be achievable by spatially varying the sensor parameters over the sensor gauge length.

Although the sensor orientation can be used to alter the sensor sensitivity along its gauge length, the relationship between sensor orientation and sensitivity becomes more complicated for more complicated structural geometries such as plates and shells. The relationship between orientation and sensitivity is also more complicated for embedded sensors. Consequently, the preferred method for changing the sensor sensitivity for more general sensor applications is variation of the sensor parameters.

The fiber core radius and cladding index of refraction represent sensor parameters that could be varied in a predetermined spatial pattern to achieve a desired spatial sensor sensitivity. The core radius can be varied by varying the speed with which the fiber is drawn during the manufacturing process, and the cladding index of refraction can be varied by spatially varying the doping of the cladding material in the preform from which the fiber is drawn. The first method - changing the radius of the fiber core - has already been used to construct a weighted modal domain optical fiber sensor [26]. Although the laser wavelength cannot be varied along the sensor gauge length, knowledge of its effect on the sensor sensitivity is important for optimizing the choice of the ranges of variation for the other two parameters.

Table 5.1.1 Nominal, maximum, and minimum values of the sensor sensitivity.

value	sensitivity	r (μm)	n_{cl}	λ (nm)	V (rad)
nominal	4.3239e+004	2.5	1.4532	632	2.938
maximum	8.1543e+004	2.1	1.450	530	3.797
minimum	7.2692e+003	3.225	1.4532	640	3.743

5.2. DISTRIBUTED-EFFECT SENSOR IMPLEMENTATION

In Chapter 4, a number of criteria were considered for selecting the weighting functions for designing distributed-effect sensors. Section 5.1 described the effects of variations in the fiber core radius and cladding index of refraction on the sensitivity of a modal domain optical fiber sensor to strain. In this section the implementation of distributed-effect sensor weighting functions using modal domain optical fiber sensors is considered.

Chapter 3 described the incorporation of the linear design model of the modal domain optical fiber sensor into the mathematical model of a flexible structure. For a straight section of fiber mounted on the surface of a flexible structure, the sensor output is proportional to

$$y_f(t) = \int_S \Delta\tilde{\beta}(s)\epsilon_1(s,t)\mathrm{d}s \ , \tag{5.2.1}$$

where $\Delta\tilde{\beta}$ denotes the sensor sensitivity to axial strain, given in (5.1.7) with $\theta = 0$, and ϵ_1 denotes the axial strain induced in the sensor. For a modal domain optical fiber sensor mounted on the surface of a flexible beam, parallel to the beam's longitudinal axis, Equation (5.2.1) becomes

$$y_f(t) = \int_\Omega \Delta\tilde{\beta}(z)\epsilon(z,t)\ \mathrm{d}z \ , \tag{5.2.2}$$

where Ω denotes the domain of the structure, and $\epsilon(z,t)$ denotes the strain at the surface of the beam.

By varying the fiber core radius and cladding index of refraction, the sensor sensitivity, $\Delta\tilde{\beta}$, can be varied in a prescribed manner. The problem with trying to implement arbitrary sensor weighting functions using modal domain optical fiber sensors is that for a single fiber the weighting function is restricted to a range of values of the form

$$a \leq \Delta\tilde{\beta}(z) \leq b \ , \tag{5.2.3}$$

where a and b are both positive. Bipolar weighting function can be implemented, however, by using differential techniques.

Let $g(z)$ denote a desired distributed-effect weighting function. If the set of realizable modal domain optical fiber sensor sensitivities are described by bounds of the form given in Equation (5.2.3), then

$$0 \leq \frac{\Delta\tilde{\beta}(z) - a}{(b-a)} \leq 1 \ . \tag{5.2.4}$$

The desired weighting function $g(z)$ can be expressed as

$$g(z) = \| g(z) \|_{\infty} \left(\ g_{+}(z) - g_{-}(z) \ \right), \tag{5.2.5}$$

where

$$g_{+}(z) = \begin{cases} g(z)/\| g(z) \|_{\infty} & , 0 \leq g(z) \\ 0 & , g(z) \leq 0 \end{cases} \tag{5.2.6}$$

and

$$g_{-}(z) = \begin{cases} 0 & , 0 \leq g(z) \\ g(z)/\| g(z) \|_{\infty} & , g(z) \leq 0 \ . \end{cases} \tag{5.2.7}$$

From the definitions of $g_{+}(z)$ and $g_{-}(z)$,

$$| \ g_{-}(z) \ | \leq 1 \ , \quad \text{and} \ | \ g_{+}(z) \ | \leq 1 \ . \tag{5.2.8}$$

The desired weighting function, $g(z)$, can be realized by defining two modal domain optical fiber sensitivity profiles

$$\Delta\beta_{+}(z) = (b-a) g_{+}(z) + a \ , \tag{5.2.9}$$

and

$$\Delta\beta_{-}(z) = (b-a) g_{-}(z) + a \ , \tag{5.2.10}$$

each of which satisfies the constraints given in (5.2.3). Subtracting the outputs of two modal domain optical fiber sensor with the sensitivity profiles $\Delta\beta_{+}(z)$ and

$\Delta\beta_{-}(z)$ respectively and scaling by an appropriate gain yields a sensor output with the corresponding weighting function

$$g(z) = \frac{\|g(z)\|_\infty}{(b-a)} \left(\Delta\beta_{+}(z) - \Delta\beta_{-}(z) \right). \tag{5.2.11}$$

A block diagram of the implementation of the distributed-effect sensor weighting function $g(z)$ described by Equation (5.2.11) is shown in Figure 5.2.1.

5.3. SUMMARY

In this chapter the effects of parameter variations on the sensitivity of modal domain optical fiber sensors were described, and a method was proposed for implementing arbitrary distributed-effect sensor weighting functions using modal domain optical fiber sensors with spatially varying sensitivity. Because the allowable parameter variations only permit bounded, positive sensor sensitivity profiles, a differential technique requiring two weighted sensors is required to implement bipolar weighting functions.

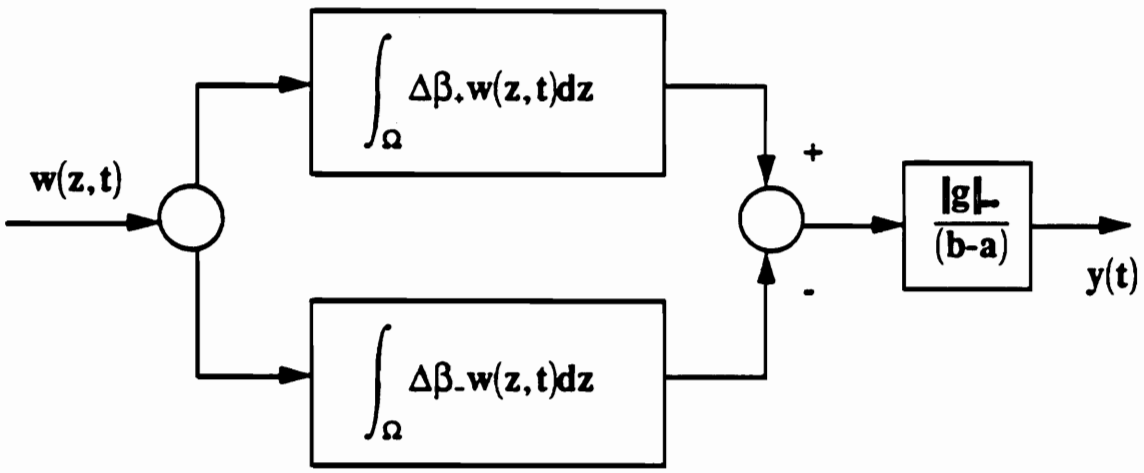

$$y(t)=\int_\Omega g(z)w(z,t)dz$$

Figure 5.2.1 Differential implementation of bipolar weighting functions.

6. The effects of weighting function errors on sensor performance

Chapter 4 described several criteria for selecting weighting functions for distributed-effect sensors, assuming no restrictions on the set of realizable weighting functions. In practice, the weighting function realized in the construction or manufacture of the sensor will differ from the desired weighting function. As a result of this deviation, the performance of a control law which uses the output of the sensor may degrade. This chapter describes the effects of errors in the weighting function of a distributed-effect on the performance of the sensor relative to the closed-loop control objectives of the system.

The effects of differences between desired and achieved weighting functions on the output of a distributed-effect sensor were reported by Lee & Moon [14]. Lee and Moon implemented a spatial filter designed to measure the first modal amplitude for a cantilevered beam using piezoelectric film. The sensor was fabricated by removing the metalic coating on the PVDF film so that the sensor's conducting electrode was in the shape of the beam's first vibrational mode. The sensor's output, however, contained a significant component attributed to the beam's second mode, in addition to the desired first mode. Examination of the sensor's conducting electrode showed that the edge of the conducting electrode was not smooth, as it should have been for the desired weighting function, but rough - indicating the presence of higher modal components in the achieved weighting function.

In order to study the effects of spatial filter errors on the performance of distributed-effect sensors, some knowledge of the nature of the errors is assumed - either global knowledge about the nature of the error, or knowledge about the spatial frequency (or modal) content of the error. Two ways of characterizing the errors are proposed - a deterministic characterization and a probabilistic characterization.

Section 6.1 describes the types of limitations that may be placed on the set

of realizable weighting functions for distributed-effect sensors. Section 6.2 defines the spatial filter error which results when the weighting function for an implemented sensor design differs from the desired weighting function and describes the relationship between the spatial filter error and the resulting error in the sensor output. Section 6.3 describes deterministic and probabilistic characterizations of the filter error. Section 6.4 describes the effects of spatial filter errors on sensor performance for several distributed-effect sensor design criteria. The effects of errors in the weighting functions of distributed-effect sensors on the measurement of strain in a cantilevered beam are demonstrated.

6.1. LIMITATIONS ON REALIZABLE SENSOR WEIGHTS

The output of a distributed-effect sensor configured to measure strain in a one-dimensional flexible structure is given by

$$y(t) = \int_{\Omega} g(z)\epsilon(z,t)\mathrm{d}z, \tag{6.1.1}$$

where Ω denotes the structures domain, and $g(z)$ is the sensor's weighting function. The design criteria for selecting the weighting function $g(z)$ that were described in Chapter 4 assumed no restrictions on the set of realizable weighting functions. The weighting function realized in the implementation of a distributed-effect sensor, however, may deviate from the desired weighting function due to limitations imposed by the manufacturing process associated with the sensor technology used.

Each type of distributed-effect sensing technology - modal domain optical fiber sensors, piezoelectric film, holographic sensing, etc. - will impose its own restrictions on the set of realizable weighting functions. Three general classes of restrictions that may be expected with any type of sensing technology include:

1. Bounds on the range of $g(z)$,
2. Bounds on the rate of change (spatial) of the weighting function,
3. Limits on the resolution of $g(z)$.

Each of these restrictions is considered below.

Bounds on the range of realizable weighting functions would restrict $g(z)$ to a set of the form

$$\mathcal{G}_1 \triangleq \left\{ g(z) \,|\, a \leq g(z) \leq b \right\}, \tag{6.1.2}$$

where a and b denote the minimum and maximum realizable values of the weighting function for a particular type of distributed-effect sensor. Technically, for all three distributed-effect sensor technologies described in Chapter 4, the lower limit in Equation (6.1.2) is $a = 0$. In piezoelectric sensors, however, bipolar weighting functions have been implemented by reversing the electromagnetic poling or the polarity of the electrical leads in different sections of the piezoelectric film. For the holographic sensor and the modal domain optical fiber sensor bipolar weighting functions are implemented using differential techniques such as the one described in Chapter 5.

When differential techniques are used in the implementation bipolar weighting functions, the set $\mathcal{G}_1$ becomes

$$\mathcal{G}_1 = \left\{ g(z) \;\; | \;\; \|g(z)\|_\infty \leq b - a \right\} , \tag{6.1.3}$$

since for differential implementation strategies the sensor should have the same range of positive and negative realizable sensor weights. For piezoelectric sensors, the upper bound on the magnitude of the realizable sensor weights is a function of the width of the piezoelectric film (or the width of the structure) or the achievable variation in the poling of the piezoelectric. For the modal domain optical fiber sensor, the maximum achievable sensitivity is related to the restrictions on the fiber's normalized frequency as described in Chapter 5.

When restrictions are placed on the spatial rate of change of the weighting function, the realizable weighting functions belong to a set of the form

$$\mathcal{G}_2 = \left\{ g(z) \,|\, c \leq \frac{\partial g(z)}{\partial z} \leq d \right\}. \tag{6.1.4}$$

If $c = -d$, then

$$\mathcal{G}_2 = \left\{ \; g(z) \;\; | \;\; \left\| \frac{\partial g(z)}{\partial z} \right\|_{\infty} \leq d \; \right\} . \tag{6.1.5}$$

Restrictions of this type would most likely be related to limits on the ability to vary the necessary parameters over the sensor's spatial domain in the sensor fabrication process. For piezoelectric sensors this means either limits on the ability to cut or etch the piezoelectric film in the desired shape, or limits on the spatial rate at which the poling of the piezoelectric material can be varied. For modal domain optical fiber sensors, the bound d in Equation (6.1.5) would be related to the manufacturing process by which the optical fiber is drawn from a preformed silica rod, or the process by which the cladding is doped in the optical fiber preform.

The final type of restriction on realizable sensor weights, limits on the resolution of the implemented weighting function, is a function of the accuracy of the manufacturing process used in the implementation of the desired distributed-effect sensor. Regardless of the sensing technology used, there will most likely be some level of error beyond which the value of the weighting function cannot be controlled. This is analogous to the signal-to-noise ratio in signal processing.

Bounds on the magnitude and spatial rate of change of realizable weighting functions can be compensated for in the design process by scaling the desired weighting functions. Suppose $g(z)$ denotes the desired weighting function determined using one of the design criteria described in Chapter 4, and let the restrictions on the set of realizable weighting functions take the form of bounds on the magnitudes of $g(z)$ and $\partial g(z)/\partial z$ as in Equations (6.1.3) and (6.1.5). Assuming $a = 0$ in Equation (6.1.3), let

$$\epsilon_B = \max\{b, d\}, \tag{6.1.6}$$

and

$$\mathrm{K} = \max \left\{ \| g(z) \|_{\infty} , \left\| \frac{\mathrm{d}g(z)}{\mathrm{d}z} \right\|_{\infty} \right\} . \tag{6.1.7}$$

If

$$\tilde{g}(z) = \frac{\epsilon_B}{\mathrm{K}} \, g(z) \, , \tag{6.1.8}$$

then

$$\|\tilde{g}(z)\|_{\infty} = \frac{\epsilon_B}{K} \|g(z)\|_{\infty} \leq \epsilon_B \leq b, \tag{6.1.9}$$

and

$$\left\|\frac{d\tilde{g}(z)}{dz}\right\|_{\infty} = \frac{\epsilon_B}{K} \left\|\frac{dg(z)}{dz}\right\|_{\infty} \leq \epsilon_B \leq d. \tag{6.1.10}$$

Therefore, $\tilde{g}(z) \in \mathcal{G}_1 \cap \mathcal{G}_2$, which implies that $\tilde{g}(z)$ is a realizable weighting function.

Because the output of a distributed-effect sensor is a linear function of the weighting $g(z)$, scaling the weighting function simply scales the sensor output, and does not effect the spatial filter function implemented by the sensor. Therefore, if $\tilde{y}(t)$ denotes the output of the distributed-effect sensor with the realizable weighting function $\tilde{g}(z)$, then the desired sensor output is given by

$$y(t) = \frac{K}{\epsilon_B} \tilde{y}(t) \, . \tag{6.1.11}$$

This shows that restrictions on the magnitude and gradient of the weighting function can be accommodated by scaling the desired weighting function; hence, most errors in the weighting function will result from limits on the resolution of $g(z)$, and not from limits on the range or spatial rate of change of the weighting function.

6.2. SPATIAL FILTER ERRORS

The weighting function that is realized when a distributed-effect sensor is fabricated may deviate from the desired weighting function.

Definition 6.2.1: If $g(z)$ denotes the desired weighting function for a spatial filter, and $\widehat{g}(z)$ denotes the weighting function achieved in the fabrication of the sensor, then

$$n(z) \triangleq \widehat{g}(z) - g(z) \tag{6.2.1}$$

is defined as the spatial filter error. □

Suppose $g(z)$ denotes the desired weighting function for a distributed-effect sensor which measures the distributed quantity $m(z,t)$, and the desired sensor output is given by

$$y(t) = \int_{\Omega} g(z)\, m(z,t)\, \mathrm{d}z, \tag{6.2.2}$$

where Ω denotes the sensor's spatial domain. If $\widehat{g}(z)$ denotes the weighting function that is realized in the fabrication of the sensor, then the sensor's actual output is given by

$$\widehat{y}(t) = \int_{\Omega} \widehat{g}(z)\, m(z,t)\, \mathrm{d}z\ . \tag{6.2.3}$$

The error in the achieved weighting function produces a corresponding error in the sensor output.

Definition 6.2.2: If $y(t)$ denotes the desired output of a distributed-effect sensor and $\widehat{y}(t)$ denotes the output that is achieved when the sensor is fabricated, then

$$e(t) \triangleq \widehat{y}(t) - y(t)\ . \tag{6.2.4}$$

is called the sensor output error. □

Substituting the expressions for the desired and achieved sensor outputs into (6.2.4) yields

$$\begin{aligned} e(t) &= \int_{\Omega} \hat{g}(z)\, m(z,t)\, \mathrm{d}z - \int_{\Omega} g(z)\, m(z,t)\, \mathrm{d}z \\ &= \int_{\Omega} \Big(\hat{g}(z) - g(z) \Big)\, m(z,t)\, \mathrm{d}z\ , \\ &= \int_{\Omega} n(z)\, m(z,t)\, \mathrm{d}z\ . \end{aligned} \tag{6.2.5}$$

Hence, an equivalent representation of the sensor output error is as the output of a distributed-effect sensor with the weighting function $n(z)$, the spatial filter error.

Section 4.3 described the integration of the distributed-effect sensor model into state-space models of flexible structures. If $m(z,t)$ is described by a set of basis functions $\{\xi_j(z)\}$, and the weighting function $g(z)$ is described by another set of basis functions $\{\gamma_j(z)\}$, then the output of the distributed-effect sensor can be written as

$$y(t) = \mathrm{C}x(t)\ , \tag{6.2.6}$$

where C is given by (4.3.7), and $x(t)$ is the corresponding state vector. If the set $\{\gamma_j(z)\}$ forms a basis for the set of all square-integrable functions defined over the spatial domain Ω, then there exists a representation of the spatial filter error such that

$$n(z) = \sum_{i=1}^{\infty} n_i\, \gamma_i(z)\ , \tag{6.2.7}$$

where

$$n_i = \int_{\Omega} n(z)\, \gamma_i(z)\, \mathrm{d}z\ . \tag{6.2.8}$$

For computational purposes, the spatial filter error is approximated by its projection on the span of some finite-dimensional subset of the basis functions $\{\gamma_j(z)\}$, so that

$$n(z) = \sum_{i=1}^{M} n_i \, \gamma_i(z) \, . \tag{6.2.9}$$

It is possible that in order to accurately model the spatial filter error the number M in (6.2.9) will be larger than the number of modes included in the state space model of the structure.

In order to incorporate the effects of the spatial filter error in the state space model of the system, the state vector, $x(t)$, can be defined as

$$x(t) = \begin{bmatrix} x_c(t) \\ x_r(t) \end{bmatrix}, \tag{6.2.10}$$

where $x_c(t)$ models the structural dynamics associated with the modes η_j for $j = 1, 2, \ldots, N$, and $x_r(t)$ models the structural dynamics associated with the modes η_j for $j = N+1, N+2, \ldots, M$. The modes included in x_c are called the residual or modelled modes, and the modes included in x_r are called residual modes.

Substituting (6.2.9) into the expression for the sensor output error, and including the residual modes in the decomposition of $m(z,t)$ yields

$$\begin{aligned} e(t) &= \sum_{k=1}^{M} \left\{ \int_{\Omega} n(z) \, \xi_k(z) \, \mathrm{d}z \right\} \eta_k(t) \\ &= \sum_{k=1}^{M} \left\{ \sum_{i=1}^{M} n_i \int_{\Omega} \gamma_i(z) \, \xi_k(z) \, \mathrm{d}z \right\} \eta_k(t) \\ &= \sum_{k=1}^{M} \delta c_k \eta_k(t) \, , \end{aligned} \tag{6.2.11}$$

where

$$\delta c_k = \sum_{i=1}^{M} n_i \int_{\Omega} \gamma_i(z) \, \xi_k(z) \, \mathrm{d}z. \tag{6.2.13}$$

Defining the $M \times M$ matrix Q_M with elements

$$q_{kj} = \int_{\Omega} \gamma_k(z) \, \xi_j(z) \, \mathrm{d}z, \tag{6.2.14}$$

equation (6.2.11) can be written in matrix form as

$$\delta \mathrm{C} = \mathrm{N}\mathrm{Q}_M \ , \tag{6.2.15}$$

where

$$\mathrm{N} = [n_1 \ n_2 \cdots n_M] \ . \tag{6.2.16}$$

If $g(z)$ is given by equation (3.3.4) and $n(z)$ by (6.2.9), then the achieved weighting function, $\widehat{g}(z)$ is given by

$$\widehat{g}(z) = \sum_{i=1}^{M} \widehat{g}_i \ \gamma_i(z) \ , \tag{6.2.17}$$

where

$$\widehat{g}_i = g_i + n_i \ , \tag{6.2.18}$$

with $g_i = 0$ for $N+1 \leq i \leq M$. Substituting (6.2.17) into the expression for the achieved sensor output and including the residual modes in the expression for the distributed signal $m(z,t)$ yields

$$\widehat{y}(t) = \sum_{i=1}^{M} \widehat{c}_i \eta_i(t) \ , \tag{6.2.19}$$

where

$$\widehat{c}_i = c_i + \delta c_i \ , \tag{6.2.20}$$

with $c_i = 0$ for $N+1 \leq i \leq M$. Using matrix notation,

$$\widehat{y}(t) = \widehat{\mathrm{C}} \ x(t) \ , \tag{6.2.21}$$

where

$$\widehat{\mathrm{C}} = \widehat{\mathrm{G}}\mathrm{Q}_M \ , \tag{6.2.22}$$

with

$$\widehat{G} = [\widehat{g}_1 \; \widehat{g}_2 \cdots \widehat{g}_M] \; . \tag{6.2.23}$$

The output of the achieved distributed-effect sensor can also be written as

$$\widehat{y}(t) = [\; C + \delta C_c \; | \; \delta C_r \;] \; x(t) \quad , \tag{6.2.24}$$

where δC_c and δC_r denote partitions of the error output matrix δC corresponding to x_c and x_r respectively.

Remark: The formulation for $\widehat{y}(t)$ given in (6.2.24) characterizes the effects of spatial filter errors as perturbations in output matrix in the structure's state space model. This formulation is useful because techniques exist for designing control laws that are robust to these types of model uncertainties [48-50].

6.3. CHARACTERIZATION OF THE SPATIAL FILTER ERROR

In order to study the effects of spatial filter errors on the performance of distributed-effect sensors, some knowledge of the nature of the errors is assumed - either global knowledge about the nature of the error, or knowledge about the spatial frequency (or modal) content of the error. This section describes two characterizations of spatial filter error - a deterministic characterization, and a probabilistic characterization. The deterministic characterization is based on an assumption that there exist reasonable deterministic bounds on the filter error; that is, the achieved weighting function is expected to deviate from the desired weighting function by less than some prescribed amount. In the probabilistic characterization the spatial filter error is modelled as a random process with an assumed mean and standard deviation. In both cases, the error characterization reflects the level of the confidence in the fabrication process used to implement weighting functions, $g(x)$.

6.3.1. Deterministic characterization

The deterministic characterization of the spatial filter error can take the form of bounds on the magnitude of either

1. $n(z)$, or
2. the weights, n_i, in Equation (6.2.9).

The first approach assumes there exists a bound $\delta_\infty \geq 0$ such that

$$\| n(z) \|_\infty \leq \delta_\infty \, . \tag{6.3.1}$$

The second approach assumes there exists a set of bounds $\{\delta_i \mid \delta_i \geq 0, i = 1,2,\ldots,M\}$ on the magnitudes of the coefficients n_i in Equation (6.2.9) such that

$$n(z) \in \left\{ n(z) = \sum_{i=1}^{M} n_i \, \gamma_i(z) \; ; \; | n_i | \leq \delta_i, \; i = 1,2,\ldots,M \right\} . \tag{6.3.2}$$

The set in Equation (6.3.2), defined by the bounds $\{\delta_i\}$, corresponds to a neighborhood in the span of the basis functions $\{\gamma_i\}$, centered at $n(z) \equiv 0$.

The bounds associated with the first deterministic characterization of the spatial filter error limits the magnitude of $n(z)$, the characterization of $n(z)$ in (6.3.2) can be used to include knowledge about the spatial frequency content of the error.

The two deterministic characterizations are related - a bound on the magnitude of $n(z)$, defines a set of bounds on the weights n_i, and bounds on the weights n_i define a bound on the magnitude of $n(z)$. Suppose there exists $\delta_\infty \geq 0$ such that $\| n(z) \|_\infty \leq \delta_\infty$. From equation (6.1.8)

$$\begin{aligned} | n_i |^2 &= \left| \int_\Omega n(z) \, \gamma_i(z) \, \mathrm{d}z \right|^2 , \\ &\leq \delta_\infty^2 \int_\Omega | \gamma_i(z) |^2 \, \mathrm{d}z \, , \end{aligned} \tag{6.3.3}$$

for $i = 1,\ldots,M$. Conversely, given a set of bounds $\{n_i\}$ such that $| n_i | \leq \delta_i$ for

each i,

$$\|n(z)\|_\infty \leq \sum_{j=1}^{M} |\delta_j| \, \|\gamma_j(z)\|_\infty \, . \tag{6.3.4}$$

The bounds associated with the deterministic characterization of the spatial filter error also determine bounds on the magnitude of the corresponding sensor output error. Suppose there exists a bound δ_∞ such that $\|n(z)\|_\infty \leq \delta_\infty$, then from (6.1.5),

$$\begin{aligned} |\, e(t) \,|^2 &= \left| \int_\Omega n(z)\, m(z,t)\, dz \right|^2 \\ &\leq \|n(z)\|_\infty^2 \int_\Omega m^2(z,t)\, dz \, . \end{aligned} \tag{6.3.5}$$

If $m(z,t)$ is structural strain, then

$$|\, e(t) \,|^2 \leq \|n(z)\|_\infty^2 \sum_{j=1}^{N} \beta_j^4 \, \eta_j^2(t) \, . \tag{6.3.6}$$

Hence, for strain sensing, the square of the output error is bounded by the magnitude of the spatial filter error and the beam's strain energy.

6.3.2. Probabilistic characterization

The spatial filter error can also be characterized as a random process. The error can be characterized by specifying statistics for $n(z)$ directly, or by specifying statistics for the weights, n_i, in Equation (6.2.9). For the purpose of analyzing the effects of the spatial filter error on system performance, a convenient representation of the error is as a zero-mean Gaussian random process.

If $n(z)$ is modeled as "white" spatial noise, (zero-mean, Gaussian, with standard deviation σ_n), then the expected value of the achieved weighting function at a point z is

$$\begin{aligned} \mathbf{E}\{\, \widehat{g}(z) \,\} &= \mathbf{E}\{\, g(z) + n(z) \,\} \\ &= g(z) + \mathbf{E}\{\, n(z) \,\} \\ &= g(z) \, . \end{aligned} \tag{6.3.7}$$

and the variance of $\widehat{g}(z)$ is

$$\mathbf{E}\{\ [\widehat{g}(z) - g(z)]^2\ \} = \mathbf{E}\{\ n^2(z)\ \} \ = \sigma_n^2\ . \tag{6.3.8}$$

The expected value of the corresponding sensor output error is

$$\begin{aligned} \mathbf{E}\{e(t)\} &= \mathbf{E}\left\{ \int_{\Omega} n(z)\ m(z,t)\ \mathrm{d}z \right\} \\ &= \int_{\Omega} \mathbf{E}\{\ n(z)\ \}\ m(z,t)\ \mathrm{d}z \\ &= 0\ . \end{aligned} \tag{6.3.9}$$

Therefore, the variance of the sensor output error is

$$\begin{aligned} \mathbf{E}\{\ e^2(t)\ \} &= \mathbf{E}\left\{ \int_{\Omega} n(z)\ m(z,t)\ \mathrm{d}z \int_{\Omega} n(u)\ m(u,t)\ \mathrm{d}u \right\} \\ &= \int_{\Omega}\int_{\Omega} \mathbf{E}\Big\{n(z)n(u)\Big\}\ m(z,t)m(u,t)\ \mathrm{d}z\ \mathrm{d}u \\ &= \int_{\Omega}\int_{\Omega} \mathcal{R}_n(z,u)\ m(z,t)\ m(u,t)\ \mathrm{d}z\ \mathrm{d}u \end{aligned} \tag{6.3.10}$$

where $\mathcal{R}_n$ denotes the autocorrelation function for the spatial filter error $n(z)$. When $n(z)$ is modeled as "white" spatial noise,

$$\mathcal{R}_n(z,u) = \sigma_n^2 \delta(z-u)\ , \tag{6.3.11}$$

which implies

$$\mathbf{E}\{e^2(t)\} = \sigma_n^2 \int_{\Omega} m^2(z,t)\ \mathrm{d}z\ . \tag{6.3.12}$$

If $m(z,t)$ is structural strain, then

$$\mathbf{E}\{e^2(t)\} = \sigma_n^2 \sum_{j=1}^{N} \beta_j^4\ \eta_j^2(t)\ . \tag{6.3.13}$$

The probabilistic characterization of $n(z)$ also characterizes the coefficients n_i in (6.2.9). When $n(z)$ is characterized as a zero-mean, Gaussian random process with variance σ_n^2,

$$\begin{aligned} \mathbf{E}\{\, n_i \,\} &= \mathbf{E}\left\{ \int_{\Omega} n(z)\, \gamma_i(z)\, dz \right\} \\ &= \int_{\Omega} \mathbf{E}\Big\{ n(z) \Big\}\, \gamma_i(z)\, dz \\ &= 0 \,. \end{aligned} \tag{6.3.14}$$

The coefficients are also uncorrelated:

$$\begin{aligned} \mathbf{E}\{\, n_i n_j \} &= \mathbf{E}\left\{ \int_{\Omega} n(z)\, \gamma_i(z)\, dz \int_{\Omega} n(u)\, \gamma_j(u)\, du \right\} \\ &= \int_{\Omega}\int_{\Omega} \mathbf{E}\Big\{ n(z) n(u) \Big\}\, \gamma_i(z)\gamma_j(u)\, dz\, du \\ &= \int_{\Omega}\int_{\Omega} \mathcal{R}_n(z,u)\, \gamma_i(z)\gamma_j(u)\, dz\, du \\ &= \sigma_n^2 \delta_{ij} \,. \end{aligned} \tag{6.3.15}$$

Therefore, each coefficient, n_i, also has zero mean and standard deviation σ_n.

Instead of characterizing $n(z)$ as a random process, the spatial filter error can be characterized in terms of the weights, n_i, in the representation of $n(z)$ with respect to a given basis. Suppose each coefficient, n_i, in (6.2.9) is an independent, zero-mean, Gaussian random variable, with variance σ_i^2. The expected value of the spatial filter error at any point z is

$$\begin{aligned} \mathbf{E}\Big\{ n(z) \Big\} &= \mathbf{E}\Big\{ \sum_{i=1}^{N} n_i\, \gamma_i(z) \Big\} \\ &= \sum_{i=1}^{N} \mathbf{E}\Big\{ n_i \Big\}\, \gamma_i(z) \\ &= 0 \,. \end{aligned} \tag{6.3.16}$$

The correlation between the error at any two points z and u is given by

$$
\begin{aligned}
\mathcal{R}_n(z,u) &= \mathbf{E}\Big\{n(z)n(u)\Big\} \\
&= \mathbf{E}\Big\{ \sum_{i=1}^{N} n_i\, \gamma_i(z) \sum_{j=1}^{N} n_j\, \gamma_j(u) \Big\} \\
&= \sum_{i=1}^{N} \sum_{j=1}^{N} \mathbf{E}\Big\{ n_i\, n_j \Big\}\, \gamma_i(z)\, \gamma_j(u) \\
&= \sum_{i=1}^{N} \sum_{j=1}^{N} \sigma_j^2\, \delta_{ij}\, \gamma_i(z)\, \gamma_j(u) \qquad (6.3.17) \\
&= \sum_{j=1}^{N} \sigma_j^2\, \gamma_j(z)\, \gamma_j(u)\ .
\end{aligned}
$$

Hence, even though the weights n_i are uncorrelated, $n(z)$ and $n(u)$ are correlated and depend on the values of the basis functions at the two points z and u.

When the coefficients in the representation of the spatial filter error in a particular basis are independent zero-mean, Gaussian random variables with standard deviation σ_i, the expected value of the resulting sensor output error is also zero,

$$
\mathbf{E}\{e(t)\} = 0\ . \qquad (6.3.18)
$$

The variance of the sensor output error is

$$
\begin{aligned}
\mathbf{E}\{\ e^2(t)\ \} &= \int_{\Omega}\int_{\Omega} \mathcal{R}_n(z,u)\, m(z,t)\, m(u,t)\, \mathrm{d}z\, \mathrm{d}u \\
&= \int_{\Omega}\int_{\Omega} \sum_{j=1}^{N} \sigma_j^2\, \gamma_j(z)\, \gamma_j(u)\, m(z,t)\, m(u,t)\, \mathrm{d}z\, \mathrm{d}u \\
&= \sum_{j=1}^{N} \sigma_j^2 \int_{\Omega} \gamma_j(z)\, m(z,t)\, \mathrm{d}z \int_{\Omega} \gamma_j(u)\, m(u,t)\, \mathrm{d}u \qquad (6.3.19) \\
&= \sum_{j=1}^{N} \sigma_j^2\, q_j^2\, \eta_j^2(t)
\end{aligned}
$$

where q_{jj} is given in (6.2.14), and is equal to β_j^2 is $m(z,t)$ is structural strain.

Comparing (6.3.13) and (6.3.19) shows that the two probabilistic characterizations of the spatial filter error yield the same value for the variance of the output error when $\sigma_j^2 = \sigma_n^2$, for $j = 1,2,\ldots,N$. Comparing the expected values

for the output error variance in the probabilistic characterization of the spatial filter error to the bound on the square value of the output error for the deterministic characterization of $n(z)$ shows that when

$$\mathbf{E}\{n^2(z)\} = \|n(z)\|_\infty^2 \tag{6.3.20}$$

the two characterizations yield similar characterizations of the output error.

Example 6.3.1

Figure 6.3.1 shows the weighting function, $g(z)$, for a distributed-effect strain sensor designed to respond only to the first vibrational mode of a flexible cantilevered beam. Scaling the desired weighting function so that $\| g(z) \|_\infty = 1$ yields the following desired sensor output

$$y(t) = \left[\frac{\sqrt{l}}{2}\beta_1^2 \quad 0 \quad 0 \quad 0\right]\eta(t)$$

Figure 6.3.2 shows a plot of

$$\hat{g}(z) = g(z) + n(z)$$

when $n(z)$ is characterized as a zero-mean, Gaussian random process with variance $\sigma_n^2 = 10^{-4}$. The resulting sensor output is given by

$$y(t) = \left[\left(\frac{\sqrt{l}}{2}\beta_1^2 + \beta_1^2 n_1\right) \quad \beta_2^2 n_2 \quad \beta_3^2 n_3 \quad \beta_4^2 n_4\right]\eta(t)$$

where each n_i is a zero-mean Gaussian random variable with variance σ_n^2. Figure 6.3.3 shows $\hat{g}(z)$ for a zero-mean, Gaussian spatial filter $n(z)$ with $\sigma_n^2 = 10^{-2}$.

The dashed lines in each plot denote the minimum and maximum values of $\hat{g}(z)$ when the magnitude of the spatial filter error is characterized by the deterministic bound $\|n(z)\|_\infty^2 \leq \sigma_n^2$; that is,

$$g(z) - \sigma_n^2 \leq \hat{g}(z) \leq g(z) + \sigma_n^2 \,.$$

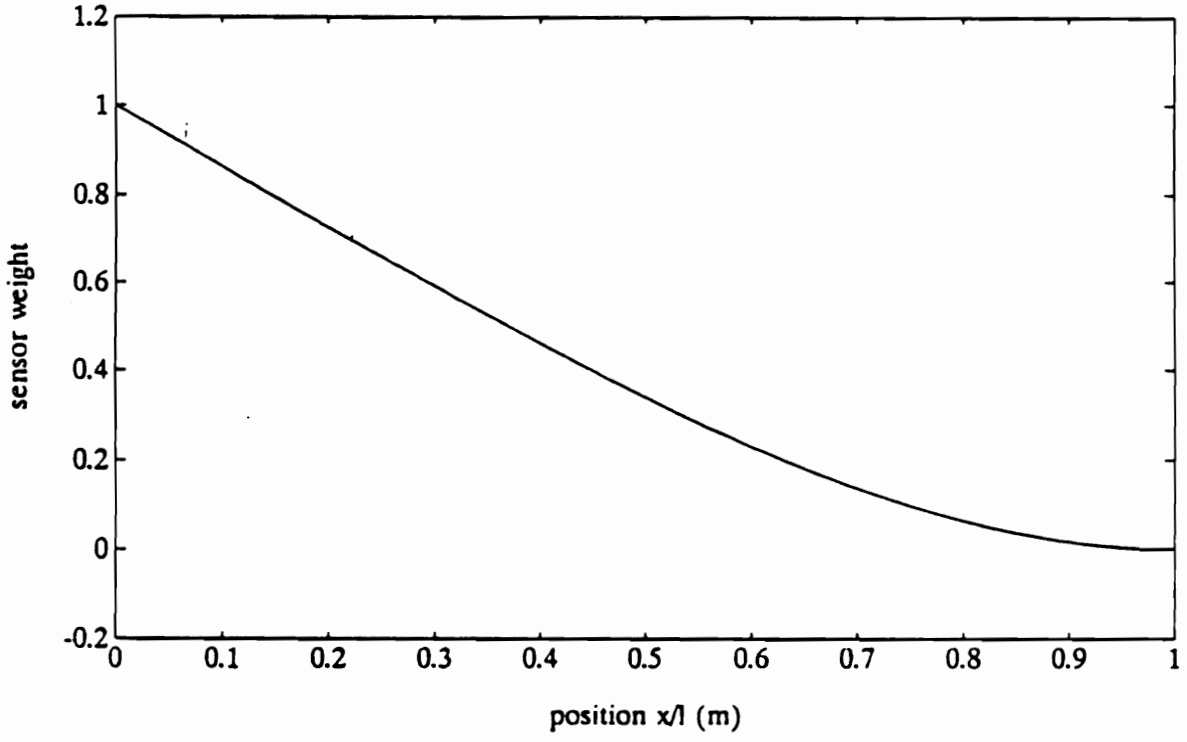

Figure 6.3.1 Spatial filter gain for a distributed-effect sensor designed to measure the modal amplitude of the first mode of the cantilevered beam described in Chapter 3.

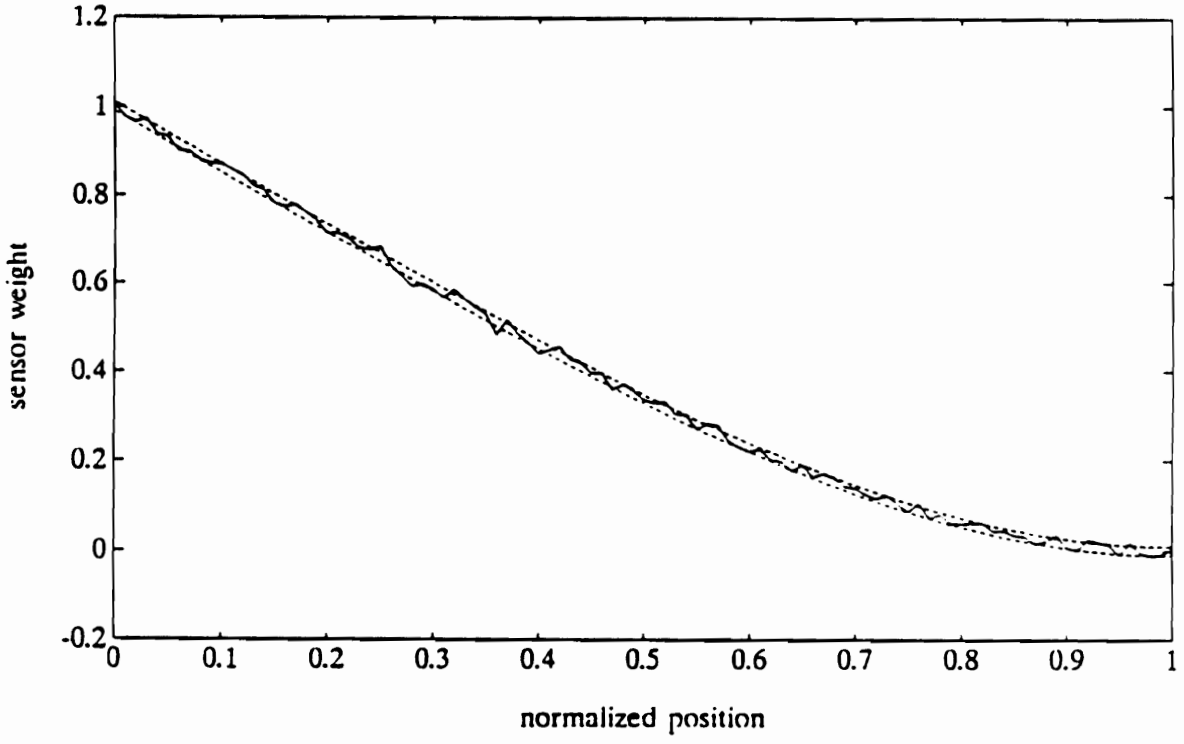

Figure 6.3.2 Spatial filter gain for a distributed-effect sensor designed to measure the modal amplitude of the first mode for the cantilevered beam described in Chapter 2, corrupted by zero-mean, Gaussian spatial noise with variance $\sigma_n^2 = 10^{-4}$.

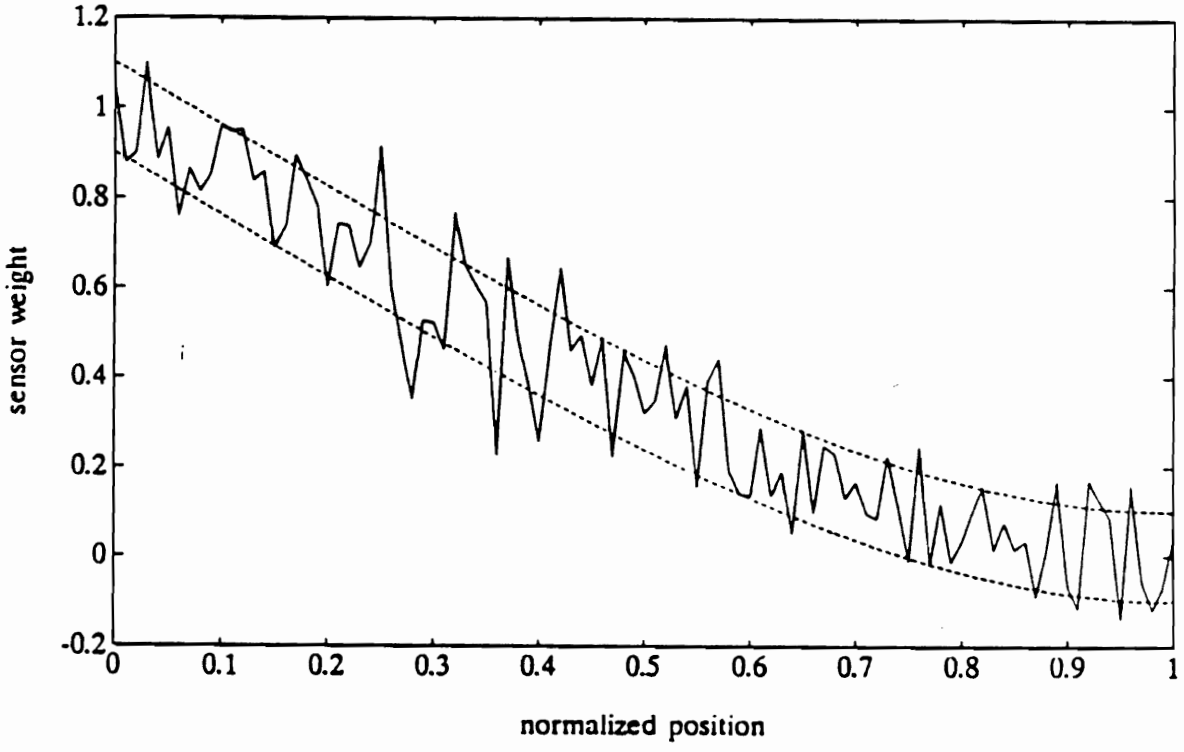

Figure 6.3.3 Spatial filter gain for a distributed-effect sensor designed to measure the modal amplitude of the first mode for the cantilevered beam described in Chapter 2, corrupted by zero-mean, Gaussian spatial noise with variance $\sigma_n^2 = 10^{-2}$.

When $g(z)$ is scaled so that $\| g(z) \|_\infty = 1$ and $\sigma_n^2 = 10^{-4}$ this deterministic characterization implies

$$| \hat{g}(z) - g(z) | \leq 0.01 \times | g(z) | \ ,$$

or 1% of the magnitude of the desired value of the weighting function $g(z)$. Similarly, $\sigma_n^2 = 10^{-2}$ corresponds to a maximum error of 10% of the magnitude of $g(z)$. □

6.4. MEASURING THE EFFECTS OF SPATIAL FILTER ERRORS

This section describes the several ways of measuring effects of spatial filter errors on system performance, including the effects of the errors on the system frequency response, measures of observability, and observation spillover. The weighting function error is included in the state-space model of the cantilevered beam described in Chapter 3 as perturbations in the output matrix C as described in Section 6.2.

6.4.1. Frequency response

Suppose the flexible structure is modelled by the set of state equations

$$\dot{x}(t) = \mathrm{A}x(t) + \mathrm{B}u(t) \ , \tag{6.4.1}$$

and the desired sensor output is given by

$$y(t) = \mathrm{C}x(t) \ . \tag{6.4.2}$$

The transfer function from the input, $u(t)$, to the ideal or desired distributed-effect sensor output, $y(t)$, is given by

$$\mathrm{H}(s) = \mathrm{C}(s\mathrm{I} - \mathrm{A})^{-1}\mathrm{B} \ . \tag{6.4.3}$$

If the output of the implemented distributed-effect sensor is given by

$$\hat{y}(t) = [\mathrm{C} + \delta\mathrm{C}]x(t) \tag{6.4.4}$$

Then transfer function from the system input to the actual sensor output, $\hat{y}(t)$, is given by

$$\hat{\mathrm{H}}(s) = \mathrm{H}(s) + \delta\mathrm{H}(s) \ , \tag{6.4.5}$$

where

$$\delta\mathrm{H}(s) = \delta\mathrm{C}(s\mathrm{I} - \mathrm{A})^{-1}\mathrm{B} \ . \tag{6.4.6}$$

Definition 6.4.1: The transfer function from the input, $u(t)$, to the sensor output error, $e(t)$ is given in (6.4.6) and is called the transfer function error or the error transfer function. □

Figure 6.4.1 shows the relationship between the transfer functions $\mathrm{H}(s)$, $\hat{\mathrm{H}}(s)$, and $\delta\mathrm{H}(s)$, for a system.

For flexible structures the transfer function $\mathrm{H}(s)$ can be written in the form

$$\mathrm{H}(s) = \sum_{i=1}^{N} \frac{c_i b_i}{s^2 + 2\zeta_i\omega_i + \omega_i^2} \ , \tag{6.4.7}$$

and $\delta\mathrm{H}(s)$ can be written as

$$\delta\mathrm{H}(s) = \sum_{i=1}^{M} \frac{\delta c_i b_i}{s^2 + 2\zeta_i\omega_i + \omega_i^2} \ . \tag{6.4.8}$$

One measure of the effects of the spatial filter error is the L_2 norm of $\delta\mathrm{H}(\omega)$, the Fourier transform equivalent of the error transfer function. In the Laplace domain, the L_2 norm of $\delta\mathrm{H}(\omega)$ is defined by

$$\| \delta\mathrm{H}(\omega) \|_2^2 = \frac{1}{2\pi j} \int_{-j\infty}^{j\infty} | \delta\mathrm{H}(s) |^2 \, \mathrm{d}s \ . \tag{6.4.9}$$

The digital analogue of this quantity has been used in digital filter analysis to

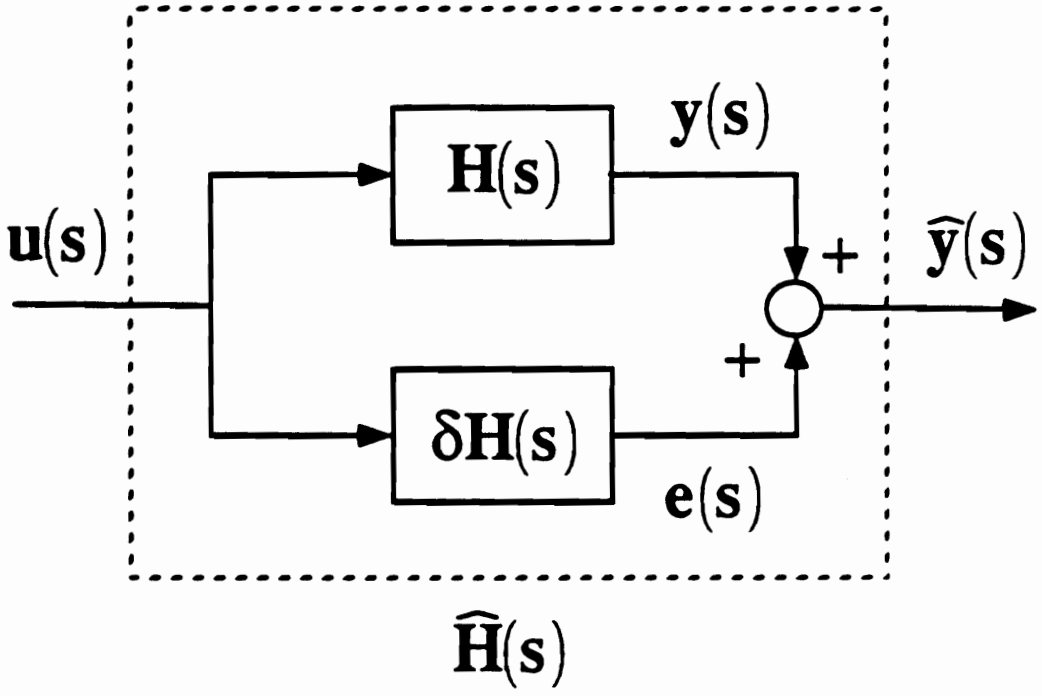

Figure 6.4.1 System block diagram showing the ideal and error transfer functions.

derive a measure of the sensitivity of filter structures to parameter uncertainties such as those represented by δC in Equation (6.4.4) [51].

Writing δH as

$$\delta H(s) = \left[\frac{\partial H(s)}{\partial c_1} \;\; \frac{\partial H(s)}{\partial c_2} \;\; \cdots \;\; \frac{\partial H(s)}{\partial c_M} \right] \delta C^T \,, \tag{6.4.10}$$

where

$$\frac{\partial H(s)}{\partial c_i} = \frac{b_i}{s^2 + 2\zeta_i \omega_i + \omega_i^2} \quad . \tag{6.4.11}$$

The L_2 norm of $\delta H(\omega)$ can be approximated as

$$\begin{aligned} \| \delta H(\omega) \|_2^2 &\leq \| \delta C \|_2^2 \; \frac{1}{2\pi j} \int_{-j\infty}^{j\infty} \left\| \left[\frac{\partial H(s)}{\partial c_1} \;\; \frac{\partial H(s)}{\partial c_2} \;\; \cdots \;\; \frac{\partial H(s)}{\partial c_M} \right] \right\|^2 ds \\ &= \| \delta C \|_2^2 \; \frac{1}{2\pi j} \int_{-j\infty}^{j\infty} \sum_{i=1}^{M} \left| \frac{b_i}{s^2 + 2\zeta_i \omega_i + \omega_i^2} \right|^2 ds \qquad (6.4.12) \\ &= \| \delta C \|_2^2 \sum_{i=1}^{M} \frac{1}{2\pi j} \int_{-j\infty}^{j\infty} \left| \frac{b_i}{s^2 + 2\zeta_i \omega_i + \omega_i^2} \right|^2 ds. \end{aligned}$$

Evaluating the integral expression in the above equation yields

$$\| \delta H(\omega) \|_2^2 \leq \| \delta C \|_2^2 \sum_{i=1}^{M} \frac{b_i^2}{4\zeta_i \omega_i^3} \quad . \tag{6.4.13}$$

The bound on the L_2 norm of the error transfer function depends on two factors. One factor depends on the perturbation of the system parameters caused by the spatial filter error. The second factor depends on the structure of the system, and is used in the signal processing literature as a measure of the sensitivity of the system structure to parameter perturbations.

The L_2 norm of the error transfer function has an interesting interpretation when the system is driven by white noise. By Parseval's theorem, the energy of the sensor output error is given by

$$\mathcal{E}\{e\} = \int_{-\infty}^{\infty} |e(t)|^2 dt = \frac{1}{2\pi} \int_{-\infty}^{\infty} |\mathcal{F}\{e(t)\}|^2 d\omega \,, \tag{6.4.14}$$

where $\mathcal{F}\{\cdot\}$ denotes the Fourier transform. If the input $u(t)$ is white noise with variance σ_u^2, then

$$\mathcal{E}\{e\} = \sigma_u^2 \frac{1}{2\pi} \int_{-\infty}^{\infty} |\delta H(\omega)|^2 d\omega = \sigma_u^2 \|\delta H(\omega)\|_2^2 . \tag{6.4.15}$$

Hence, Equation (6.4.13) gives an upper bound on the energy in the sensor output error when the system is driven by white noise.

Both characterizations of the spatial filter error described in the preceding section yield similar approximations for the L_2 norm of the error transfer function. When the spatial filter error is characterized by a deterministic bound of the form $\|n(z)\|_\infty \leq \delta_\infty$,

$$|n_i|^2 \leq \|n(z)\|_\infty^2 , \tag{6.4.16}$$

for $i = 1, 2, \ldots, M$ in (6.2.9). When $m(z,t)$ denotes structural strain, $\delta c_i = \beta_i^2 n_i$, and (6.4.16) implies

$$\|\delta C\|_2^2 \leq \delta_\infty^2 \sum_{i=1}^{M} \beta_i^4 . \tag{6.4.17}$$

When $n(z)$ is characterized by deterministic bounds on the amplitudes of the coefficients n_i,

$$\delta c_i^2 = \beta_i^2 |n_i|^2 \leq \delta_i , \tag{6.4.18}$$

and

$$\|\delta C\|_2^2 \leq \sum_{i=1}^{M} \delta_i^2 \beta_i^4 . \tag{6.4.19}$$

Therefore, when $\delta_i = \delta_\infty$ for $i = 1, \ldots, M$, the two deterministic characterizations yield the same bound for $\|\delta C\|_2$.

When $n(z)$ is characterized as a random process,

$$\mathbf{E}\{\|\delta C\|_2^2\} = \sum_{i=1}^{M} \mathbf{E}\{\delta c_i^2\} \tag{6.4.20}$$

where

$$\mathbf{E}\left\{\delta c_i^2\right\} = \beta_i^4\, \mathbf{E}\left\{n^2(z)\right\}, \tag{6.4.21}$$

so that

$$\mathbf{E}\left\{ \| \delta \mathbf{C} \|_2^2 \right\} = \sigma_n^2 \sum_{i=1}^{N} \beta_i^4 . \tag{6.4.22}$$

Similarly, when $n(z)$ is characterized as a weighted sum of orthonormal basis functions in which the weights, n_i, are random variables, then

$$\mathbf{E}\left\{\delta c_i^2\right\} = \beta_i^4\, \mathbf{E}\left\{ n_i^2 \right\}, \tag{6.4.23}$$

and

$$\mathbf{E}\left\{ \| \delta \mathbf{C} \|_2^2 \right\} = \sum_{i=1}^{N} \beta_i^4\, \sigma_i^2 . \tag{6.4.24}$$

Therefore, both probabilistic characterizations of the spatial filter error yield the same expected value of $\| \delta \mathbf{C} \|_2^2$. Comparing the expected value of $\| \delta \mathbf{C} \|_2^2$ for the probabilistic characterization of the spatial filter error to the bound on $\| \delta \mathbf{C} \|_2^2$ for the deterministic characterizations shows that both types of characterizations yield similar characterizations for the L_2 norm of the perturbation in the output matrix; therefore, from (6.4.13) they also yield a similar bound on the L_2 norm of the error transfer function.

Example 6.4.1

Example 6.3.1 illustrated the effects of spatial noise on the weighting function for a distributed-effect sensor designed to measure the modal amplitude of the first vibrational mode of a cantilevered beam. The transfer function from the system input to the ideal distributed-effect sensor output given in Example 6.2.1 is given by

$$H(s) = \frac{c_1 b_1}{s^2 + 2\zeta_1\omega_1 + \omega_1^2} \quad ,$$

where

$$c_i = \frac{\sqrt{l}}{2}\beta_1^2 \, .$$

When spatial filter errors are present, the transfer function from the system input to the output of the implemented distributed-effect sensor becomes

$$\hat{H}(s) = \frac{c_1 b_1}{s^2 + 2\zeta_1\omega_1 + \omega_1^2} + \sum_{i=1}^{M} \frac{\delta c_i b_i}{s^2 + 2\zeta_i\omega_i + \omega_i^2} \, .$$

For spatial filter errors $n(z)$ characterized as zero-mean, Gaussian spatial noise with variance σ_n^2,

$$\delta c_i = \beta_i^2 \, n_i$$

where n_i has zero mean and variance σ_n^2 .

Figure 6.4.2 shows plots of the frequency response of the ideal system, with transfer function $H(s)$, from the actuator input $u(t)$ to the desired distributed-effect sensor output, and the expected value of the magnitude of $\hat{H}(s)$, for a spatial filter error due to "white" spatial noise with $\sigma_n^2 = 10^{-4}$ (1% error). Figure 6.4.3 shows a plot of the expected value of the difference between the magnitudes of $H(\omega)$ and $\hat{H}(\omega)$:

$$\left| \; |H(\omega)| \; - \; \mathbf{E}\{ |\hat{H}(\omega)| \} \; \right| \, ,$$

and Figure 6.4.4 shows a plot of the variance of this quantity. Figures 6.4.5-7 show the same plots for $\sigma_n^2 = 10^{-2}$.

Figure 6.4.8 shows a magnitude plot of the frequency response of the structural model from the input $u(t)$ to the output of the ideal distributed-effect sensor, and from the input to the output of a strain gauge located at the base of the beam. Figure 6.4.2 shows that although the attenuation of the higher order structural modes is degraded by the spatial error in the sensor's weighting

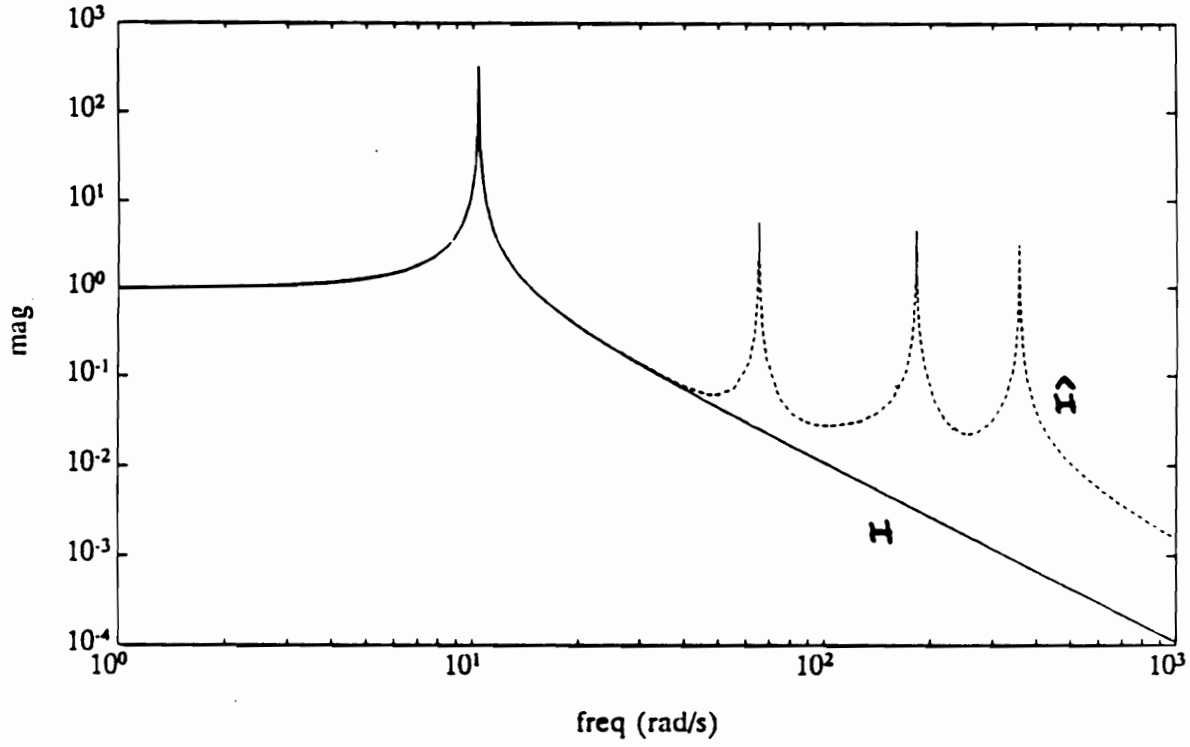

Figure 6.4.2 Magnitude frequency response of the transfer function, H(s), from the system input to the desired output of a distributed-effect sensor designed to measure the modal amplitude of the first mode of a cantilevered beam, and the expected value of the magnitude frequency response of the achieved transfer function $\widehat{\mathrm{H}}(s)$ for spatial filter errors with $\sigma_n^2 = 10^{-4}$.

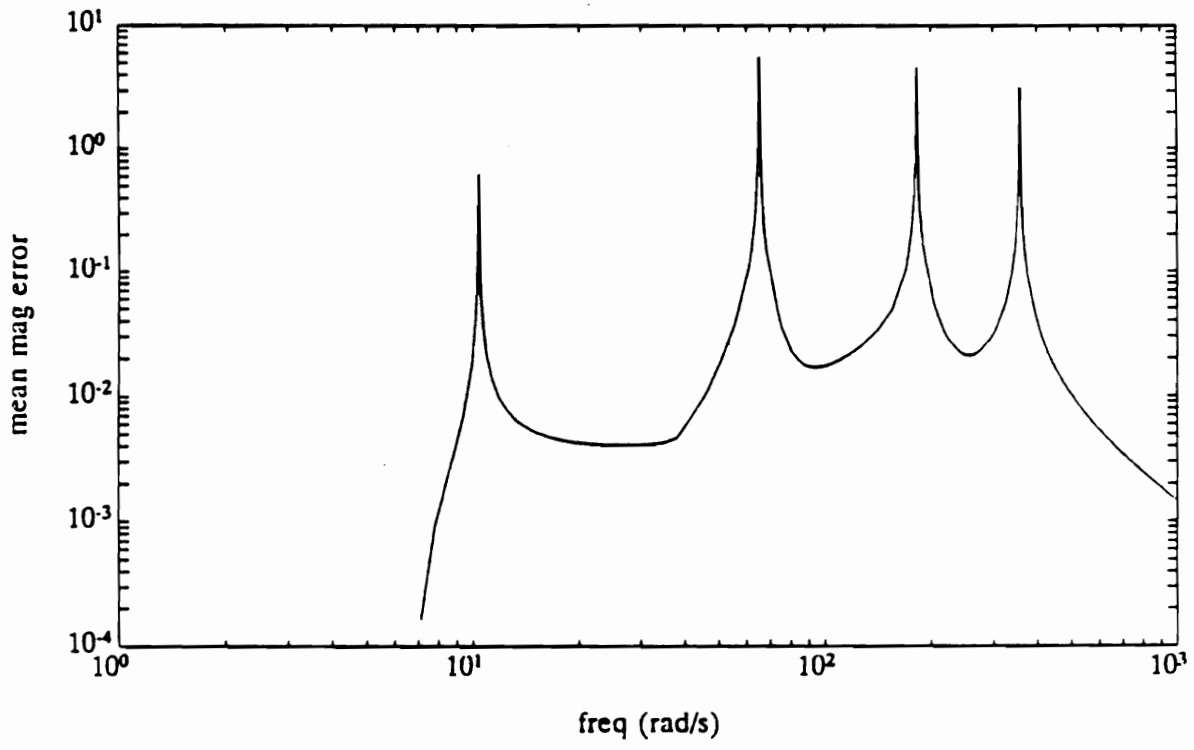

Figure 6.4.3 Expected value of the error $\left|\ |H| - E\{|\hat{H}|\}\ \right|$, for spatial filter errors with $\sigma_n^2 = 10^{-4}$.

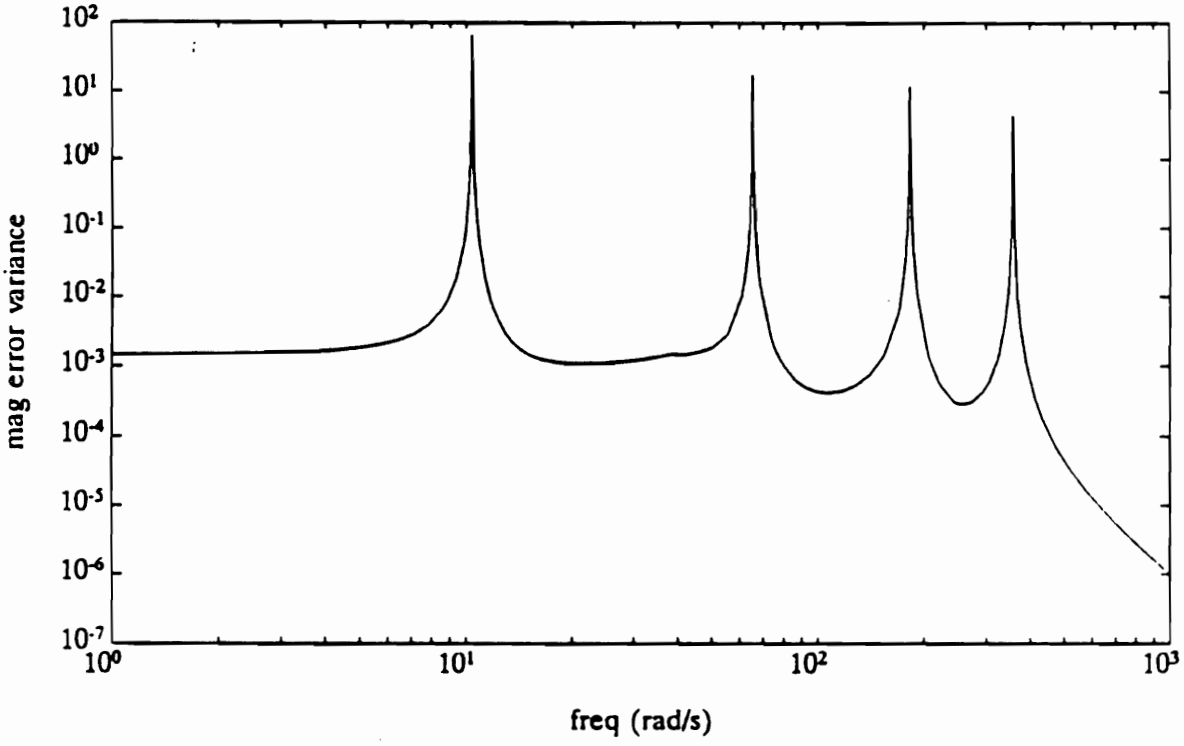

Figure 6.4.4 Variance of the error $| \, |H| - |\widehat{H}| \, |$, for spatial filter errors with $\sigma_n^2 = 10^{-4}$.

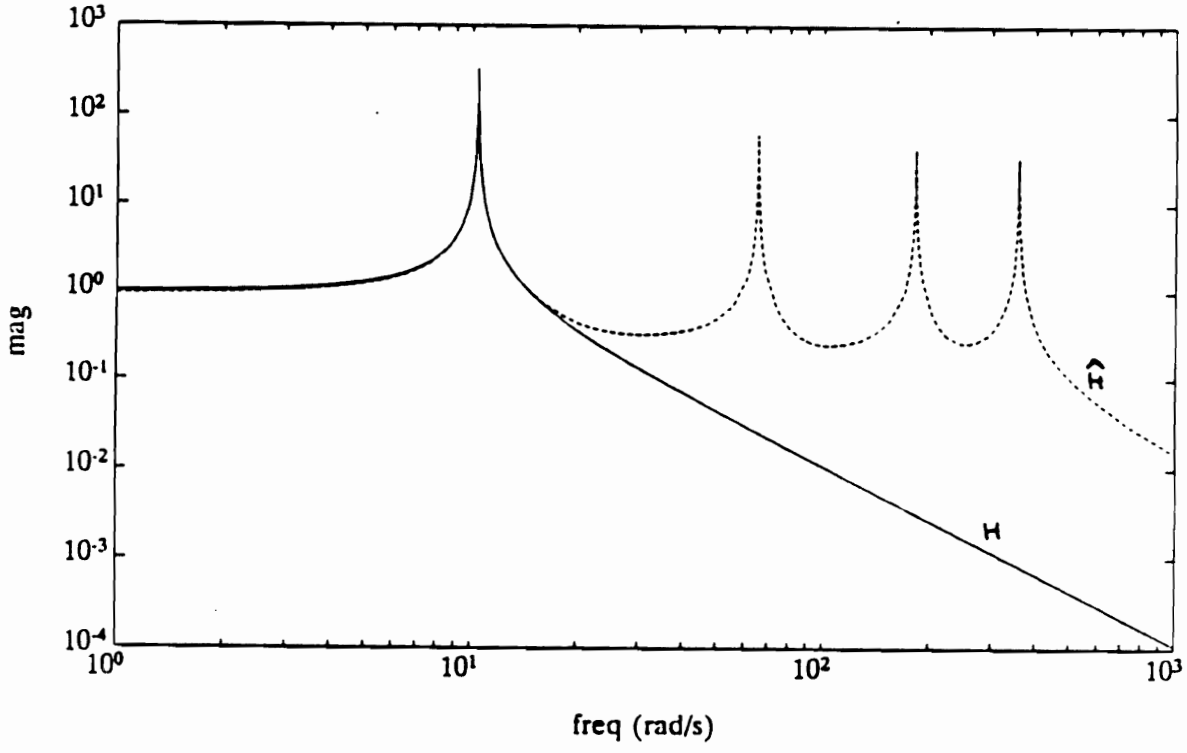

Figure 6.4.5 Magnitude frequency response of the transfer function, H(s), from the system input to the desired output of a distributed-effect sensor designed to measure the modal amplitude of the first mode of a cantilevered beam, and the expected value of the magnitude frequency response of the achieved transfer function $\widehat{\mathrm{H}}(s)$ which is subject to spatial filter errors with $\sigma_n^2 = 10^{-2}$.

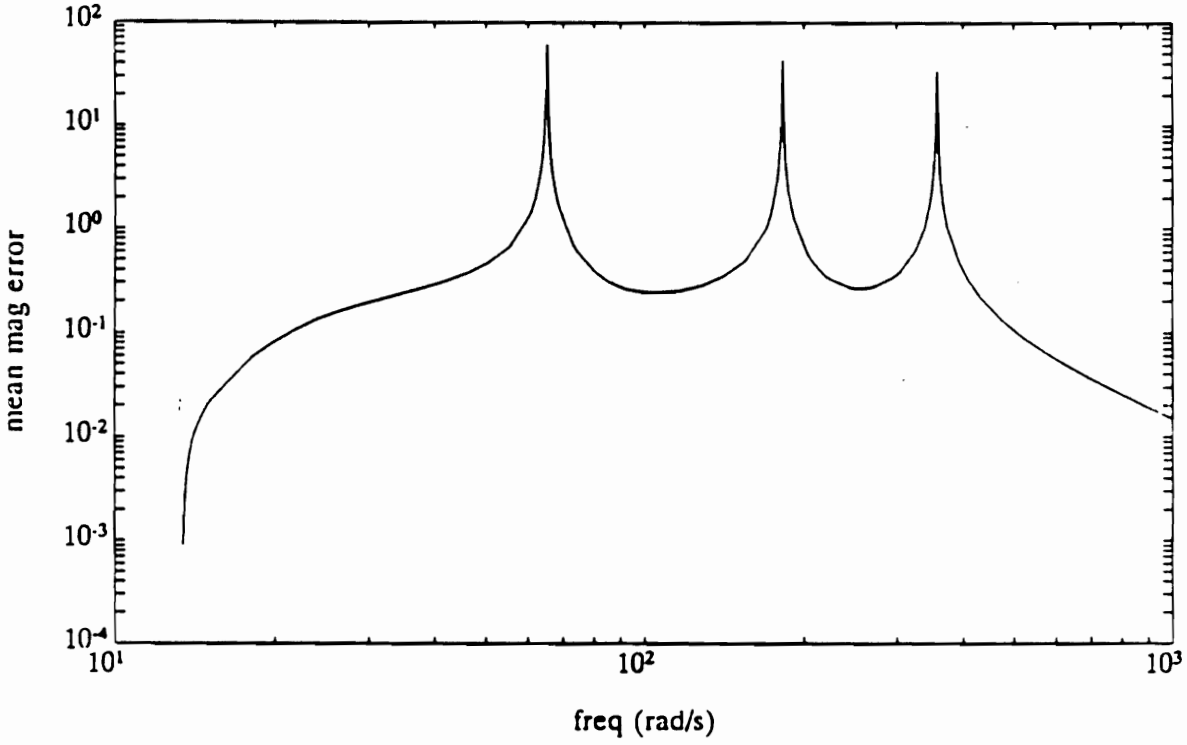

Figure 6.4.6 Expected value of the error $\big|\ |H| - \mathbb{E}\{|\hat{H}|\}\ \big|$, for spatial filter errors with $\sigma_n^2 = 10^{-2}$.

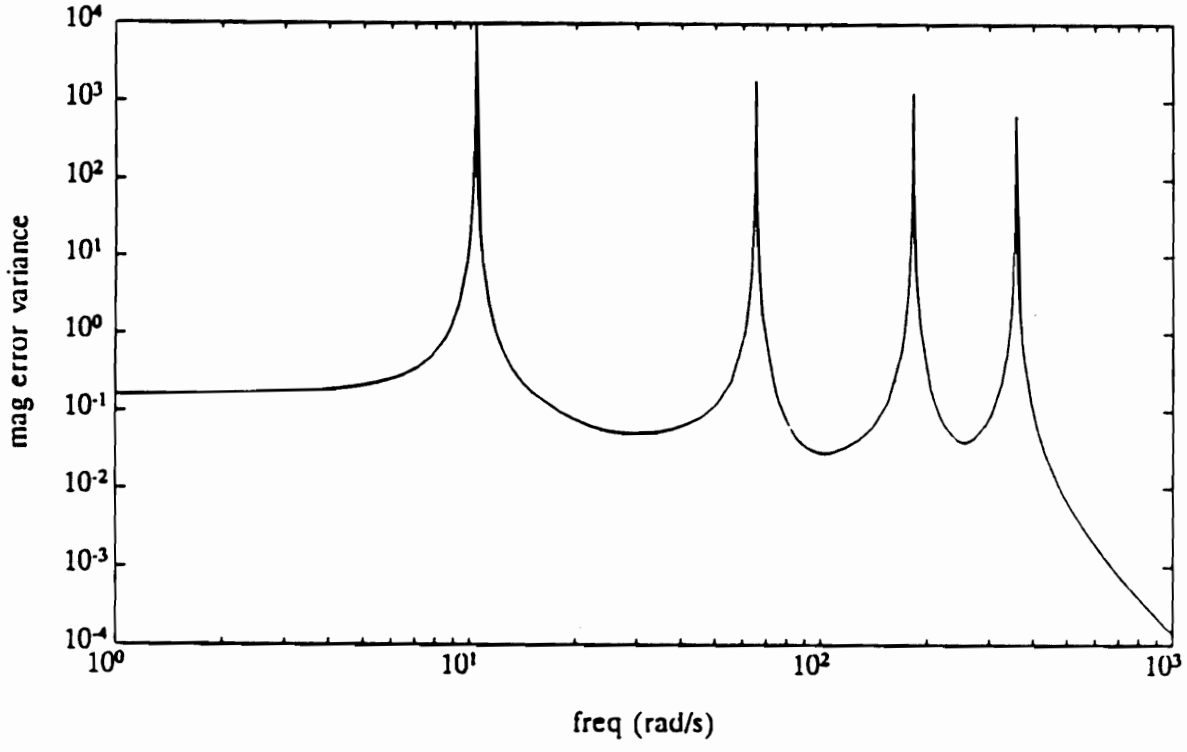

Figure 6.4.7 Variance of the error $| \, |H| - \mathbf{E}\{|\widehat{H}|\} \, |$, for spatial filter errors with $\sigma_n^2 = 10^{-2}$.

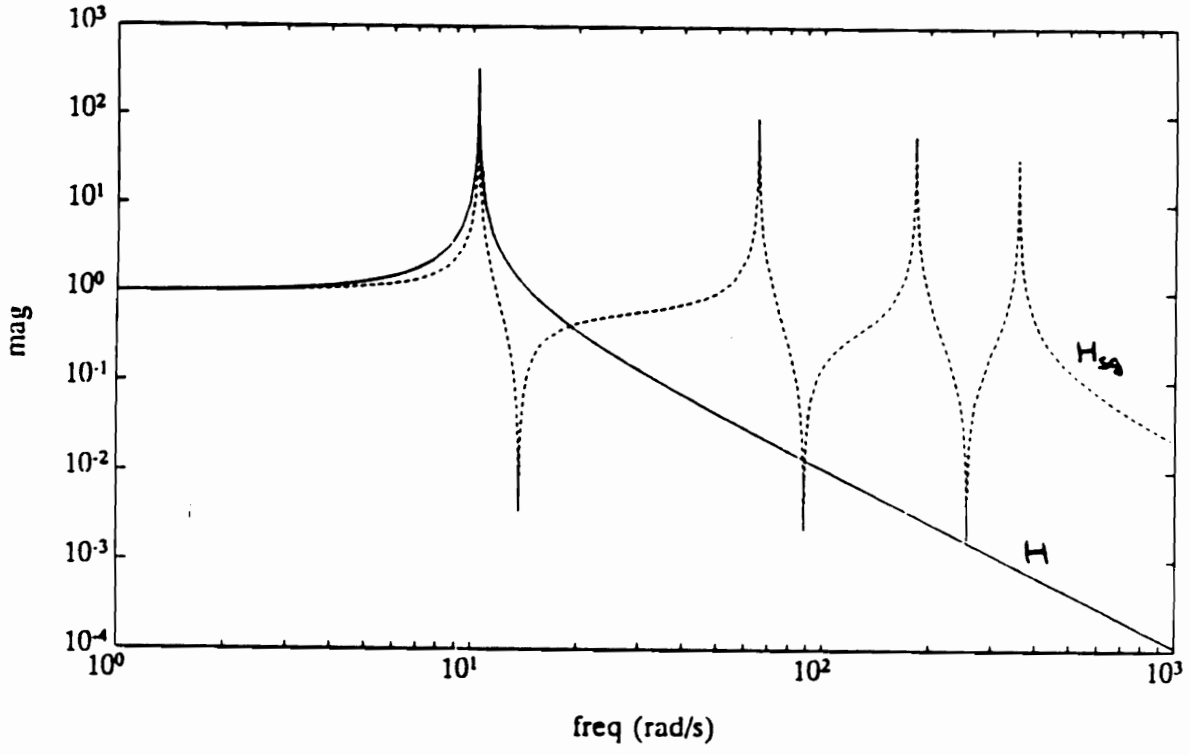

Figure 6.4.8 Magnitude frequency response of the transfer function H, from the system input to the output of a distributed-effect sensor designed to measure the modal amplitude of the first mode of a cantilevered beam, and the transfer function H_{sg} from the system input to a strain gauge located at the base of the beam.

function the magnitude of the frequency response at the higher modes is still an order of magnitude below the magnitude of the frequency response associated with the strain gauge at the corresponding frequencies.

A comparison of Figure 6.4.5 and Figure 6.4.8, however, shows that for spatial filter errors on the order of 10%, the frequency response of the transfer function from the system input to the output of the distributed-effect sensor shows no significant attenuation of the higher order modes compared to the frequency response associated with the strain gauge. These results can also be predicted from Figures 6.4.3 and 6.4.6 which show that the expected value of the magnitude of the transfer function error is an order of magnitude higher at the higher order modes for the larger spatial filter error.

Recall that the L_2 norm of the error transfer function provides an upper bound on the square energy in the output error when the system input $u(t)$ is white noise with variance $\sigma_u^2 = 1$. For this example,

$$\sum_{i=1}^{M} \frac{b_i^2}{4\zeta_i\omega_i^3} = \sum_{i=1}^{4} \frac{b_i^2}{4\zeta_i\omega_i^3} = 1.5 \times 10^{-5} , \tag{6.4.25}$$

hence

$$\| \delta H(\omega) \|_2^2 \leq \sigma_n^2 \, (1.5 \times 10^{-5}) . \qquad \square$$

6.4.2. Measures of observability

Recall the modal measure of observability defined in Chapter 4:

$$\mu_k = \frac{| C \; p_k |}{\sqrt{2 \, | \, Re\{\lambda_k\} \, |}} . \tag{6.4.26}$$

The spatial filter function associated with a particular distributed-effect sensor design determines the output matrix C, but does not affect the system eigenvalues or eigenvectors. When the distributed-effect sensor is subject to errors in the spatial filter weighting function, the measure of observability for the k-th mode becomes

$$\widehat{\mu}_k = \frac{| [C + \delta C] \; p_k |}{\sqrt{2 \, | \, Re\{\lambda_k\} \, |}} . \tag{6.4.27}$$

For structures such as the flexible beam described in Chapter 3, (6.4.27) becomes

$$\widehat{\mu}_k = \frac{|\, c_k + \delta c_k \,|}{\sqrt{2\zeta_k \omega_k (1+\omega_k^2)}} \quad . \tag{6.4.28}$$

Example 6.4.2

Table 6.4.1 shows the average measures of observability for the first four modes of the cantilevered beam described in Chapter 3 associated with the output of a distributed-effect sensor designed to respond only to the structure's first flexible mode subject to spatial filter errors modeled as zero-mean, Gaussian random processes with variance σ_n^2. The first column contains the measures of observability associated with the desired sensor output. The second and third columns contain the average measures of observability for each mode for the sensor output corresponding to spatial filter error noise variances of $\sigma_n^2 = 10^{-4}$, and $\sigma_n^2 = 10^{-2}$ respectively. The fourth column shows the corresponding measures of observability for a strain gauge located at the base of the beam, where the strain gauge output has been scaled to yield the same measure of observability as the ideal distributed-effect sensor for the first mode.

Comparing the different columns in Table 6.4.1 shows that although increasing the level of the spatial error noise increases the measures of observability of the higher order modes, the distributed-effect sensor still rejects those modes relative to the strain gauge output. Recall that based on frequency domain analysis, in Example 6.4.1, the distributed-effect sensor did not appear to reject the higher order modes for spatial filter errors on the order of 10%. □

6.4.3. Observation spillover

For state feedback control laws, observers are often used to provide estimates of the system states to the controller. Observation spillover - the presence of unmodelled system dynamics in the measurements provided to the

Table 6.4.1 Measures of observability for a distributed-effect sensor subject to weighting function errors.

mode	$\sigma_n^2 = 0$	$\sigma_n^2 = 10^{-4}$	$\sigma_n^2 = 10^{-2}$	strain gauge
1	1.9787	1.9793	1.9845	1.9787
2	0.0	0.0151	0.1509	0.6470
3	0.0	0.0094	0.0941	0.3079
4	0.0	0.0068	0.0681	0.1628

observer - can cause instability in the closed-loop system [7]. Distributed-effect sensors are often designed to eliminate observation spillover by making the unmodelled dynamics unobservable. Spatial filter errors, however, can lead to observation spillover through changes in the observability of the unmodeled system dynamics.

Partitioning the system state vector in Chapter 3 as

$$x(t) = \begin{bmatrix} x_c \\ x_r \end{bmatrix} \tag{6.4.29}$$

where x_c denotes the modeled or controlled system states, and x_r denotes the unmodeled or residual modes, the state equations which describe the system dynamics become

$$\begin{bmatrix} \dot{x}_c \\ \dot{x}_r \end{bmatrix} = \begin{bmatrix} A_{cc} & A_{cr} \\ A_{rc} & A_{rr} \end{bmatrix} \begin{bmatrix} x_c \\ x_r \end{bmatrix} + \begin{bmatrix} B_c \\ B_r \end{bmatrix} u \, . \tag{6.4.30}$$

If the distributed-effect sensor is designed to eliminate observation spillover, then the desired sensor output is given by

$$y = [\, C \vdots 0 \,] \begin{bmatrix} x_c \\ x_r \end{bmatrix} . \tag{6.4.31}$$

When the weighting function realized in the manufacture of the sensor deviates from the desired weighting function, the achieved sensor output can have the form

$$\hat{y} = [\, C + \delta C_c \vdots \; \delta C_r \,] \begin{bmatrix} x_c \\ x_r \end{bmatrix} , \tag{6.4.32}$$

The full-order state observer for the controlled modes is described by the set of equations:

$$\dot{\hat{x}}_c = A_{cc}\hat{x}_c + B_c u + L(y - C\hat{x}_c) \, . \tag{6.4.33}$$

Applying the state feedback control law,

$$u = -K\hat{x}_c + v \, , \tag{6.4.34}$$

and substituting the actual sensor output, $\widehat{y}$, for y in Equation (6.4.33), the closed-loop state equations become

$$\begin{bmatrix} \dot{x}_c \\ \dot{x}_r \\ \dot{\widehat{x}}_c \end{bmatrix} = \begin{bmatrix} A_{cc} & A_{cr} & -B_cK \\ A_{rc} & A_{rr} & -B_rK \\ L(C+\delta C_c) & L\delta C_r & A_{cc}-B_cK-LC \end{bmatrix} \begin{bmatrix} x_c \\ x_r \\ \widehat{x}_c \end{bmatrix} + \begin{bmatrix} B_c \\ B_r \\ B_c \end{bmatrix} v \ . \quad (6.4.35)$$

Defining the state estimation error

$$e_c = x_c - \widehat{x}_c \ , \quad (6.4.36)$$

equation (6.4.35) becomes

$$\begin{bmatrix} \dot{x}_c \\ \dot{e}_c \\ \dot{\widehat{x}}_c \end{bmatrix} = \begin{bmatrix} A_{cc}-B_cK & B_cK & A_{cr} \\ -L\delta C_c & A_{cc}-LC & A_{cr}-L\delta C_r \\ A_{rc}-B_rK & B_rK & A_{rr} \end{bmatrix} \begin{bmatrix} x_c \\ e_c \\ \widehat{x}_c \end{bmatrix} + \begin{bmatrix} B_c \\ 0 \\ B_c \end{bmatrix} v \ . \quad (6.4.37)$$

For structural models, the states can be choose such that $A_{cr} = A_{rc}^T = 0$; hence, in the absence of spatial filter errors

$$\begin{bmatrix} \dot{x}_c \\ \dot{e}_c \\ \dot{\widehat{x}}_c \end{bmatrix} = \begin{bmatrix} A_{cc}-B_cK & B_cK & 0 \\ 0 & A_{cc}-LC & 0 \\ -B_rK & B_rK & A_{rr} \end{bmatrix} \begin{bmatrix} x_c \\ e_c \\ \widehat{x}_c \end{bmatrix} + \begin{bmatrix} B_c \\ 0 \\ B_c \end{bmatrix} v \ . \quad (6.4.38)$$

From equation (6.4.38) the closed-loop eigenvalues of the system are given by the set

$$\Lambda_{cl} = \lambda(A_{cc}-B_cK) \cup \lambda(A_{cc}-LC) \cup \lambda(A_{rr}) \ , \quad (6.4.39)$$

where $\lambda(F)$ denotes the eigenvalues of the matrix F. When observation spillover is

eliminated - through the design of the distributed-effect sensor - the addition of the unmodeled system dynamics does not cause instability [7]. The presence of the terms δC_c and δC_r in Equation (6.4.37), resulting from the spatial filter error, can change the closed-loop eigenvalues of the system, and may lead to instability.

Example 6.4.3

Figure 6.4.9 shows a scatter plot of the closed-loop poles for the state feedback control law designed in Chapter 4 and implemented using a full-order observer. The system measurement for this example is provided by a distributed-effect sensor designed so that each of the first four structural modes has the same measure of observability and all higher order modes are unobservable, eliminating observation spillover. The x's denote the nominal closed-loop poles, and the dots denote the perturbed closed-loop poles for spatial filter errors with variance $\sigma_n^2 = 10^{-4}$. Figure 6.4.10 shows the effect on the closed-loop poles of spatial filter errors with variance $\sigma_n^2 = 10^{-2}$. Comparing Figures 6.4.9 and 10 shows that while small errors in the achieved weighting function may alter the closed-loop damping of the system, it remains stable, but for larger errors the system may become unstable. □

The perturbations in the output matrix caused by spatial filter errors also affects the closed-loop poles of the system when feedback control laws are implemented using functional observers. The functional observer is described by a pair of equations of the form

$$\begin{aligned} \dot{z} &= \mathrm{F}z + \mathrm{G}x + \mathrm{H}u \\ w &= \mathrm{M}z + \mathrm{P}x \ , \end{aligned} \tag{6.4.40}$$

where the observer is designed so that

$$\lim_{t \to \infty} w(t) = \mathrm{K}x(t) \ , \tag{6.4.41}$$

for the desired state feedback gain matrix K. The spatial filter weights for the

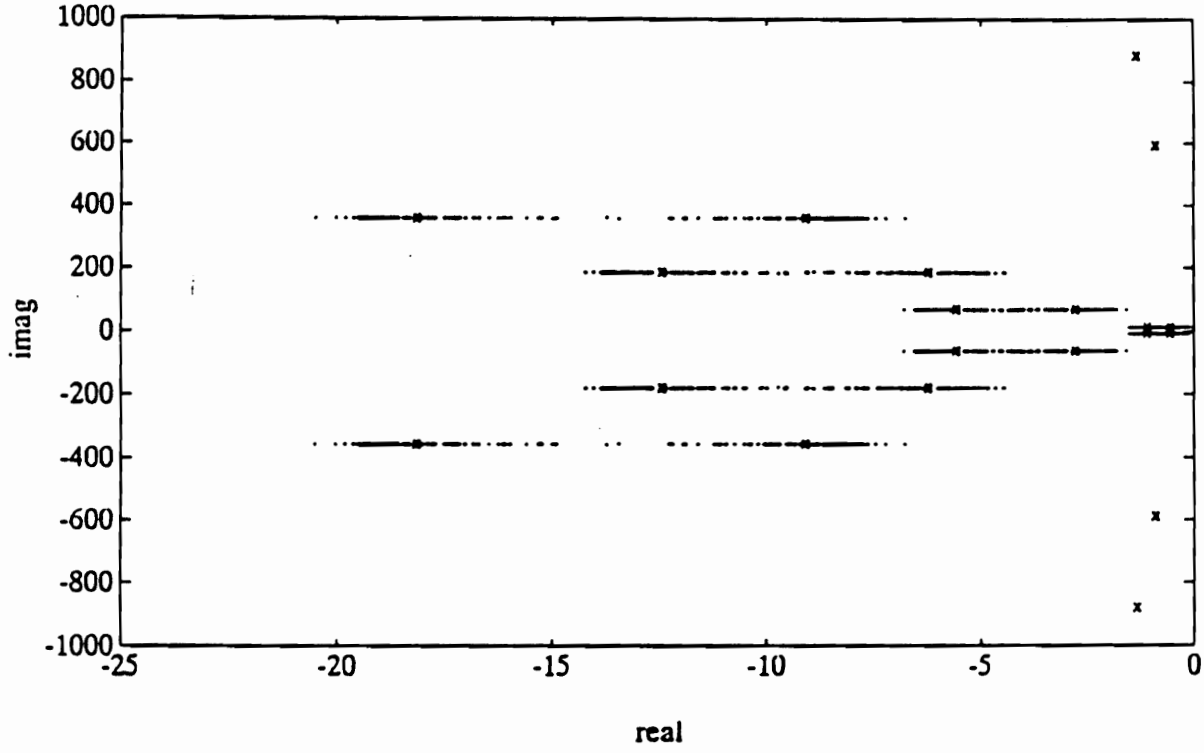

Figure 6.4.9 Closed-loop poles for state feedback control with a full-order observer, subject to spatial filter errors in the distributed-effect sensor design. The x's indicate nominal closed-loop pole locations, and dots indicate closed-loop pole locations for spatial filter errors with variance $\sigma_n^2 = 10^{-4}$.

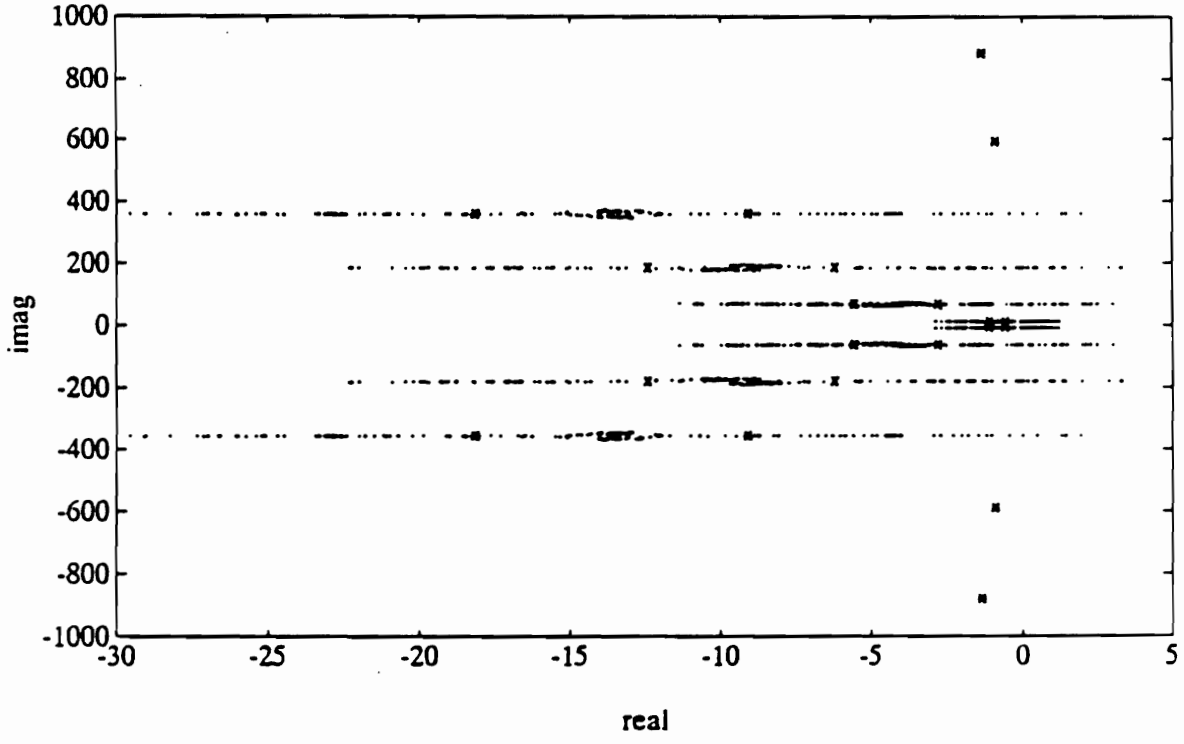

Figure 6.4.10 Closed-loop poles for state feedback control with a full-order observer, subject to spatial filter errors in the distributed-effect sensor design. The x's indicate nominal closed-loop pole locations, and dots indicate closed-loop pole locations for spatial filter errors with variance $\sigma_n^2 = 10^{-2}$.

distributed-effect sensors used to implement the functional observer are chosen so that

$$\mathrm{G}x = \bar{\mathrm{G}}x_c, \text{ and } \quad \mathrm{P}x = \bar{\mathrm{P}}x_c \,. \tag{6.4.42}$$

When spatial filter errors are present,

$$\mathrm{G}x = (\bar{\mathrm{G}} + \delta\bar{\mathrm{G}}_c)\, x_c + \delta\bar{\mathrm{G}}_r\, x_r \tag{6.4.43}$$

and

$$\mathrm{P}x = (\bar{\mathrm{P}} + \delta\bar{\mathrm{P}}_c)\, x_c + \delta\bar{\mathrm{P}}_r\, x_r \,. \tag{6.4.44}$$

Applying the control law

$$u = -w + v \tag{6.4.45}$$

the state equations for the closed-loop system become

$$\begin{bmatrix} \dot{x}_c \\ \dot{x}_r \\ \dot{z} \end{bmatrix} = \begin{bmatrix} \mathrm{A}_{cc} - \mathrm{B}_c(\bar{\mathrm{P}} + \delta\,\bar{\mathrm{P}}_c) & \mathrm{A}_{cr} - \mathrm{B}_c\delta\bar{\mathrm{P}}_r & -\mathrm{B}_c\mathrm{M} \\ \mathrm{A}_{rc} - \mathrm{B}_r\,(\bar{\mathrm{P}} + \delta\,\bar{\mathrm{P}}_c) & \mathrm{A}_{rr} - \mathrm{B}_r\delta\bar{\mathrm{P}}_r & -\mathrm{B}_r\mathrm{M} \\ (\bar{\mathrm{G}} + \delta\bar{G}_c) - \mathrm{H}\,(\bar{\mathrm{P}} + \delta\bar{\mathrm{P}}_c) & \delta\bar{G}_r - \mathrm{H}\delta\bar{\mathrm{P}}_r & \mathrm{F} - \mathrm{HM} \end{bmatrix} \begin{bmatrix} x_c \\ x_r \\ \dot{z} \end{bmatrix} + \begin{bmatrix} \mathrm{B}_c \\ \mathrm{B}_r \\ \mathrm{M} \end{bmatrix} \tag{6.4.46}$$

For structural models with $\mathrm{A}_{cr} = \mathrm{A}_{rc}^{\mathrm{T}} = 0$, Equation (6.4.46) becomes

$$\begin{bmatrix} \dot{x}_c \\ \dot{x}_r \\ \dot{z} \end{bmatrix} = \begin{bmatrix} \mathrm{A}_{cc} - \mathrm{B}_c(\bar{\mathrm{P}} + \delta\,\bar{\mathrm{P}}_c) & -\mathrm{B}_c\delta\,\bar{\mathrm{P}}_r & -\mathrm{B}_c\mathrm{M} \\ -\mathrm{B}_r\,(\bar{\mathrm{P}} + \delta\,\bar{\mathrm{P}}_c) & \mathrm{A}_{rr} - \mathrm{B}_r\delta\bar{\mathrm{P}}_r & -\mathrm{B}_r\mathrm{M} \\ (\bar{\mathrm{G}} + \delta\bar{G}_c) - \mathrm{H}\,(\bar{\mathrm{P}} + \delta\bar{\mathrm{P}}_c) & \delta\bar{G}_r - \mathrm{H}\delta\bar{\mathrm{P}}_r & \mathrm{F} - \mathrm{HM} \end{bmatrix} \begin{bmatrix} x_c \\ x_r \\ \dot{z} \end{bmatrix} + \begin{bmatrix} \mathrm{B}_c \\ \mathrm{B}_r \\ \mathrm{M} \end{bmatrix} \tag{6.4.47}$$

In the absence of spatial filter errors, the closed-loop state equation becomes

$$\begin{bmatrix} \dot{x}_c \\ \dot{x}_r \\ \dot{z} \end{bmatrix} = \begin{bmatrix} \mathrm{A}_{cc} - \mathrm{B}_c\bar{\mathrm{P}} & 0 & -\mathrm{B}_c\mathrm{M} \\ -\mathrm{B}_r\,\bar{\mathrm{P}} & \mathrm{A}_{rr} & -\mathrm{B}_r\mathrm{M} \\ \bar{\mathrm{G}} - \mathrm{H}\,\bar{\mathrm{P}} & 0 & \mathrm{F} - \mathrm{HM} \end{bmatrix} \begin{bmatrix} x_c \\ x_r \\ \dot{z} \end{bmatrix} + \begin{bmatrix} \mathrm{B}_c \\ \mathrm{B}_r \\ \mathrm{M} \end{bmatrix} v \,. \tag{6.4.48}$$

and the system's closed-loop eigenvalues are given by

$$\Lambda_{cl} = \lambda(A_{cc} - B_c K) \cup \lambda(F) \cup \lambda(A_{rr}) \; . \tag{6.4.49}$$

When spatial filter errors are present, however, the perturbations $\delta\bar{P}$ and $\delta\bar{G}$ in Equation (6.4.47) may lead to unstable closed-loop eigenvalues.

Example 6.4.4

Figure 6.4.11 shows a scatter plot of the closed-loop poles for the state feedback control law designed in Chapter 4 and implemented using a functional observer, when the system output is provided by a distributed-effect sensor designed to implement the functional observer design. The x's denote the nominal closed-loop poles, and the dots denote the perturbed closed-loop poles for spatial filter errors with variance $\sigma_n^2 = 10^{-4}$. Figure 6.4.12 shows the effect on the closed-loop poles of spatial filter errors with variance $\sigma_n^2 = 10^{-2}$. Comparing Figures 6.4.11 and 6.4.12, shows that while spatial errors with $\sigma_n^2 = 10^{-4}$ can degrade the damping in the closed-loop poles, they do not appear to cause instability. As the variance of the error increases, however, the larger perturbations in the measurement matrices can cause the system to become unstable. □

6.5. SUMMARY

This chapter described the effects of errors in the weighting functions associated with distributed-effect sensor designs. The errors in the achieved weighting functions were modelled as small deviations in the normalized values of the actual weighting functions from their desired values. The spatial filter errors were characterized in terms of deterministic bounds, and as random processes. The effects of errors in the spatial filter functions on several measures of system performance were examined. In examples of the application of distributed effect sensing to a flexible cantilevered beam, it was shown that small errors (on the order of 1%) could be tolerated, but that larger errors (on the order of 10%)

caused a significant change in the characteristics of the sensor.

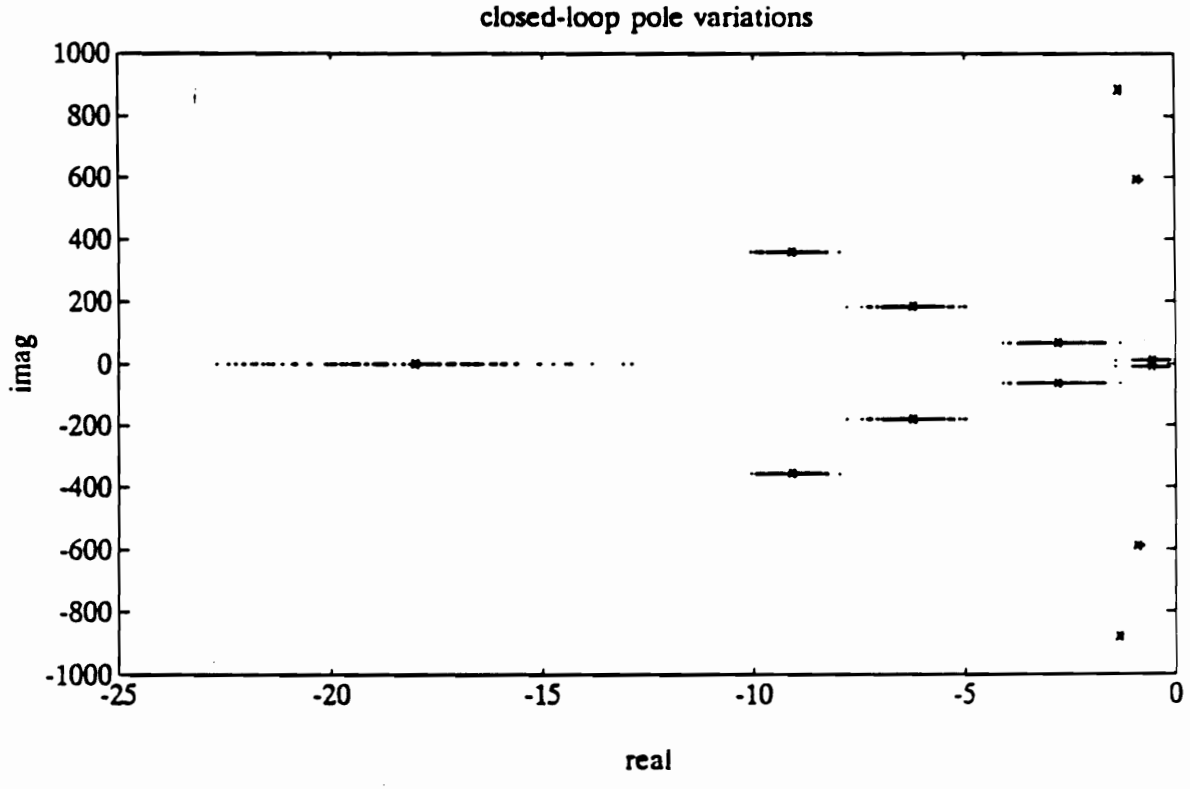

Figure 6.4.11 Closed-loop poles for state feedback control with a functional observer, subject to spatial filter errors in the distributed-effect sensor design. The x's indicate nominal closed-loop pole locations, and dots indicate closed-loop pole locations for spatial filter errors with variance $\sigma_n^2 = 10^{-4}$.

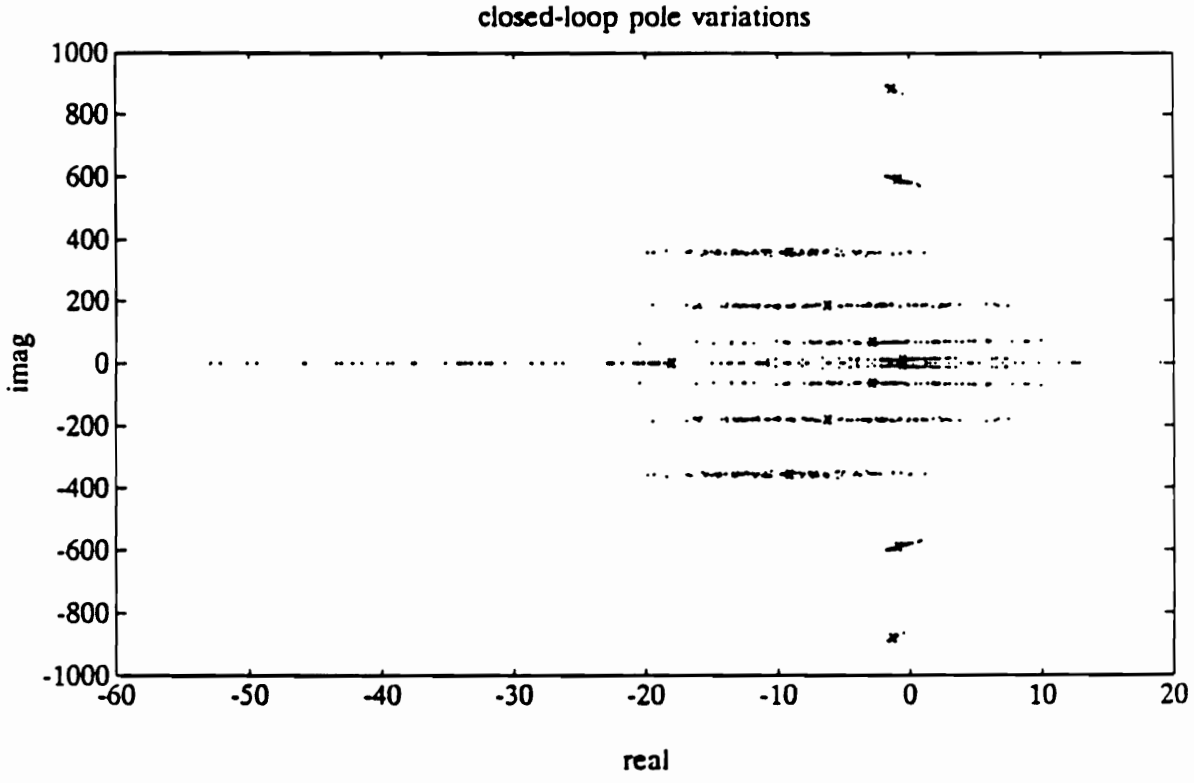

Figure 6.4.12 Closed-loop poles for state feedback control with a functional observer, subject to spatial filter errors in the distributed-effect sensor design. The x's indicate nominal closed-loop pole locations, and dots indicate closed-loop pole locations for spatial filter errors with variance $\sigma_n^2 = 10^{-2}$.

7. Conclusions

The recent development of sensors capable of providing spatially filtered measurements of distributed quantities, has lead to many proposed applications in structural control. This thesis described the use of distributed-effect sensors in structural control, and considered the effects of sensor weighting function errors on the outputs of distributed-effect sensors. Several methods for implementing distributed-effect modal domain optical fiber sensors were also described.

Distributed-effect sensors respond to environmental changes along a significant gauge length but have scalar outputs. The sensors can be manufactured with spatially varying sensitivity to a desired distributed measurand and act as spatial filters by converting the spatially distributed measurements into scalar signals. The spatial variation in the sensor sensitivity is known as the sensor's weighting function and determines the spatial filter operation performed by the sensor.

The distributed-effect sensor's weighting function represents an additional design parameter for structural control system design. There is a one-to-one correspondence between the sensor's weighting function and the representation of the sensor output when the sensor model is incorporated into a state space model of a flexible structure. Given a desired scalar system output, there exists a weighting function such that the output of the distributed-effect sensor provides the desired measurement; thus, distributed-effect sensors can also be interpreted as generalized point sensors and offer a possible solution to the well-known sensor placement problem in structural control.

Through the proper selection of the weighting function, distributed-effect sensors can measure directly many system quantities which can not be measured directly using point sensors. One criterion for the selection of the weighting function for a distributed-effect sensor is the implementation of modal filters.

Using the orthogonality of the mode shapes for structures such as cantilevered beams, the distributed-effect sensor can be designed to directly measure desired modal amplitudes; thus, distributed-effect sensors act as band-pass filters in the structure's spatial frequency domain. An important application of this type of spatial filtering in structural control is the elimination of observation spillover.

Another design criterion for selecting the weighting function for a distributed-effect sensor is the specification of measures of observability for different structural modes. Instead of simply making modes observable or unobservable, as in modal filtering, the weighting function can be chosen such that each structural mode has a specified measure of observability from the sensor output. In this dissertation, the design of weighting functions based on measures of observability was demonstrated using a measure of observability defined by the distance from the origin to the observability Grammian defined by the sensor's output.

Distributed-effect sensors can also be designed to implement reduced-order functional observers for structural control systems. A state feedback control law that would require a full-order observer of order 2N, can be implemented using a functional observer of order one and two distributed-effect sensors designed to provide the necessary system measurements. This result is particularly attractive in structural control, where the system order, N, may be quite large.

Although distributed-effect sensors offer increased capability for sensing applications in structural control, many of their advantages depend on the ability to arbitrarily specify and implement desired weighting functions. Unfortunately, the weighting functions that are realized in the fabrication of distributed-effect sensors can be expected to differ from those specified in the design of the sensors. Errors in the weighting functions of distributed-effect sensors can seriously degrade the performance of control laws designed to use the sensor outputs.

Causes of differences in the achieved and desired weighting functions for distributed-effect sensors include limits on the magnitude and spatial rate of change of the weighting functions for a particular sensor technology and application, and the process used to manufacture the sensor. Limits on the magnitude and spatial rate of change of the weighting function can be accounted

for in the design of the sensor by scaling the desired weighting function. Limitations imposed by the accuracy of the process used to fabricate the sensor, however, will generate errors in the implemented sensor weighting function.

The deviation of the implemented weighting function from the desired weighting function can be incorporated into the state-space representation of the sensor model as a perturbation in the corresponding output matrix. The weighting function error can be characterized in terms of deterministic bounds on the magnitude of the error, or as a random process. The error can also be characterized in terms of its spatial frequency content.

The characterization of the weighting function error, either deterministic or probabilistic, also characterizes the perturbations in the sensor's output matrix in the state space model of the structure to which it is attached. For this reason, it is convenient to characterize the error as white spatial noise, since techniques exist for designing control laws that are robust to the corresponding errors that are produced in the sensor's output matrix.

Errors in the weighting function of a distributed-effect sensor generate corresponding errors in the sensor output, which can degrade the performance of control laws which use the sensor. The effect of errors in the sensor's weighting function can be measured by examining the frequency response of the system from the sensor output, the measures of observability associated with the output of the implemented sensor, and the resulting closed-loop poles when the sensor is employed in a feedback control system.

A comparison of the desired and achieved frequency response of a flexible structure from the control input to the output of a distributed-effect sensor designed to measure only the first modal amplitude shows that for small errors in the weighting function, the sensor output contains some components due to the higher order modes, but still offers better performance than is available using a point sensor. For larger errors in the weighting function, however, the distributed-effect sensor fails to reject the higher order modes. Comparing the measures of observability for the same sensor outputs shows similar results. The presence of weighting function errors in distributed-effect sensors designed to implement functional observers for the control of a flexible beam can destabilize

the closed-loop system. Small errors in the weighting function tend to decrease the damping added by the control system, but large errors can cause some of the closed-loop poles to become unstable.

Examples of distributed-effect sensors include sensors constructed from piezoelectric film, holographic sensors, and modal domain optical fiber sensors. Optical fiber sensors are particularly well suited for applications in smart structures and materials. Several mechanisms for implementing modal domain optical fiber sensors with spatially weighted strain sensitivity were presented in this dissertation. The fabrication of weighted distributed-effect modal domain optical fiber sensors served as the motivation for the study of the effects that errors in the implemented weighting functions have on sensor performance.

This dissertation described the use of distributed-effect sensors for structural control. Perhaps most importantly, the effects of deviations in the weighting functions realized in the fabrication of distributed-effect sensors were examined and related to errors in the sensor output. The implementation of weighted modal domain optical fiber sensors was also considered. Using this research as a foundation, several areas that merit further investigation can be identified.

One area that deserves further investigation is the selection of weighting functions for distributed-effect sensors. One of the key advantages of distributed-effect sensors is their ability to perform spatial signal processing. Spatial filters can be designed to implement complex signal processing algorithms in the spatial domain. There is an inherent tradeoff in the design of these spatial filters, however, between a reduction in the complexity of the associated control laws and flexibility. With todays distributed-effect sensor technology, the weighting functions can not easily be changed after the sensor is fabricated; hence, if the system or structure changes over time, the distributed-effect sensor may no longer provide the desired system measurement. Thus, distributed-effect sensors must be designed with weighting functions that are robust to plant changes.

Another important area for future research is the development of new distributed-effect sensor technology. At this time, most applications of distributed-effect sensors have used piezoelectric film. Recently, a modal domain

optical fiber sensor was fabricated with spatially varying sensitivity to strain, but the ability to manufacture modal domain optical fiber sensors with prespecified spatial sensitivity to strain is still not available. Holographic sensing, which is still in the developmental stages for structural control applications, may offer the ability to implement distributed-effect sensors with adaptive weighting functions.

Finally, one area of research that must be pursued if distributed-effect sensor are to become generally accepted for structural control applications is the effects of errors on sensor performance. Although the results presented here can be used to describe the effects of certain types of errors on the sensor output, much work still needs to be done concerning the characterization of the types of errors that can be expected in the fabrication of the sensors. Better characterizations of the errors that can be expected in the weighting functions would result in better predictions of the effects of those errors on the sensor outputs. This information would also be useful for the design of robust control laws for systems employing distributed-effect sensors.

REFERENCES

[1] W. H. Chen and J. H. Seinfeld, "Optimal Location Of Process Measurements," *International Journal Of Controls*, Vol 21, No. 6, pp. 1003-1014, 1975.

[2] C. N. Viswanathan, R. W. Longman, and P. W. Likins, "A definition of the degree of controllability - a criterion for actuator placement," *Proceedings of the Second VPI&SU/AIAA Symposium on Dynamics and Control of Large Flexible Spacecraft*, Blacksburg, VA, June 1979.

[3] J. D. Chiu and R. E. Skelton, "Optimal Selection Of Inputs And Outputs In Linear Stochastic Systems," *Journal Of Astronautical Sciences*, Vol 31, No. 3, pp. 399-414, July-Sept. 1983.

[4] A. El Jai and A. J. Pritchard, "Sensors and actuators in distributed systems," *International Journal of Control*, Vol 46., No. 4, pp 1139-1153, 1987.

[5] H. Baruh and K. Choe, "Sensor placement in structural control," *Journal of Guidance and Control*, Vol. 13, No. 3, pp 524-533, May-June 1990.

[6] R. E. Skelton and G. A. Norris, "Selection Of Dynamic Sensors And Actuators In The Control Of Linear Systems," *Journal of Dynamic Systems, Measurement, and Control*, Vol. 111, pp. 389-397, Sept. 1989.

[7] M. J. Balas, "Feedback control of flexible systems," *IEEE Transactions On Automatic Control*, Vol. AC-23, No. 4, pp 673-679, August 1978.

[8] L. Meirovitch and H. Baruh, "The implementation of modal filters for control of structures," *Journal of Guidance and Control*, Vol. 8, No. 6, pp 707-716,

Nov.-Dec. 1985.

[9] M.F. Barsky, K.M. Reichard, D.K. Lindner, and R.O. Claus, "Distributed sensing methods for controlling flexible structures," in *Proceedings of the 7th* VPI&SU/AIAA Symposium on Dynamics and Control of Large Structures, May 8-10, 1989.

[10] D.K. Lindner, K.M. Reichard, W.T. Baumann, and M.F. Barsky, "Measurement and control of flexible structures using distributed sensors," *Proceedings of the 29th IEEE Conference on Decision and Control*, Honolulu, HI, pp2588-92, 1990.

[11] S. E. Miller and J. Hubbard, "Observability of a Bernoulli-Euler beam using PVF_2 as a distributed sensor," *Proceedings of the 6th VPI&SU/AIAA Symposium on Dynamics and Control of Large Structures*, Blacksburg, VA, June 1987.

[12] S. E. Burke and J. E. Hubbard, Jr., "Active vibration control of a simply supported beam using a spatially distributed actuator," *IEEE Control Systems Magazine*, Vol. 7, No. 4, pp25-30, Aug. 1987.

[13] C. -K. Lee and W. W. Chiang, "Critical active damping control of a flexible slender plate using a distributed modal actuator and sensor," *Proceedings of the 1989 American Controls Conference*, Pittsburgh, PA, June 1989.

[14] C.-K. Lee and F.C. Moon, "Modal sensor / actuators," *Transactions of the ASME,* Vol. 57, June, pp434-441, 1990.

[15] M. F. Barsky, "Holographic sensing for control of flexible structures," Ph.D. Dissertation, Bradley Department of Electrical Engineering, Virginia Tech, Blacksburg, VA, Jan. 1990.

[16] S. S. Welch, and D.E. Cox, "Characteristics of a dynamic holographic sensor for shape control of a large reflector," *Proceedings of the SPIE Conference*

on OE/Aerospace Sensing, paper #1480-01, Orlando, FL, April 1991.

[17] K. Murphy, M.S. Miller, A.M. Vengasarker, and R.O. Claus, "Elliptical-core, two-mode, optical fiber sensor implementation methods," *Journal of Lightwave Technology*, Vol. 8, pp.1688-1696, 1990.

[18] K.M. Reichard and D.K. Lindner, "Modeling the effects of arbitrary stress on the response of modal domain optical fiber sensors," Internal Research Report, Virginia Tech Fiber & Electro-Optics Research Center, Virginia Tech, Blacksburg, VA, March, 1990.

[19] S.A. Collins, D.W. Miller, and A.H. vonFlotow, "Piezopolymer spatial filters for active structural control," *Proceedings of the Workshop on Recent Advances in Active Control of Sound and Vibrations*, Blacksburg, VA, pp 219-236, 1991.

[20] D. Cox and D.K. Lindner, "Active control for vibration suppression in a flexible beam using a modal domain optical fiber sensor," accepted for publication in *ASME Journal of Vibration and Acoustics*, 1991.

[21] D.K. Lindner, W.T. Baumann, F.S. Ho, and E. Bielecki, "Modal domain optical fiber senosrs for control of acoustic radiation," presented at Workshop on Recent Advances in Active Control of Sound and Vibration, Blacksburg, VA, April 15-17, 1991.

[22] D. Cox, D. Thomas, K. Reichard, D.K. Lindner, and R.O. Claus, "Modal domain fiber optic sensor for closed loop vibration control of a flexible beam," in *Proceedings of the SPIE Conference on OE/Fibers*, Vol. 1170, pp 372-383, Boston, MA, Sept. 1989.

[23] D. Cox, D. Thomas, K. Reichard, D.K. Lindner, and R.O. Claus, "Vibration control of a flexible beam using a distributed fiber optic sensor," in *Proceedings of the 28th* IEEE Conference on Descision and Control, Tampa, FL, pp. 2685-2686, Dec. 1989.

[24] D. E. Cox, "Active control of flexible structures using fiber optic modal domain sensors," M.S. Thesis, Bradley Department of Electrical Engineering, Virginia Tech, Blacksburg, VA, June 1990.

[25] R.O. Claus, K.D. Bennett, A.M. Vengsarkar, and K.A. Murphy, "Embedded optical fiber sensors for materials evaluation," *Journal of Non-Destructive Evaluation*, Vol. 8, No. 2, pp. 371-381, 1989.

[26] A. Vengsarkar, "Weighted fiber sensors for vibration analysis," *Proceedings of the Smart Materials Workshop,* Virginia Polytechnic Institute and State University, Blacksburg, VA, April 1991.

[27] K.D. Bennett, "Optical fiber modal domain sensors for dynamic strain measurements," Ph.D. Dissertation, Bradley Department of Electrical Engineering, Virginia Tech, Blacksburg, VA, 1990.

[28] J.S. Sirkis and H.W. Haslach, Jr., "Interferometric strain measurement by arbitrarily configured, surface-mounted, optical fibers," *Journal of Lightwave Technology,* Vol. 8, No. 10, pp 1497-1503, Oct. 1990.

[29] A. Safaai-Jazi and R.O. Claus, "Synthesis of interference patterns in few-mode optical fibers," *Proceedings of the SPIE Symposium on Optoelectronic and Fiber Optic Devices and Applications*, Boston, MA, pp. 180-185, Sep., 1989.

[30] M.R. Layton and J.A. Bucaro, "Optical fiber acoustic sensor utilizing mode-mode interference," *Applied Optics,* Vol. 18, No. 5, pp. 666-670, 1979.

[31] B.Y. Kim, J.N. Blake, S.Y. Haung, and H.J. Shaw, "Use of highly ellipical core fibers for two-mode fiber devices," *Optics Letters*, Vol. 12, No. 9, pp. 729-731, 1987.

[32] J.K. Shaw, A.M. Vengsarkar, and R.O. Claus, "Theoretical analysis of two-

mode, elliptical-core optical fiber sensors," *Proceedings of the SPIE Conference on Fiber Optic Smart Structures and Skins III*, Vol. 1370, San Jose, CA, 1990.

[33] Zvonar, G.A., and P. Delos, "Fringe counting device for modal domain optical fiber sensors," Internal report, Fiber & Electro-Optic Research Center, Bradley Department of Electrical Engineering, Virginia Tech, Blacksburg, VA, 1990.

[34] A.W. Snyder and J.D. Love, *Optical Waveguide Theory*, London: Chapman and Hall, 1983.

[35] D. Gloge, "Weakly guiding fibers," *Applied Optics*, Vol. 10, No. 10, pp. 2252-2258.

[36] C. DiFrancia and R.O. Claus, "Structure/property correlations of several polyimide optical fiber coatings for embedding in an epoxy matrix," *Proceedings of the SPIE Conference on OE/Fibers*, Vol. 1170, pp. 505-512, Boston, MA, 1989.

[37] J.S. Sirkis and A. Dasgupta, "Optimal coatings for intelligent structure fiber optic sensors," *Proceedings of the SPIE Symposium on Optoelectronic and Fiber Optic Devices and Applications*, SanJose, CA, pp 129-141, Sept. 1990.

[38] J.S. Sirkis and H.W. Haslach, Jr., "Complete phase-strain model for structurally embedded interferometric optical fiber sensors," accepted for publication in the Journal of Intelligent Material Systems and Structures, 1991.

[39] A.C. Ugural and S.K. Fenster, *Advanced Strength and Applied Elasticity*, NewYork: Elsevier Science Publishing Co., Inc., 1981.

[40] L. Meirovitch and H. Baruh, "Control of self-adjoint distributed-parameter systems", *Journal of Guidance and Control*, Vol. 5, No. 1, pp 60-66, Jan-Feb

1982.

[41] T. Bailey and J. E. Hubbard Jr., "Distributed piezoelectric-polymer active vibration control of a cantilevered beam," *Journal of Guidance, Control, and Dynamics*, Vol. 8, No. 5, pp605-611, Sept-Oct 1985.

[42] M. F. Barsky and D. K. Lindner, "Distributed sensing for robust control of flexible structures," in *Proceedings of the 1989 Allerton Controls Conference*, Urbana, IL, Sept. 1989.

[43] C. N. Viswanathan, R. W. Longman, and P. W. Likins, "A degree of controllability definition: Fundamental concepts and application to modal systems," *Journal of Guidance and Control*, Vol. 7, No. 2, pp 222-230, March - April 1984.

[44] D. K. Lindner, J. Babendreier, and A. M. A. Hamdan, "The dual GHR, zeros, and residues," *System and Control Letters*, Vol. 10, pp 245-250, 1988.

[45] B. C. Moore, "Principal component analysis in linear systems: controllability, observability, and model reduction," *IEEE Transactions on Automatic Control*, Vol. AC-26, pp. 17-32, 1981.

[46] R. E. Skelton and M. L. DeLorenzo, "Selection of Noisy Actuators And Sensors In Linear Stochastic Systems," *Journal of Large Scale Systems, Theory and Applications*, Vol. 4, pp. 109-136, Apr. 1983.

[47] C-T Chen, *Linear System Theory and Design*, Holt, Rinehart and Winston, 1984.

[48] M. Tahk and J. L. Speyer, "Modeling of parameter variations and asymptotic LQG synthesis," *IEEE Transactions on Automatic Control,* Vol 32, No 9, pp 793-801, 1987.

[49] M. Tahk and J. L. Speyer, "Parameter robust linear-quadratic-Gaussian

design synthesis with flexible structure control applications," *Journal of Guidance, Control, and Dynamics*, Vol 12, pp 460-468, 1989.

[50] J.-Y. Lin, *Robust Design of LQG Controllers*, Ph.D. Dissertation, University of California, Los Angeles, CA, 1989.

[51] V.D. DeBrunner, *Sensitivity Analysis of Digital Filter Structures*, M.S. Thesis, Virginia Polytechnic Institute ans State University, Blacksburg, VA, 1986.

Vita

Karl Martin Reichard was born in Baltimore, MD in 1962, and moved to Forest Hill, MD in 1966. He attended Forest Hill Elementary School, Bel Air Middle School, and graduated from Bel Air Senior High School in 1980.

Mr. Reichard graduated Summa Cum Laude from Virginia Polytechnic Institute and State University (Virginia Tech) in 1985 with the degree of Bachelor of Science in Electrical Engineering. He received the degree of Master of Science in Electrical Engineering from Virginia Tech in 1988.

Mr. Reichard was the recipient of Office of Naval Research and E.I. duPont graduate fellowships. He is a member of the Pi Kappa Alpha Fraternity, the Tau Beta Pi, Eta Kappa Nu, and Phi Kappa Phi honor societies, and the IEEE Control Systems Society.